

# **ABSTRACT**

## **FETUS PHANTOM CONSTRUCTIONS FOR OVERWEIGHT AND OBESE PREGNANT FEMALES FOR RADIOLOGICAL APPLICATIONS**

by Rasha Makkia

July 2019

Director of Dissertation: Dr. Michael Dingfelder

### **DEPARTMENT OF PHYSICS**

Radiation exposure and associated radiation risks are major concerns for fetal development for pregnant patients in general, and in particular for overweight and obese pregnant patients who undergo diagnostic imaging or radiation therapy procedures. This dissertation describes a detailed research project related to the construction of hybrid computational phantoms, including the fetus and the pregnant female with the focus on overweight and obese patients, which can be used in radiological applications. In detail, a series of three hybrid computational fetus phantoms corresponding to a fetal age of 20, 31, and 35 weeks of pregnancy were constructed using high-quality magnetic resonance imaging (MRI) sets obtained for three different patients. A total of 29 fetal organs were outlined from radiological images via the Velocity Treatment Planning System (TPS) and were imported to the three-dimensional (3D) modeling software package Rhinoceros for further reconstruction. The hybrid computational female phantom was constructed from the adult ICRP reference model which was converted from voxels into a non-uniform rational basis spline (NURBS) or mesh surface based phantom. A total of 35 different female organs and tissues

were identified. All fetal and female organ masses were individually matched with the ICRP 89 Publication reference values. The hybrid computational pregnant female phantom series was constructed by individually adding the hybrid fetus model series to the hybrid female phantom. Fetal positions and locations were carefully adapted from MRI data and verified by a clinical specialist. Ultrasound data has also been used to determine the fetus body masses. Overweight and obese pregnant phantom models were derived from the developed standard hybrid computational pregnant series by adding different amounts of fat under the skin, except in the eye regions. They were carefully modeled using NURBS and/or polygon mesh geometry and include specified amounts of adipose tissue below the skin. The NURBS and mesh-based pregnant phantoms were then voxelized using the Binvox software and checked for consistency using the Viewvox and ImageJ software packages. This resulted in a set of pregnant female phantoms with body mass indexes ranging from 22.58 kg/m<sup>2</sup> (normal body weight) to 34.24 kg/m<sup>2</sup> (morbidly obese). This set of new phantoms can be used in the future to study the optimization of image quality and radiation dose for patients of different weight classifications. The ultimate goal is to create a library of all the data derived from these phantoms into a comprehensive dosimetry database defined in the Virtual Dose software. The new series of hybrid computational fetus models provide realistic anatomical details that can be useful in evaluating fetal radiation doses in pregnant patients undergoing diagnostic imaging or radiotherapy where realistic fetal computational human phantoms are required.



**FETUS PHANTOM CONSTRUCTIONS FOR OVERWEIGHT AND  
OBESE PREGNANT FEMALES FOR RADIOLOGICAL APPLICATIONS**

A Dissertation

Presented to the Faculty of the Department of Physics

East Carolina University

In Partial Fulfillment of the Requirements for the Degree

Doctor of Philosophy in Biomedical Physics

by

Rasha Makkia

July 2019

© Rasha Makkia, 2019

**FETUS PHANTOM CONSTRUCTIONS FOR OVERWEIGHT AND  
OBESE PREGNANT FEMALES FOR RADIOLOGICAL APPLICATIONS**

By

Rasha Makkia

APPROVED BY:

DIRECTOR OF: \_\_\_\_\_  
DISSERTATION Michael Dingfelder, Ph. D.

COMMITTEE MEMBER: \_\_\_\_\_  
Keith Nelson MD

COMMITTEE MEMBER: \_\_\_\_\_  
Habib Zaidi, Ph.D.

COMMITTEE MEMBER: \_\_\_\_\_  
Robert McLawhorn, Ph.D.

COMMITTEE MEMBER: \_\_\_\_\_  
Regina DeWitt, Ph.D.

COMMITTEE MEMBER: \_\_\_\_\_  
Jefferson Shinpaugh, Ph.D.

CHAIR OF THE DEPARTMENT  
OF PHYSICS: \_\_\_\_\_  
Jefferson Shinpaugh, Ph.D.

DEAN OF THE  
GRADUATE SCHOOL: \_\_\_\_\_  
Paul J. Gemperline, Ph.D.

## **ACKNOWLEDGMENTS**

I would like to thank Dr. Michael Dingfelder for his greatest support and guidance during my entire graduate studies and research projects. It was my honor to work with him and learn from his experience and advice. His welcoming attitude, which expects much from candidates made this project a joy to pursue. His office door is and was always open, and he always made himself available, no matter how busy his schedule is and was.

I also would like to thank Dr. Keith Nelson whom I had the honor to work with him. Thank you for sharing your clinical experience which made this project unique, accurate and more detailed. Thank you for reviewing and editing on my manuscripts and posters. In addition, thank you for the time you spent in the Radiation Oncology Department confirming all the clinical contours and segmentation in my work. I would also like to thank your father and mother for gifting the atlas fetus book to me with their author signatures in it. You and your parents gave a very special and excellent clinical touch to this project.

It was my honor to work with one of the most experienced professors at the core of this project, Dr. Habib Zaidi who made this work possible and saw it to completion. Your input was very valuable and fundamental to this project. Thank you also for the help provided by your lab members, in particular by Dr. Xie Tianwu. Thank you for all your ongoing advice and generous guidance, helping to complete the final input models well, and making the space and time for my work in your very busy schedule.

Thank you to the dissertation committee members, Dr. Michael Dingfelder, Keith Nelson, Dr. Habib Zaidi, Regina Dewitt, Dr. Jefferson Shinpaugh, and Robert McLawhorn for their dissertation review and helpful suggestions. I also would like to thank the physics staff who helped me in the best way possible: Mr. Dan Criminger, Mrs. Brenda Doss, Mr. Brandi Griffin, and Rhonata Hurwitz. I am fortunate in having met so many great people on my journey through this degree program.

I would not have known how to find the strength and motivation to complete it if it had not been for these truly kind and warm-hearted people who have helped me greatly during these years. They all have become my second family on this other side of the world. I would also like to thank my family for being understanding and supportive of hours dedicated to my studies and research, and of the years being away from home.

Many thanks and love to my parents, my mother-in-law, my brother, and my sister in law, and to all my relatives for their utmost support and love. Thank you to my dear friends for their great support.

Finally, I sincerely thank and appreciate my husband, Safaa Al-Qaysi, for joining me on this journey, as well as on the previous and other ongoing journeys, for all of his motivation and support. I could not have done it without his patience and help. And my lovely and adorable son, Zain Alqaysi, who has indirectly influenced me to create this project in 2015: the moment I knew I had him in my life, I started thinking more about other mothers, who also care so much for their children's health and safety.



# TABLE OF CONTENTS

<b>LIST OF TABLES .....</b>	<b>x</b>
<b>LIST OF FIGURES .....</b>	<b>xi</b>
<b>LIST OF ABBREVIATIONS .....</b>	<b>xv</b>
<b>CHAPTER ONE: INTRODUCTION .....</b>	<b>1</b>
1.1 BACKGROUND .....	1
1.2 PREVIOUS PREGNANT FEMALE MODELS AND THEIR LIMITATIONS.....	5
1.2.1 MATHEMATICAL OR STYLIZED PHANTOMS .....	6
1.2.2 VOXELIZED OR TOMOGRAPHY PHANTOMS.....	7
1.2.3 HYBRID PHANTOMS .....	9
1.3 RADIATION EFFECTS ON THE FETUS .....	12
1.4 COMMON DIAGNOSTIC IMAGING PROCEDURES DURING PREGNANCY .....	13
1.5 OBJECTIVE OF THIS RESEARCH.....	15
<b>CHAPTER TWO: HYBRID COMPUTATIONAL FETUS PHANTOM CONSTRUCTIONS.....</b>	<b>18</b>
2.1 TARGET FETAL AGES .....	18
2.2 IMAGE ACQUISITION .....	19

2.3 IMAGE SEGMENTATION.....	20
2.4 CONVERSION TO 3D MODELING FILE FORMAT.....	24
2.5 NURBS AND POLYGON MESH MODELING.....	25
2.6 MATCHING WITH ICRP PUBLICATION 89.....	28
2.7 RESULTS.....	29
2.7.1 COMPARING FETAL ORGAN MASSES WITH ICRP RECOMMENDATION.....	29
2.7.2 FETAL POSITION IN UTERO.....	33
2.8 DISCUSSION.....	36

## **CHAPTER THREE: HYBRID COMPUTATIONAL PREGNANT FEMALE**

### **PHANTOM CONSTRUCTIONS.....41**

3.1 ICRP FEMALE AND FILE FORMAT .....	42
3.2 NURBS AND POLYGON MESH MODELING.....	43
3.3 STANDARD HYRBID FEMALE PHANTOM .....	45
3.4 STANDARD FETUS POSITION IN UTERO .....	46
3.5 PREGNANT FEMALE PHANTOM CONSTRUCTIONS.....	47
3.5.1 PREGNANT FEMALE PHANTOM – 20 WEEKS .....	48
3.5.2 PREGNANT FEMALE PHANTOM – 31 WEEKS .....	48
3.5.3 PREGNANT FEMALE PHANTOM – 35 WEEKS .....	49
3.6 RESULTS.....	50

3.6.1 THE ICRP ADULT FEMALE MODEL.....	51
3.6.2 THE FETUS PHANTOMS INSIDE THE UTERO.....	55
3.6.3 THE HYBRID PREGNANT COMPUTATIONAL PHANTOMS .....	57
3.7 DISCUSSION.....	67
<b>CHAPTER FOUR: HYBRID OBESE COMPUTATIONAL PREGNANT PHANTOM CONSTRUCTIONS.....</b>	<b>69</b>
4.1 PREGNANT FEMALE MODELS COMPLETED .....	69
4.2 VOXELIZATION .....	70
4.2 OVERWEIGHT AND OBESE PREGNANT FEMALE PHANTOM .....	73
<b>CHAPTER FIVE: CONCLUSION AND FUTURE WORK .....</b>	<b>93</b>
5.1 CONCLUSION .....	93
5.2 FUTURE WORK .....	96
<b>REFERENCES.....</b>	<b>98</b>
<b>APPENDIX A: SEGMENTED ORGANS OF THE PREVIOUS PREGNANT PHANTOM IN COMPARISON WITH THE CURRENT DEVELOPED MODEL.....</b>	<b>102</b>
<b>APPENDIX B: VOXELIZED PREGNANT PHANTOM MODELS INFORMATION.....</b>	<b>103</b>

B-1 Voxelization bounding box, organ ID, and voxel resolution for 20-week Pregnant  
Female Phantom..... 104

B-2 Voxelization bounding box, organ ID, and voxel resolution for 31-week Pregnant  
Female Phantom..... 106

B-3 Voxelization bounding box, Organ ID and voxel resolution for 35-week Pregnant  
Female Phantom..... 108

**APPENDIX C: SELECTED PUBLISHED, ABSTRACTS, AND AWARDS**

.....110

**APPENDIX D: THE UNIVERSITY & MEDICAL CENTER**

**INSTITUTIONAL REVIEW BOARD (UMCIRB)**Error! Bookmark not defined.

## LIST OF TABLES

Table 2.1 Three case studies of fetal organ mass densities, compared with the provided ICRP reference data. ....	31
Table 2.2 Fetal organ mass densities, matching ICRP reference data. ....	32
Table 3.1 An Adult ICRP reference female mass volume and density. ....	52
Table 3.2 31-Weeks Pregnant Female Phantom Model mass volume and density ....	598
Table 3.3 35-Weeks Pregnant Female Phantom Model mass volume and density ....	59
Table 3.4 Flow chart describing the steps for developing hybrid computational pregnant phantom models. ....	660
Table 3.5 Flow chart describing the steps for developing hybrid computational pregnant phantom models. ....	66
Table 4.1 The weight classifications of ICRP reference model and female pregnant phantoms, excluding fetus weight. ....	788

## LIST OF FIGURES

Figure 2.1 Sample of an MR coronal image of a 35-week pregnant female. (a) Original MR slice, (b) The same MR slice segmented, in “seen” view 3D mode, using the Velocity Software (TPS). .....	21
Figure 2.2 Representative CT, the sagittal image of 30-weeks and 3-dimension pregnant female: (a) Original CT slice, (b) Segmentation result of the original CT image, (c) 3D model in “seen” view mode, using Velocity Software (TPS). .....	23
Figure 2.3 Illustration of the 3D-model, using Velocity software (TPS) MR coronal image segmentation of a 31-weeks pregnant female (a) Original, unsegmented slice (b) Segmented placenta and umbilical cord (c) Segmented placenta, umbilical cord, and uterus.....	25
Figure 2.4 An example of extracting the placenta in different steps: (a) The original triangle mesh of the placenta model extracted from a 2D MR image. (b) The extracted contours of the original model. (c) The 3D NURBS surface representation of the placenta model. (d) The 3D NURBS surface representation after adding the surface color feature. ....	27
Figure 2.5 An example of the 31-week fetus model development, in this case, of the brain, eyes, and liver. (a) The original triangle mesh model extracted from 2D MR imaging. (b) The extracted contours from the original mesh model. (c) The completed 3D non-uniform rational basis spline (NURBS) surface, constructed from the original mesh polygons. (d) A comparison between the constructed 3D NURBS surface and the original mesh model.....	34
Figure 2.6 A snapshot of the 20-, 31-, and 35-week uterus with the fetus inside it. ....	35

Figure 2.7 A Snapshot of the 20- (a), 31- (b), and 35-week (c) fetus, showing the fetal body, the placenta, and the umbilical cord, with the help of Rhinoceros software. ....	40
Figure 3.1 Illustration of a polygon mesh object with triangle facets of a 35-week fetal brain organ. (a) The red gab between triangle faces. (b) The red hole was repaired using the FillMeshHoles command in Rhinoceros software [50]. ....	43
Figure 3.2 Frontal and back views of the standard reference female model, after removing the skin of the initial voxels in a polygon mesh. ....	53
Figure 3.3 Frontal and back views of the ICRP adult reference female in NURBS surfaces of the standard reference female model. ....	54
Figure 3.4 Three-dimensional front representations of hybrid fetus phantom models at 20, 31, and 35 weeks of gestation. (a) 20-week of gestation, (b) 31-week of gestation, (c) 31 week of gestation. ....	56
Figure 3.5 The steps necessary to create ICRP pregnant computational phantom sets by adding the fetus phantom developed inside ICRP reference female after removing selected organs from the non-pregnant model at (a) 20, (b) 31, and (c) 35 weeks of gestation. ....	62
Figure 3.6 Frontal views of pregnant female phantom series. (a) ICRP female phantom, (b) 20-week pregnant phantom, (c) 31-week pregnant phantom, (d) 35-week pregnant phantom. ....	63
Figure 3.7 Side views of pregnant female phantom series. (a) ICRP female phantom, (b) 20-week pregnant phantom, (c) 31-week pregnant phantom, (d) 35-week pregnant phantom. ....	64
Figure 3.8 Side and the original views of pregnant female phantom series. (a) ICRP female phantom, (b) 20-week pregnant phantom, (c) 31-week pregnant phantom, (d) 35- week pregnant phantom.....	65

Figure 4.1 An example of the left lung at 35 weeks of gestation, in a closed polygon mesh after it has been given (a) an identity of 57 and a bounding box, and (b) an identity of 56 and a bounding box.....75

Figure 4.2 The same example of the left lung at 35 weeks of gestation, in a closed polygon mesh, after it has been given (a) a Binvox command prompt of the left lung, as an example of the left lung voxelization process, using the same ID and maximum voxel resolution calculated from its bounding box, and (b) a Viewvox command prompt, in order to visualize and check the initial voxelization step in (a). (c) The output result from step (b), showing the resulting voxelized left and right lungs, repeating the steps outlined above. ....77

Figure 4.3 The back and original orientation of the voxelized pregnant female phantom series, using ImageJ 3D viewer. (a) ICRP female phantom, (b) 20-weeks pregnant phantom, (c) 31-weeks pregnant phantom, (d) 35-weeks pregnant phantom.....79

Figure 4.4 Frontal views of voxelized pregnant female phantom series, using ImageJ 3D viewer. (a) ICRP female phantom, (b) 20-weeks pregnant phantom, (c) 31-weeks pregnant phantom, (d) 35-weeks pregnant phantom. ....80

Figure 4.5 Side views of the voxelized pregnant female phantom series, using ImageJ 3D viewer. (a) ICRP female phantom, (b) 20-weeks pregnant phantom, (c) 31-weeks pregnant phantom, (d) 35-weeks pregnant phantom. ....81

Figure 4.6 Side views ICRP reference female phantom series. (a) ICRP female phantom, (b) Overweight female phantom (c) Obese pregnant phantom. ....82

Figure 4.7 Top views of the ICRP reference female phantom series. (a) ICRP female phantom, (b) Overweight female phantom (c) Obese pregnant phantom.....83



Figure 4.8 Frontal views of 20-weeks voxelized pregnant female phantom series. (a) ICRP pregnant phantom, (b) Overweight pregnant phantom, (c) Obese pregnant phantom.....	84
Figure 4.9 Side views of 20-weeks voxelized pregnant female phantom series. (a) ICRP pregnant phantom, (b) Overweight pregnant phantom, (c) Obese pregnant phantom.....	85
Figure 4.10 Top views of voxelized 20-week pregnant female phantom series. (a) ICRP pregnant phantom, (b) Overweight pregnant phantom, (c) Obese pregnant phantom.....	86
Figure 4.11 Front views of 31-weeks voxelized pregnant female phantom series. (a) ICRP pregnant phantom, (b) Overweight pregnant phantom, (c) Obese pregnant phantom.....	87
Figure 4.12 Side views of 31-weeks pregnant female phantom series. (a) ICRP female phantom, (b) 20-weeks pregnant phantom, (c) 20-weeks overweight pregnant phantom.....	88
Figure 4.13 Top views of 31-weeks voxelized pregnant female phantom series. (a) ICRP pregnant phantom, (b) Overweight pregnant phantom, (c) Obese pregnant phantom.....	89
Figure 4.14 Front views of 35-weeks voxelized pregnant female phantom series. (a) ICRP pregnant phantom, (b) Overweight pregnant phantom, (c) Obese pregnant phantom.....	90
Figure 4.15 Side views of voxelized 35-week pregnant female phantom series. (a) ICRP pregnant phantom, (b) Overweight pregnant phantom, (c) Obese pregnant phantom.....	921
Figure 4.16 Top views of voxelized 35-week pregnant female phantom series. (a) ICRP pregnant phantom, (b) Overweight pregnant phantom, (c) Obese pregnant phantom.....	92

## LIST OF ABBREVIATIONS

AAPM	The American Association of Physicists in Medicine
ALARA	As Low As Reasonably Achievable
BMI	Body Mass Index
CT	Computational Tomography
DICOM	Digital Imaging and Communication in Medicine
FOV	Field of View
ICRP	International Commission on Radiological Protection
ICRU	International Commission on Radiation Units and Measurements
IMRT	Intensity Modulation Radiation Therapy
IRB	Institutional Review Board
MRI	Magnetic Resonance Imaging
MC	Monte Carlo
NURBS	Non-Uniform Rational Basis Spline Surface
OBGYN	Obstetrics and Gynecology
OBJ	Wavefront Object
ORNL	Oak Ridge National Lab
PC	Post Conception

PDD	Percentage Depth Dose
PET	Positron Emission Tomography
SAT	Subcutaneous Adipose Tissue
SMR	Severe Mental Retardation
SPECT	Single Photon Emission Computerized Tomography
STL	Standard Triangle Length
3D	Three Dimension
TG	Task Group
TLD	Thermoluminescent Dosimetry
TPS	Treatment Planning System
US	Ultrasound
VAT	Visceral Adipose Tissue

# CHAPTER ONE: INTRODUCTION

## 1.1 BACKGROUND

Obese patients represent potential health problems worldwide [1]. The National Health and Nutrition Examination Survey reported that 60% of the adult American population is either overweight or obese [2]. Overweight is defined as having a BMI in the range of 25 kg/m<sup>2</sup> to 29.9 kg/m<sup>2</sup> and obesity is defined as having a body mass index (BMI) in the range of 30 kg/m<sup>2</sup> and more [2]. The BMI is calculated as the body mass divided by the square of body height. Various medical conditions are associated with obesity: different types of cancer, such as endometrial (uterus) cancer, breast cancer, ovarian cancer, cervical cancer, colon cancer, and other negative health risks such as fetus birth defects and infertility [3]. Typical abdominal CT examinations for obese patients result in insufficient image quality: there is too much image noise because fat (subcutaneous and visceral) absorbs a higher dose. To obtain a decent quality image with less noise, a modified CT protocol is needed for obese patients, in order to improve image quality. This can be achieved by increasing the x-ray output, which can, in turn, be done by either increasing the tube voltage or the tube current. However, this step would also increase the in-field organ dose as well as the out-of-field healthy organ dose that are located further away from the scanned beam field. [2].

Researchers have shown that the number of CT diagnostic examinations in the US has increased by up to 400% over the last a few years [4]. The American Association of Physicists in Medicine (AAPM) Radiation Therapy Committee Task Group 36 (TG-36) in 1995 has also

reported that up to four thousand pregnant women in the United States receive radiotherapy every year [5]. Invasive cancer is the number one cause of death in women aged 35 to 54 years, and the most common invasive cancer types in pregnant women being breast cancer, cervical cancer, lymphoma, malignant melanoma, and thyroid cancer [4]. Radiation therapy, surgery and /or both are the three primary methods in the treatment of pregnant women [6]. The number of patients undergoing radiation therapy has increased because of the vast improvement in cancer detection, treatment, and survival of patients. However, they are at relatively high risk of secondary malignancies due to the exposure of the patient body to radiation [7-8]. Many concerns apply to the fetus, too, if the mother is treated with radiation during pregnancy [5]. Custom lead or apron shielding devices such as the Bridge Over Patient device or the Table Over Treatment Couch device are not always available in small clinics which is why mothers should be referred to larger institutions which have the shielding equipment available for best treatments[5,9-10]. It is essential to calculate the dose absorbed by a sensitive structure such as the fetus in a pregnant patient and to evaluate the associated potential risk of any particular procedure such as Intensity Modulation Radiation Therapy (IMRT) to better estimate the clinical benefits for the mother and the risks to the fetus [7].

The AAPM TG-36 report provides guidelines for managing radiation therapy for pregnant women and for estimating the total measurement dose absorbed by the fetus in pregnant patients who undergo external beam radiotherapy. The estimated dose range to the fetus is calculated using three points of measurement: the funds, symphysis pubic, and umbilicus, where the dosimeters can be placed on the surface of the patient skin and underneath the shielding material, to simulate full-scatter geometry. A water phantom was used to simulate this measurement on the surface of the

pregnancy patient at three different depths, to ensure that the phantom measurements were valid for patient treatment. Part of the AAPM TG-36 procedure was to evaluate the unshielded dose to the fetus by measuring the out-of-field dose without shielding, then to add sufficient shielding material to protect the fetus during radiation therapy treatment [5].

Although AAPM TG-36 provides excellent recommendations to reduce the fetus dose outside the treatment field due to scatter, such as using open collimators, avoiding blocks, offering different shielding designs, etc., AAPM TG-36 uses many approximations to make it easy for medical physicists to apply it in the clinic [5]. Many research studies have repeated the TG-36 procedure, and they found that approximations, such as using limited field sizes and shapes can potentially lead to uncertainty in out-of-field dose measurements compared with what TG-36 has reported. According to Kry, Starkschall, et al. in 2007, the out-of-field dose was underestimated because of the small water tank used, and because of poor anatomical detail of the pregnant patient [11]. Kry et al. reported having conducted an experimental study in 2007 to evaluate the measured fetal dose using the TG-36 protocol. The fetal dose was calculated and measured in the same locations as TG-36 had measured in eight pregnant patients at MD Anderson Cancer Center. Measurements were acquired with ion chambers placed in a water tank; either there was an anthropomorphic phantom attached to the water tank (if the primary tumor site was superior to the fetus) or a cylinder phantom was connected to the water tank (for extremities like legs). Two measurements were made for each, taking into consideration the distance parameter between the fetal point and the field edge and field size parameters. Kry et al. reported that TG-36 had underestimated the measured fetal dose values by 31% [11]. These results indicate that fetal dose

determination has accurately addressed the uncertainty in phantom measurements, such as water phantom vs. patient or the computational pregnant model.

Other theoretical studies were published aiming to modify TG-36 and to better estimate the fetal dose from a 6MV photon irradiation to a pregnant patient, for example Bednarz and Xu [8]. Xu and his coworkers have developed different pregnancy models derived from Computed Tomography (CT) images, along with full Varian accelerator head modeling designed for Monte Carlo (MCNPX code) in-field and out-of-field dose calculations. Percentage depth dose (PDD) was used to compare MC calculations with TG-36 measurements, with a result of 11-20% difference at different depths. The values were higher beyond the in-field region (25% at 50 cm). Their paper suggested that computational pregnant phantom sets provide an accurate dose over the entire fetus volume in each trimester, rather than choosing three measurement points as in TG-36 [5,8].

Many studies have also quantified the accuracy of out-of-field measurements acquired by Commercial Treatment Planning Systems (TPS) in anthropomorphic male reference phantoms with thermoluminescent dosimeter TLD capsules placed within each slice of the phantom at a total of 238 points of measurement. In this study, both mean dose and standard deviation were calculated for each TPS and phantom with TLD doses. They found that TPS underestimates out-of-field doses by  $40\% \pm 20\%$ , the values increase with distance up to 55% at 11.25 cm from the field edges [12].

A very recent Monte Carlo simulation study was performed for the early and middle periods of pregnancy, in order to estimate the fetus dose for breast cancer patients with 6MV, using

two stylized or mathematical phantoms in the first two trimesters of gestation [13]. The limitation of this study was that the mathematical phantoms made by Stabin et al. in 1995 relied on simple geometry objects that represented the pregnant patient. This work was the very first step towards creating a realistic phantom model reflecting patient anatomy. Hence, the results did not register any conflicts with the results TG-36 had reported. No research has been done on any obese pregnant patients who have undergone radiotherapy procedure during pregnancy.

## **1.2 PREVIOUS PREGNANT FEMALE MODELS AND THEIR LIMITATIONS**

The evolution of anatomical models for radiation dosimetry and radiation protection dosimetry began to be introduced between 1910 and the late 1960s [14-15]. These models also called phantoms come in different designs, sizes, and types, which serve different purposes and needs. Because it is difficult to measure the total dose received by the human body that is exposed to external and internal radiation, physicists have developed phantoms to simulate patient human bodies for the purposes of dose measurement. Computational anthropomorphic phantoms are classified as one of three types: stylized phantoms, voxelized phantoms, and hybrid phantoms [16].



## 1.2.1 MATHEMATICAL OR STYLIZED PHANTOMS

The first computational phantom was developed by the Oak Ridge National Laboratory (ORNL) in the 1950s. Mathematical-stylized phantoms represented anatomical structures which were defined by simple solid geometrical objects, such as spheres, cylinders, slabs, and cones to describe very generally the shape of organs' positions and the geometry of the human body [17]. Stabin et al. in 1995 introduced the first mathematical stylized human fetus model set for the end of each trimester. They adopted a female phantom from stylized family phantoms and added the developed stylized fetus phantom and placenta in order to create the first three stylized pregnant models for the end of each pregnancy trimester, for nuclear medicine applications [17]. In 2002, the International Commission of Radiation Protection, Publication 89 (ICRP-89) introduced the reference (or population average) human in its report ICRP-89. The report lists properties of different organs, tissues, etc. such as density, size, weight [18]. After ICRP 89 Publication was established in 2002, Chen et al., in 2004 extended the stylized pregnant female models by modifying the four stylized pregnant models with the new reference values of ICRP 89 Publication to represent four pregnant stylized model sets at different ages: 8 weeks, 3, 6, and 9 months [19]. In addition to the skeleton and soft tissues, which had been previously modeled by Stabin, Chen included the brain tissue in his models for ionizing dosimetry calculations [19]. With its basic building shapes and simple surface equations, this model is considered very simple and geometrically flexible. Thus, the model lacks appropriate information regarding accurate locations and overall shapes of organs to present a realistic human body [16].

## 1.2.2 VOXELIZED OR TOMOGRAPHY PHANTOMS

These phantoms were constructed during the 1980s to 2000s from whole-body computed tomography (CT) or magnetic resonance images (MRI) of humans. The radiological image data set contains two-dimensional (2D) slices of anatomic image sets. The three-dimensional (3D) voxel volume is calculated by multiplying the pixel size by the thickness of the image slice [20]. This realistic model has become promising only after advances in computer power and medical imaging technology had been made [16]. Voxel phantoms are composed of many small cubes, assembled to represent different anatomical structures in 3D voxels, where each voxel has a unique identification number that represents the tissue of interest [20]. Becker et al. segmented a 24 week of gestation fetus from an abdominal MR image of a patient and modified their already existing reference female voxel phantom Katja accordingly to create a virtual pregnant model for dose calculations [21].

A large number of voxels were segmented and classified to create organs and tissues of interest. Adult male and female models were created first and then extended to include pregnant phantom models. The reason for this was that CT scans are prohibited for pregnant patients and even if they exist, it would be difficult to find a full CT scan of a pregnant patient body. However, Shi and Xu's group developed the first human fetus model from a set of CT images during a life-saving procedure. The patient was discovered to be pregnant at 30 weeks, and the CT scan covered only a portion of her body starting from the upper liver to below the pubic symphysis [22]. This model represents a realistic individual specific model, and not a reference pregnant woman, mainly because the patient was larger than the average woman. Even though the anatomical details of the

voxel phantom model were enhanced compared to the stylized model, the resolution of the image slices was limited to 7 mm thickness, and since the scan did not cover the entire patient body, the model needed to be combined manually with another existing one. Another limitation of this study is that this model represents a patient-specific model rather than a reference pregnant woman, and the segmented fetal organs were limited to the fetal skeleton and soft tissues [22].

Cech et al. in 2007 also developed a pregnant female model named SILVY, which was derived from MR images (7 mm thick) of an 89-kg woman which is in a good agreement with the known weight of the pregnant patient at 30 weeks of pregnancy, who had a malformed fetus. The MR images of the fetus were replaced with the CT images of the 30-week fetus made available by Shi and Xu (2004). The SILVY model was used for only non-ionizing radiation and was limited to the uterus, the placenta, fetal soft tissue, and the skeleton to investigate the interaction of low frequency electric and magnetic fields in pregnant women primarily with the fetus [23]. Nagaoka et al. (2007) [24] in Japan developed a 26-week fetus model with high resolution for a 22-year-old volunteer pregnant woman, using magnetic resonance (MR) imaging of the abdominal region. The Japanese fetus model was used to calculate specific absorption rates of the human body when it is exposed to an electromagnetic field. The fetal organ model includes fetal body, brain, amniotic fluid, placenta, and urine wall. They also developed a pregnant model by combining this fetus model with the previous non-pregnant adult Japanese woman model [24-25]. Another set of voxel models of a pregnant female was developed by Angel et al. in 2008 [26], derived from CT images with a slice thickness resolution ranging from 1.25-10 mm, and used for ionization dosimetry, however, the fetus model was also limited to the fetal bone and soft tissue.

A very recent study showed the construction of a voxel-based phantom with twins at 25 and 35 weeks of gestation, who received positron emission tomography and computed tomography PET/CT scans. These models were patient-specific voxel phantoms to estimate the fetus and maternal absorbed dose that was received from radiation dosimetry, using Monte Carlo simulations. The results suggest that the fetal organ dose is based on the fetal position inside the womb [27].

### **1.2.3 HYBRID PHANTOMS**

The third generation of the computational phantom are hybrid phantoms invented by Xu et al. in the 2000s. The hybrid phantom model combined the voxelized phantom with the stylized phantom. In this model, organ boundaries and outer body contours are described by combinations of polygon mesh surfaces [15]. To highlight the advantages of the hybrid models over the stylized and voxel models, the voxel models were clear improvement compared to the stylized ones; however, regional defects and discontinuities are still evidently noticeable. The hybrid model has clearly enhanced upon the discontinuities generated from the original voxel model. Thus, it is certainly more realistic and represents a substantial improvement over the previous two models [16].

Since gathering body images of pregnant patients is not possible due to ethical reasons, hybrid phantoms were needed, which use 3D-surface modeling technologies. Xu's group released a set of pregnant models, with a fetus which was derived from CT-images of a 7-month pregnant patient. The fetus model was scaled to match the ICRP 89 recommended weights for three gestational ages: 3, 6, and 9-month. Although the maternal organs were highly detailed, as they

had been adopted from ICRP female phantom, the fetus segmentation was limited to the fetal brain, bones, soft tissues, and placenta [15]. Another study was conducted in France by Bibin et al. in 2010, who generated nine hybrid pregnant models at different gestational ages and positions, using ultrasound (US) and magnetic resonance images (MRI). Because of the MR image resolution thickness of 4mm, the MR images suffered from numerical artifacts such as tissue interferences, with the surfaces. Also, all fetus models were limited to a maximum of eight organ structures, based on their gestational ages. The limitations of this work were that the anatomical models of fetal tissue at different stages of pregnancy were not modeled in detail, leading to generate some artifacts. In addition, only two different fetal positions were addressed by a medical specialist [28].

Maynard et al. developed the University of Florida (UF) family of hybrid phantoms representing the human fetus at 8, 10, 15, 20, 25, 30, 35 and 38 weeks from MR and CT images. Although those models were highly detailed, representing most of the anatomical structures of the fetus at different ages, a scaling method was used to construct the target fetal ages for an average ICRP pregnant model [29]. A recent study in Iran in 2014 developed a 9-month pregnant hybrid phantom for nuclear medicine application. This model included twenty different fetal organs, segmented from MR and CT images at two different gestational ages. The fetus model which they developed was generated from the MR images of a 5-month-old fetus, and with CT images at 9 months of pregnancy. This fetus model was limited because it was produced with images from fetuses at different ages [30]. The same pregnant phantom model was also used to estimate the maternal and fetal dose assessment for diagnostic scans during pregnancy, using a Monte Carlo dose study [31].

Zaidi et al. [32] in Switzerland developed computational female and fetus models to study the radiation dose delivered to the embryo/fetus and to the pregnant patient during PET examinations for radiation risk assessment. A series of eight pregnant computational phantom series was developed in this study to cover the entire pregnancy period with 35 identified tissues included in this model. However, the models were constructed by modifying previous computational models and a scaling method was applied here, too. The models were used for radiation dose assessment for embryos/fetuses and pregnant patients from positron-emitting radiotracers [33]. In addition, a patient-specific computational phantom was also developed for dosimetry calculations, using a PET/CT scan of a patient pregnant with twins [34].

The average pregnant computational phantom [22, 33-35] was adapted and recommended by ICRP as the standard pregnant patient. However, no computational obese pregnant phantom has been developed yet, and this large segment of all pregnant patients has been entirely ignored. In addition, so far, very limited realistic fetus phantoms have been created for each gestational age to demonstrate the anatomical fetal development stages, as well as the fetal position and angle inside the uterus.

### **1.3 RADIATION EFFECTS ON THE FETUS**

The influence of ionizing radiation on the embryo or fetus during pregnancy can have a lethal effect on the fetus, primarily because of the large radiation doses received by the abdomen region in the early stages of pregnancy. In many cases, these doses lead to abortion. Ionizing radiation can also cause severe mental retardation (SMR) in the fetus, which has been extensively studied in Japanese atomic bomb survivors in Hiroshima and Nagasaki in 1945. These survivors are considered the primary source of documentation on SMR in utero. Other risks to the fetus following exposure are growth retardation, sterility, cancer induction, a genetic effect involving either heredity gene mutation to future offspring, or a somatic effect involving individuals who undergo the radiation. Some periods during pregnancy are highly sensitive to radiation, and irradiation during these times will increase some risks based on the dose-response relationship [5].

The threshold fetal dose is 100 mGy, equivalent to 100 mSv. A threshold dose below 100 mGy is considered safe for continuing a pregnancy. However, a dose above 100 mGy is considered as carrying a high risk of potentially harming the fetus and could result in birth defects. An informal possibility of terminating the pregnancy should be considered, upon individual agreement [36], [37]. During the early stages of pregnancy (between weeks 1 to 7), radiation exposure results in a loss of normal developmental cells, causing the death of the fetus. Thus, radiation exposure during the early stages of pregnancy can only cause an early abortion, not birth defects. If radiation occurs between weeks 8 to 25, then the central nervous system is damaged, and the result is fetal mental

retardation and IQ reduction [5,37].

Although it is impossible to avoid all radiation to the fetus during radiation therapy, shielding unexposed regions, such as the abdomen, with a lead-rubber apron can significantly reduce the radiation dose scatter, particularly between weeks 8 to 25. If the uterus is directly exposed to radiation, then the method of reducing the dose to the fetus is “as low as reasonably achievable” i.e. following the ALARA principle [4,37]. The effects of radiation on the fetus are not well understood and cannot be predicted with certainty; the severity and frequency of adverse deterministic effects increase with the total radiation dose, and the probability of their occurrence is directly dependent on the radiation dose. Stochastic effects are assumed to have no lower threshold for the incident because they are not limited to any threshold dose. Therefore, the reduction of the fetal dose to the necessary minimum is, of course, advisable in order to reduce the potential risks of stochastic effects on the fetus [5,37].

## **1.4 COMMON DIAGNOSTIC IMAGING PROCEDURES DURING PREGNANCY**

Identifying malignant lesions can confirm the presence of cancer [4]. Once cancer has been diagnosed, treatment of the disease is recommended in certain cases [37]. X-ray diagnostic imaging procedures must be estimated based on the ALARA principle. The patient should be informed about all the risks and benefits associated with the proceedings, and the patient must decide to continue or discontinue the examination. In case of a pregnancy, most of the radiological



examinations happen where the x-ray beam is not directed at the uterus or pelvis of the pregnant patient. Shielding protection of the mother's abdomen region is necessary to protect the fetus from radiation exposure [37]. The standard imaging modalities include ultrasound, digital mammography, magnetic resonance imaging (MRI), computed tomography (CT), and hybrid PET/CT [4].

Ultrasonography is considered the first and safest imaging modality with the least radiation exposure during pregnancy because it is inexpensive and safe for the fetus. Although some studies in mice have shown that ultrasound exposure could represent a biological risk to the fetal brain and decrease fetal birth weight [37-38]. The second image modality that has been used is MRI, which detects invasive cancers, such as breast cancer, during pregnancy without using iodine-based contrast in order to avoid it being delivered into the circulation of the fetus. MR Image is considered very safe and offers excellent image contrast, but it is costly to use; unlike ultrasound, no side effects have been observed in a study on mice which were exposed to MR in utero [39].

Another diagnostic imaging modality necessary in the clinic is CT imaging for pregnant patients who are suspected of suffering from a pulmonary embolism, acute appendicitis or trauma [26]. Because the radiation dose to the fetus cannot be measured directly, it is not well known what quantity of radiation the fetus receives during CT examinations [26]. Unfortunately, CT images, if they are made, are mostly obtained for the partial body, and are rarely available for pregnant patients [40]. Most of the existing images that are currently available were taken when the pregnancy was still unknown or in order to examine the health of the mother or of the fetus [41].

## 1.5 OBJECTIVE OF THIS RESEARCH

The goal of this project is to develop methods for accurately estimating the fetal dose. In order to achieve this aim, the hypothesis was made that developing a realistic computational fetus phantom model, derived from human pregnant patients, would significantly increase the accuracy of fetal dose estimations, and estimations made for other organs at risk. The next step is to combine an adult ICRP reference female computational model with the fetus models we have developed, in order to build computational obese pregnant model sets by taking into consideration all the factors that can contribute to the fetal dose. Such factors include the weight a patient has gained, patient body changes, fetal development, fetal position, and detailed anatomy of the fetus inside the patient's body, which can be accomplished using MR and/or CT of pregnant patients. US data have also been used, prior to or after MR image sets had been taken. This can reflect the detailed patient body, which can lead to designing realistic model sets that are specific to the standard pregnant computational phantom series and to the obese pregnant computational phantom series, so that the field of medical physics can rely on them in the future when estimations regarding the fetal dose are made in order to avoid any future cancer in the patient or in the fetus.

To successfully reach this goal, the following specific aims were identified:

1. Construct a realistic computational fetus phantom series at three target ages: 20, 31, 35 weeks of pregnancy. The process starts with segmenting the major fetal organs necessary for dose calculations, derived from radiological images for each target age. The next step is to import the radiation therapy structure (RT-Structure) created through

- segmentation into 3D-modeling software to develop computational fetus phantom models for each trimester. Then, the developed fetus phantoms are matched with the corresponding ICRP 89 Publication.
2. A realistic computational female phantom is constructed. This is achieved by using an adult ICRP reference female voxel model and convert it to a non-uniform rational basic spline (NURBS) surface model in order to construct a hybrid computational female phantom as a mother to the fetus created in step 1.
  3. In order to create a complete standard pregnant computational phantom set at 20, 30, and 35 weeks of pregnancy, the mother's internal female organs developed in step 2 are removed, and the fetus phantom developed in step 1 is added to the female pelvis, using 3D-modeling software.
  4. With the aid of radiological image sets which had originally been used to construct the fetus models, each fetus' position and rotation inside the uterus is adopted. Then, start remodeling and/or modifying the female internal organs with the maternal internal organs.
  5. A total of four overweight models are developed to include: one overweight female model, and three overweight pregnant female models at different gestation ages: 20, 31, and 35 weeks. These models are derived from an ICRP reference female created in step 2 and the whole pregnant female models created in step 4.
  6. Finally, four obese models are created which is the ultimate goal of this work: one obese female model and three obese pregnant models at three gestation periods: 20, 31

and 35 weeks. Both the overweight models and the obese models are created by adding different amounts of fat layers underneath the skin.

## **CHAPTER TWO: HYBRID COMPUTATIONAL FETUS PHANTOM CONSTRUCTIONS**

This chapter describes the efforts taken to develop a hybrid computational fetus phantom set based on research aim number one: Construct realistic computational fetus phantom series at three target ages: 20, 31, 35 weeks of pregnancy. The process starts with segmenting the major fetal organs necessary for dose calculations derived, from radiological images for each target age. The next step is to input the radiation therapy structure (RT-Structure) created through segmentation into 3D-modeling software to develop computational fetus phantom models for each trimester. Then, the developed fetus phantoms are matched with the corresponding ICRP 89 Publication. The development of the computational fetus phantom set was an important and essential step toward developing the pregnant phantom model set.

### **2.1 TARGET FETAL AGES**

A total of three fetal ages, 20, 31, and 35 weeks post-conception (PC) were chosen to represent the anatomical development of fetal organs in the second and third trimester. Since the pregnant patient does not typically undergo X-ray or CT imaging during the first trimester, there was a limited number of image sets available. During the first trimester, almost all the image sets were of poor quality, where the fetal anatomical organs were not clearly visible. The International Commission of Radiation Protection Task Group 89 (ICRP-89) [18] has provided anatomical and physiological reference data which are to be used as radiological protection reference values. The

ICRP 89 Publication has also categorized the fetal ages per week as follows: the first trimester goes from 1 week to 13 weeks; the second trimester represents the period from 13 weeks to 25 weeks, and the third trimester stretches from 26 to 38 weeks. Consequently, our target models at 20, 31, and 35 weeks mostly represent the middle period of the second and third trimester [18]. A total of eleven MR and CT image sets were used for this study to develop a hybrid computational fetus phantom model for each gestational period.

## **2.2 IMAGE ACQUISITION**

For ethical reasons, pregnant patients are not typically recommended to undergo x-ray or CT-examinations during the first trimester, except for a few cases when the pregnancy is unknown, the mother's life is in danger, or there is a suspicion that the fetus may have a birth defect. For this study, the radiological images of the pregnant patients were obtained from Vidant Medical Center hospital in Greenville, North Carolina. The acquired images were anonymized from the archive under an approved (IRB) protocol. All radiological images were also screened by an obstetrics and gynecology (OBGYN) specialist to address any physical abnormalities the fetus may have and the question of whether the images cover the entire fetus before segmentation. Both MR and CT image sets were used for this study. The MR and CT images covered most of the patient's abdomen, starting from the patient's chest to below the patient's cervix. The MR scans were acquired with a 1.5T static field strength, performed on a Signa HDxt manufacture model (GE Medical Systems).

Independent sagittal, axial, and coronal T2-weighted scans were performed with parameters. Typical acquisition parameters were a flip angle of 90 degree, a field of view (FOV) of 480, a slice thickness/gap of 2/1.3 mm, a matrix of 512×512 pixels, and voxel sizes (2 mm<sup>3</sup>). The CT parameters used in this study were a tube voltage of 120 kVp, matrix size 512x512 pixels, a slice thickness of 2.5 mm, a pixel spacing of 0.985/0.985 mm, performed on a LightSpeed VCT model, GE Medical System.

## **2.3 IMAGE SEGMENTATION**

Three computational phantoms were constructed, starting from anonymized high-quality MR images, to build a complete, anatomically accurate fetus, gravid uterus, and placenta. Image segmentation is an essential step to obtain a three-dimensional (3D) model of fetal anatomy. It was performed to isolate and define the necessary organs and structures for organ dose calculations based on the definition of effective doses in ICRP Publication 60 [42]. The segmentation of MR image sets was performed on a clinical contouring tool, using the Velocity 3.1 Treatment Planning System (TPS) (Varian Medical Systems, Palo Alto, CA). The original MR images, including the sagittal, axial, and coronal views in Digital Imaging and Communications in Medicine (DICOM) format, were directly imported into Velocity TPS, which provides powerful segmentation tools with a highly interactive interface. A 3D-image viewer such as this is a helpful tool for checking the overall segmentation while contouring the images. Velocity TPS software is a clinical contouring tool which imports and exports images in DICOM format.

All the original MR images, including the sagittal, axial, and coronal views were in DICOM format and were directly imported into the Velocity TPS software. The anatomical structures of interest were contoured slice by slice and were segmented manually; no automatic segmentation was applied to any of the images as shown in Figure 2.1. Manual segmentation was primarily based on the author’s knowledge of human anatomy and was supplemented by fetal anatomical manuals [43-44]. Finally, to confirm the proper organ segmentations, locations, and overall shape, all organ and tissue segmentation results were verified by Keith H. Nelson, MD, a primary specialist in OBGYN at East Carolina University, Greenville, NC.

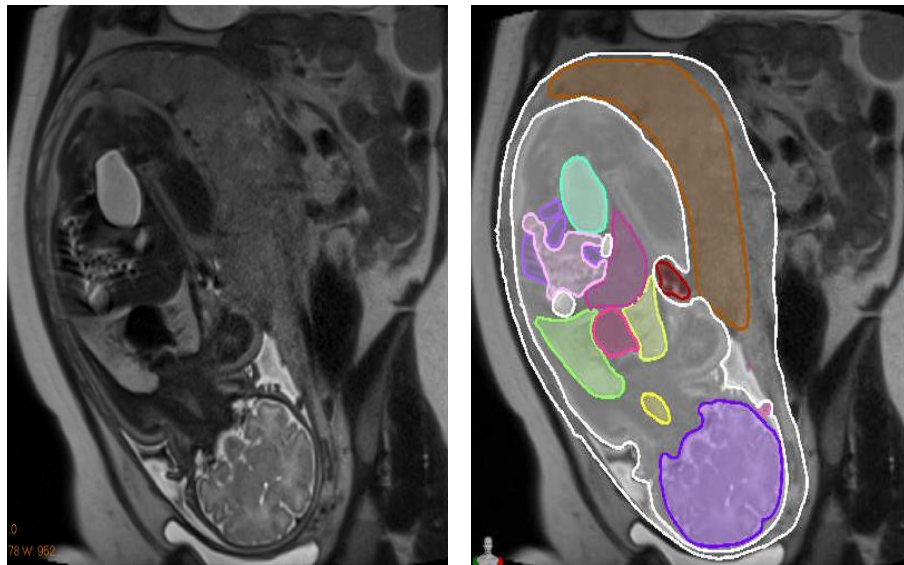


**Figure 2.1** Sample of an MR coronal image of a 35-week pregnant female. (a) Original MR slice, (b) The same MR slice segmented, in “seen” view 3D mode, using the Velocity Software (TPS).



A total of 29 fetal anatomical tissue and organ structures were identified as follows: uterus, placenta, umbilical cord, fetal body, amniotic fluid, brain, eyes, tooth buds, tongue, pituitary gland, trachea, bronchus, liver, heart, esophagus, lungs, stomach, small intestine, large intestine, kidneys, pancreas, spleen, thymus, thyroid gland, urinary bladder, adrenal glands, spine, spinal cord, and gallbladder. However, some fetal organs were difficult to segment at 20 weeks: because the thyroid and adrenals could not be confidently identified at 20 weeks, models were created and added, based on their accurate location [24-25].

Because of the overall small fetal skeleton tissue size, all skeletal tissue was segmented from CT images as a homogeneous mixture of skull, ribs, vertebrae, and femur bones. The accuracy of the fetal skeletons was carefully confirmed with an OBGYN specialist. Figure 2.2 compares an original CT slice with the same slice after it has been segmented and classified. In order to create a 3D model, the entire segmentation was carried out in sagittal view, axial view, and coronal view. The segmentations were verified, using “Sense,” a built-in 3D visualization model provided by Velocity software as shown in Figure 2.3. All segmentations were subsequently confirmed by an OBGYN specialist for further verification. Once all the necessary segmentation had been completed and approved, all the organ contours in the MR images were exported into RT-STRUCTURE which is a separated DICOM file format that stores the segmented contours by Velocity TPS software.

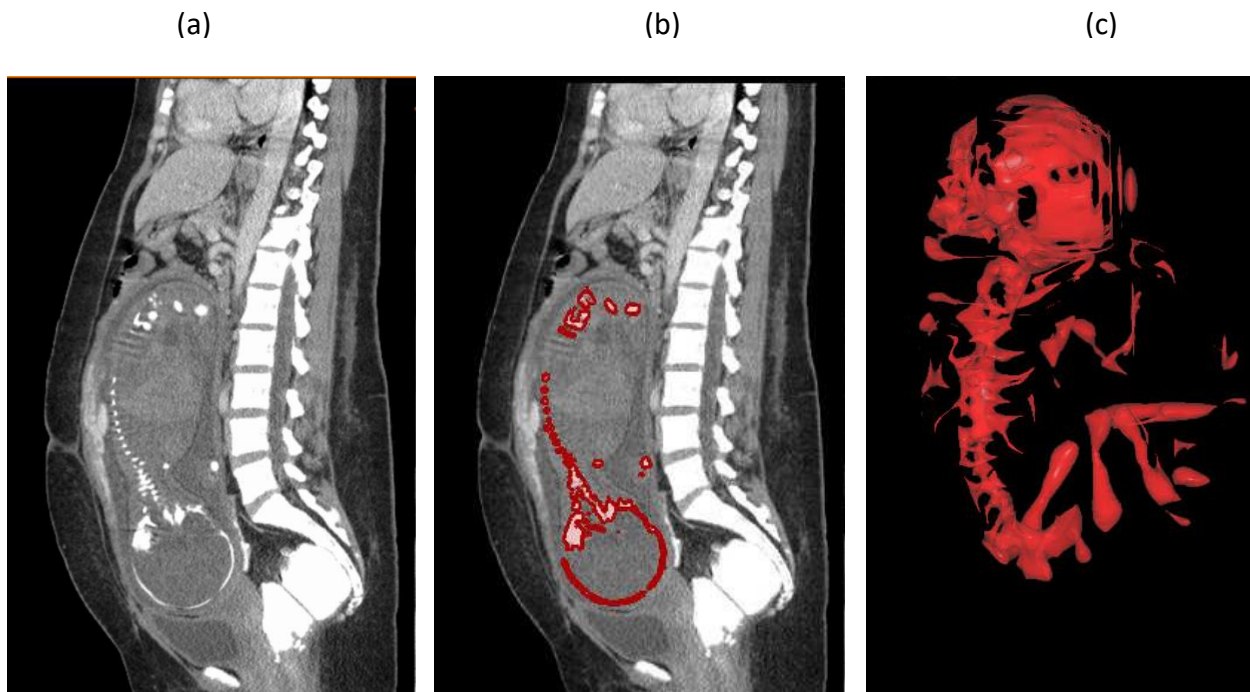


**Figure 2.2** Representative CT, the sagittal image of 30-weeks and 3-dimension pregnant female: (a) Original CT slice, (b) Segmentation result of the original CT image, (c) 3D model in “seen” view mode, using Velocity Software (TPS).

## 2.4 CONVERSION TO 3D MODELING FILE FORMAT

Once all the necessary organs had been successfully identified and completed, the exported RT-STRUCTURE in DICOM file format was automatically generated from Velocity software. To create a 3D polygon mesh representation, a 3D Slicer software (3DSlicer 4.6) was used to export the RT-STRUCTURE in DICOM format into either a simple Standard Triangular Language (STL) or to convert it into a more complex format, called Wavefront Object (OBJ). Almost all the organs were successfully exported into Wavefront object format, so it was possible to preserve more information for each polygon mesh of the 3D object and to represent it as a mesh file in order to smoothen the NURBS surfaces for later modification. In addition, the OBJ file format preserves the position, texture, color, dimension, and identity information of the segmented tissue, which are easily imported into the 3D modeling software package. To check if the imported segmented organs from the 3D-Slicer had preserved the same organ volumes, all the contoured organ volumes were measured in Velocity software as well as being measured at another time later in the process, after they had been imported to Rhinoceros<sup>TM</sup> (McNeel North America, Seattle, WA, Version 5.0) software. The percentage differences were less than 5% for all organs, which proves that the measured volumes generated by Velocity software were almost the same as the segments imported into 3D modeling software.

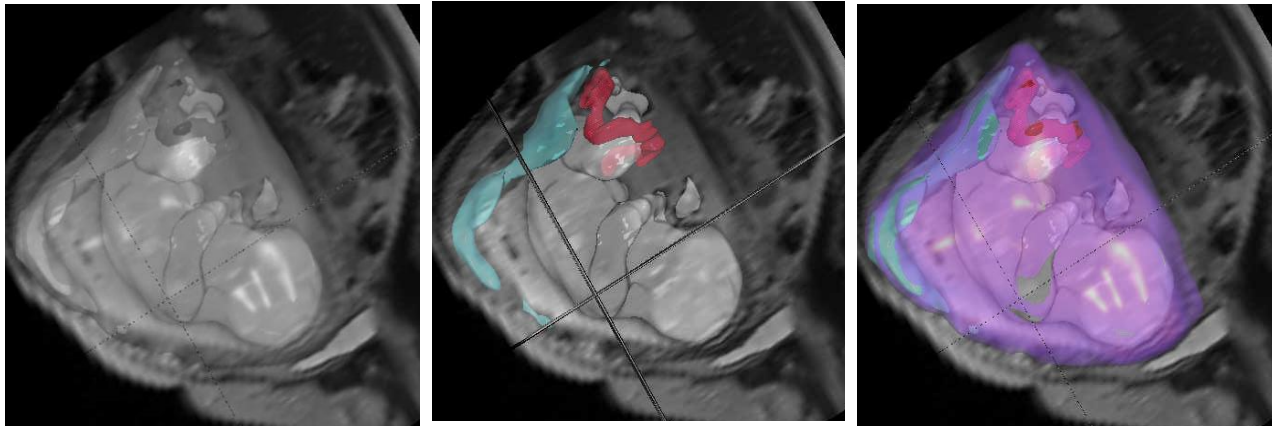


**Figure 2.3 Illustration of the 3D-model, using Velocity software (TPS) MR coronal image segmentation of a 31-weeks pregnant female (a) Original, unsegmented slice (b) Segmented placenta and umbilical cord (c) Segmented placenta, umbilical cord, and uterus.**

## **2.5 NURBS AND POLYGON MESH MODELING**

The polygon mesh representation of the Wavefront object of the MR image set was directly imported into Rhinoceros<sup>TM</sup> (McNeel North America, Seattle, WA, Version 5.0). Rhinoceros software offers many useful 3D-tools for geometrical manipulation, such as deformation, fitting, scaling, volume checking, and editing tools, as well as other 3D-surface-rendering options. These tools were used to create a non-uniform rational basis spline (NURBS) surface and a polygon mesh model for each organ structure. The NURBS surface model for each fetal organ tissue was manually created, using both the contouring and the lofting commands [15,45]. The contour command was used to create a spaced series of planar curves around the outer shape of a given

polygon mesh organ, along with the user-defined axis. The loft command was used to fit a surface through created profile curves. The created curves define the original organ surface shape from the contouring command, wrapping NURBS surfaces around the specified organ volume. The original polygon mesh is no longer needed, after creating NURBS surfaces for all organs. Some other modification tools, such as rebuilding and smoothing commands, were necessary for complex NURBS objects. A complete example of the NURBS surface process for the placenta, eyes, and liver are shown in Figure 2.4, Figure 2.5. The following organs were modeled in NURBS surfaces: brain, gall bladder, heart, kidneys, liver, lungs, pancreas, spleen, stomach, thymus, trachea, urinary bladder, uterus, and placenta. The fetal body, skeleton (from CT images), umbilical cord, tongue, tooth buds, as well as the small and large intestines, were kept in their original polygon mesh. Eyes and lenses were replaced with spherical and ellipsoid objects, whose shapes match the initially segmented organs. Finally, all organs were confirmed by an OBGYN specialist to check their proper position, particularly of the organs which had been added later.

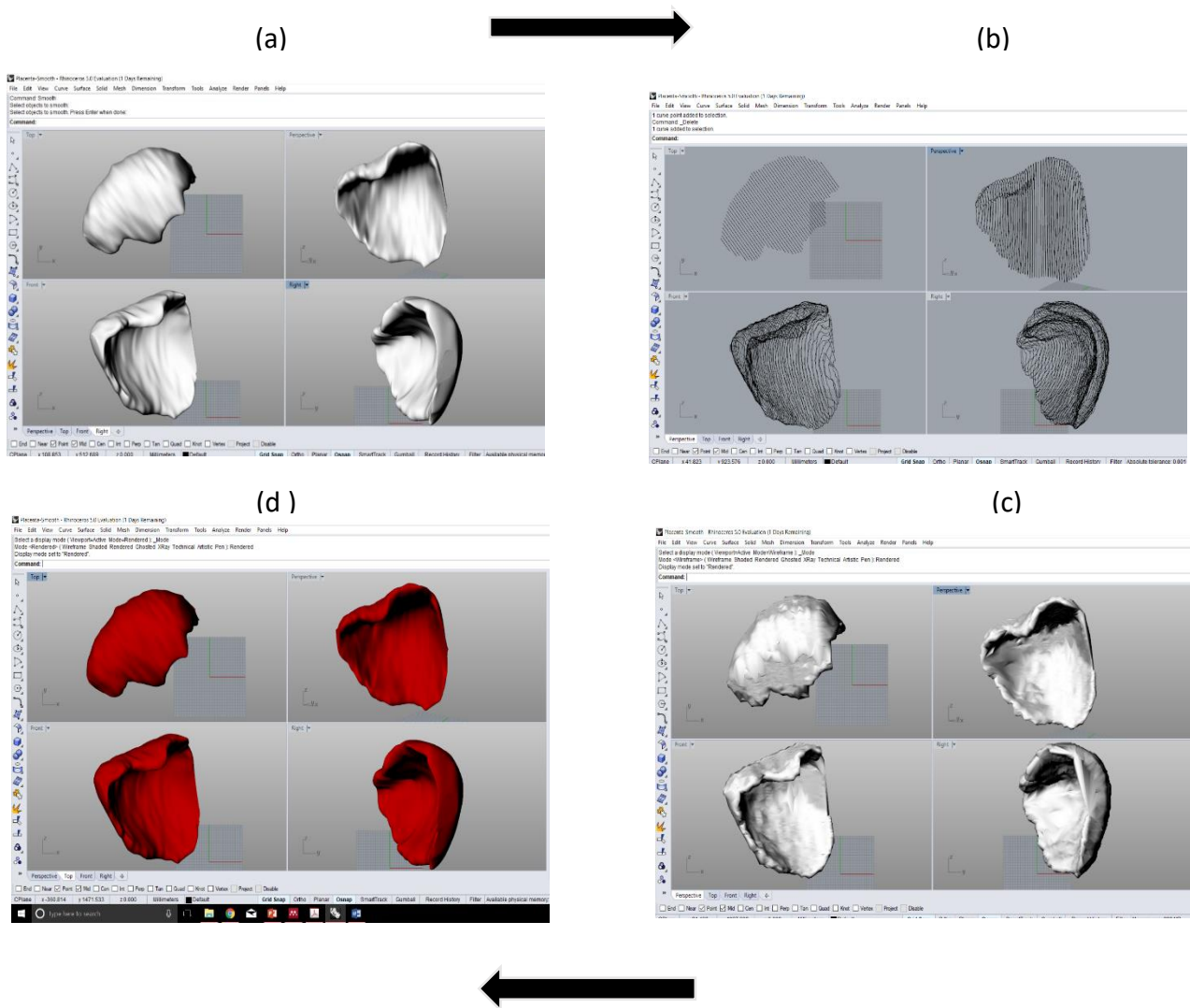


**Figure 2.4** An example of extracting the placenta in different steps: (a) The original triangle mesh of the placenta model extracted from a 2D MR image. (b) The extracted contours of the original model. (c) The 3D NURBS surface representation of the placenta model. (d) The 3D NURBS surface representation after adding the surface color feature.

## 2.6 MATCHING WITH ICRP PUBLICATION 89

The organ masses of the fetus phantoms were modified to match the size of the organs so that there would be better agreement with the reference data for organs in ICRP 89 publication [18]. ICRP Publication 89 from 2002 contains the most comprehensive data available from men, women, embryos, and fetuses from both Europe and North America. ICRP 89 Publication provides reference values for basic anatomical and physiological data in the development of the embryo and fetal organs as a function of age, for use in radiological protection. This publication provides data such as fetal dimensions, mass, body composition, and surface area for each fetal tissue per gestational week.

Since the computational phantoms are volume-based, mass densities were essential in order to be able to convert organ volumes to their organ masses. Reference masses for each trimester for each organ were derived directly from data presented in ICRP Publication 89 or from recent publications on fetuses [22,29]. Modifying the organs of interest in order to make the fetus phantoms of individuals more accurate and so that they matched the reference values for the 50th percentile required more work, using the 3D scaling command in Rhino to adjust the organ volumes of interest to the desired reference volumes, with a tolerance value of less than 1%, the scaling method was accomplished for the entire fetus at once. Transform commands in Rhinoceros were used to adjust the organ and tissue volumes to match reference volumes. As a final step, the complete internal anatomy of all fetus phantoms and the pregnant female was reviewed for accuracy by a clinical OBGYN obstetrician and suggested corrections were implemented as

needed. The 3D mesh fetus models as well as the fetal skin at 20, 31, and 35 weeks were later obtained during the voxelization step in the next section.

## **2.7 RESULTS**

The comparison between the constructed 3D NURBS surface and its original mesh model, using Rhinoceros 3D modeling software, is summarized in Figure 2.5. A complete example of the NURBS surface process for the brain, eyes, and liver are shown in Figure 2.5. The developed hybrid computational fetus phantom sets are presented in Figure 2.6, which contains a snapshot of the 20-, 31-, and 35-week uterus and fetus inside the mother's abdomen. The fetal organ masses and densities are shown in Table 2.1. All fetal volume masses were matched within 1% of their average reference data, provided in ICRP 89 Publication, as shown in Table 2.2.

### **2.7.1 COMPARING FETAL ORGAN MASSES WITH ICRP RECOMMENDATION**

The complete organ masses and densities of fetus phantoms at 20, 31, and 35 weeks of gestation were compared with ICRP 89 Publication reference masses [18], as shown in Table 2.1. Because the computational phantoms are volume-based, mass densities were required to convert between organ volumes and organ masses. The mass reported in Table 2.1 was obtained directly



from Rhinoceros<sup>TM</sup>; great care was taken to keep NURBS surfaces or mesh polygon volumes with the same original organ volumes that were obtained from the Radiation Therapy DICOM-structure file (RT Structure). To represent a realistic fetus model for each gestational stage, the organ volume masses obtained initially from organ segmentation in TPS match within 1% the organ volumes developed in Rhinoceros. To preserve the real organ shape and location, file formats were converted in 3D modeling file format. Fetal soft tissue densities and masses were taken from ICRP 89 Publication [18] and ICRU 46 Report [46]. The percentage differences between developed fetal mass and average fetal mass reported in ICRP 89 Publication about the 50<sup>th</sup> percentile were also reported in Table 2.2.

**Table 2.1 Three case studies of calculated fetal organ masses, compared with the provided ICRP reference data.**

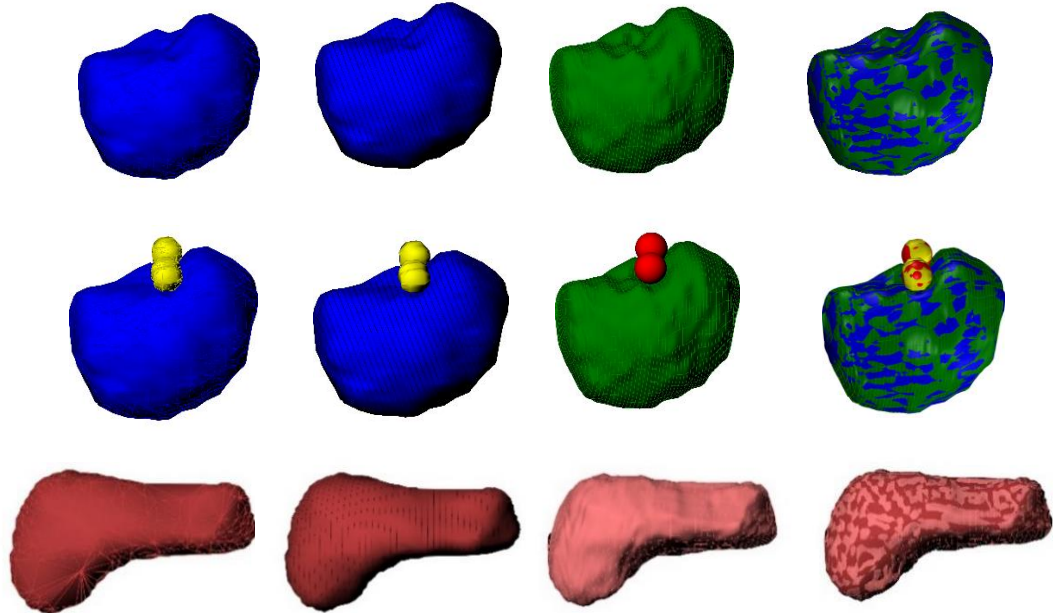
Fetus Organs	Density (g/cm <sup>3</sup> )	This Work Volume (cm <sup>3</sup> )			This Work Mass (g)			ICRP-89 Reference Mass (g)			Percentage Error			Scaling Factor		
		20-w	31-w	35-w	20-w	31-w	35-w	20-w	31-w	35-w	20-w	31-w	35-w	20-w	31-w	35-w
Adrenal glands	1.03	0.95	3.08	4.41	0.98	3.10	4.54	0.98	3.00	4.60	0.17	3.33	1.23	1.00	0.99	1.00
Amniotic fluid	1.00	542.60	4236.88	3554.54	542.60	4236.88	2186.15	350.00	750.00	725.00	55.03	464.92	201.54	0.86	0.56	0.69
Brain	1.03	72.31	339.38	343.00	74.48	349.56	353.29	62.00	213.57	300.00	20.13	63.67	17.76	0.94	0.85	0.95
Bronchi	1.07	0.04	0.13	0.34	0.04	0.14	0.37	-	-	-	-	-	-	-	-	-
Eyes	1.03	1.87	6.28	9.60	1.93	6.47	9.89	-	-	-	-	-	-	-	-	-
Eye Lenses	1.07	0.40	0.90	1.02	0.43	0.96	1.09	-	-	-	-	-	-	-	-	-
Fetal body	1.03	355.13	1767.00	2443.00	365.78	1820.01	2516.29	300.00	1500.00	2800.00	21.93	21.33	10.13	0.94	0.94	1.04
Gallbladder	1.03	0.62	1.02	1.23	0.64	1.05	1.27	-	-	-	-	-	-	-	-	-
Heart	1.04	4.45	21.92	29.50	4.63	22.80	30.68	3.00	10.57	15.00	54.27	115.64	104.53	0.87	0.77	0.79
Intestines	1.03	16.60	71.00	68.00	17.10	73.13	70.04	-	-	-	-	-	-	-	-	-
Kidneys	1.03	2.85	26.10	21.70	2.94	26.88	22.35	3.80	13.88	20.00	22.75	93.65	11.76	1.09	0.80	0.96
Liver	1.04	13.76	94.60	122.42	14.31	98.38	127.32	19.00	67.28	100.00	24.69	46.23	27.32	1.10	0.88	0.92
Lungs	1.04	21.84	62.41	107.10	22.71	64.91	111.38	15.00	40.58	51.00	51.42	59.95	118.40	0.87	0.86	0.77
Nasal Septum	1.03	0.23	0.77	0.29	0.24	0.79	0.30	-	-	-	-	-	-	-	-	-
Pancreas	1.03	2.24	3.92	4.39	2.31	4.03	4.53	2.30	4.06	4.50	0.31	0.63	0.57	1.00	1.00	1.00
Pituitary gland	1.03	0.05	0.07	0.08	0.05	0.07	0.08	-	-	-	-	-	-	-	-	-
Placenta (Mother)	1.04	98.58	1361.00	550.90	102.52	1415.44	572.94	170.00	459.18	565.00	39.69	208.25	1.40	1.18	0.69	1.00
Spinal Cord	1.02	2.33	1.71	1.81	2.38	1.74	1.86	-	-	-	-	-	-	-	-	-
Spine	1.03	8.04	12.20	19.61	8.28	12.57	20.20	-	-	-	-	-	-	-	-	-
Spleen	1.04	0.34	1.07	3.01	0.36	1.11	3.13	0.36	2.88	5.80	1.29	61.33	45.97	1.00	1.37	1.23
Stomach	1.00	3.78	6.03	12.20	3.78	6.03	12.20	-	-	-	-	-	-	-	-	-
Tongue	1.05	0.75	3.40	4.28	0.79	3.57	4.49	-	-	-	-	-	-	-	-	-
Tooth Buds	1.22	0.79	4.09	6.13	0.97	4.99	7.48	-	-	-	-	-	-	-	-	-
Trachea	1.07	0.77	2.07	5.64	0.82	2.22	6.03	-	-	-	-	-	-	-	-	-
Thymus	1.07	1.36	4.20	3.28	1.46	4.49	3.51	1.50	6.19	9.70	2.99	27.44	63.82	1.01	1.11	1.40
Thyroid Gland	1.05	0.17	0.60	0.95	0.18	0.63	1.00	0.18	0.67	1.00	0.62	6.36	0.25	1.00	1.02	1.00
Umbilical cord	1.04	21.33	73.60	127.00	22.18	76.54	132.08	-	-	-	-	-	-	-	-	-
Urinary Bladder	1.01	1.52	8.29	19.90	1.54	8.37	20.10	-	-	-	-	-	-	-	-	-
Uterus (Mother)	1.03	1003.00	7329.00	5148.00	1033.09	7548.87	5407.46	430.00	683.30	950.00	140.25	1004.77	469.21	0.75	0.45	0.56

**Table 2.2 Fetal organ mass densities, matching ICRP reference data.**

Fetus Organs	Density (g/cm3)	This Work Volume (cm3)			This Work Mass (g)			ICRP-89 Reference Mass (g)			Percentage Differences			Scaling Factor		
		20-w	31-w	35-w	20-w	31-w	35-w	20-w	31-w	35-w	20-w	31-w	35-w	20-w	31-w	35-w
Adrenals (2)	1.03	0.83	2.92	4.41	0.98	3.01	4.19	0.98	3.00	4.60	0.17	0.28	8.91	1.00	1.00	1.03
Amniotic Fluid	1.00	542.60	4236.88	3554.54	517.17	2671.77	2512.69	350.00	750.00	725.00	200.00	200.00	200.00			
Brain	1.03	60.48	207.58	288.83	62.29	213.80	297.50	62.00	213.57	300.00	0.47	0.11	0.84	1.00	1.00	1.00
Bronchi	1.07	0.03	0.13	0.36	0.03	0.14	0.39	-	-	-	-	-	-	-	-	-
Eye Balls	1.03	1.94	6.37	9.60	2.00	6.57	9.89	-	-	-	-	-	-	-	-	-
Eye Lenses	1.07	0.04	0.09	0.10	0.04	0.10	0.11	-	-	-	-	-	-	-	-	-
Fetus body	1.03	360.00	1740.00	2552.00	370.80	1792.20	2628.56	300.00	1500.00	2800.00	21.11	17.75	6.32	0.93	0.94	1.02
Gall Bladder	1.03	0.18	0.52	2.53	0.19	0.53	2.61	-	-	-	-	-	-	-	-	-
Heart	1.04	2.87	10.06	14.35	2.98	10.46	14.92	3.00	10.57	15.00	0.51	1.06	0.53	1.00	1.00	1.00
Small Intestine	1.03	2.18	11.42	45.44	2.24	11.77	46.81	-	-	-	-	-	-	-	-	-
Large Intestine	1.03	0.76	2.27	46.63	0.78	2.34	48.03	-	-	-	-	-	-	-	-	-
Kidneys (2)	1.03	3.72	13.57	19.38	3.83	13.98	19.96	3.80	13.88	20.00	0.69	0.67	0.19	1.00	1.00	1.00
Liver	1.04	18.20	63.91	96.46	18.92	66.47	100.32	19.00	67.28	100.00	0.40	1.20	0.32	1.00	1.00	1.00
Lungs (2)	1.04	14.39	38.77	48.38	14.97	40.32	50.32	15.00	40.58	51.00	0.23	0.64	1.35	1.00	1.00	1.00
Nasal Septum	1.03	0.02	0.58	0.27	0.03	0.60	0.28									
Pancreas	1.03	2.24	3.92	4.40	2.31	4.03	4.54	2.30	4.06	4.50	0.38	0.61	0.81	1.00	1.00	1.00
Pituitary gland	1.03	0.05	0.07	0.08	0.05	0.07	0.08	-	-	-	-	-	-	-	-	-
Placenta (Mother)	1.04	112.50	442.00	550.92	117.00	459.68	572.96	170.00	459.18	565.00	36.93	0.11	1.40	1.13	1.00	1.00
Spinal Cord	1.02	0.00	1.27	1.13	0.00	1.30	1.15	-	-	-	-	-	-	-	-	-
Spin	1.03	0.78	8.93	16.50	0.80	9.20	17.00	-	-	-	-	-	-	-	-	-
Spleen	1.04	0.34	2.77	5.53	0.36	2.88	5.75	0.36	2.88	5.80	1.29	0.03	0.85	1.00	1.00	1.00
Stomach	1.00	0.65	1.96	24.89	0.65	1.96	24.89	-	-	-	-	-	-	-	-	-
Tongue	1.05	0.33	2.85	2.84	0.34	2.99	2.99	-	-	-	-	-	-	-	-	-
Tooth Buds	1.22	0.20	2.48	5.37	0.24	3.02	6.55	-	-	-	-	-	-	-	-	-
Trachea	1.07	0.08	0.35	0.36	0.09	0.37	0.39	-	-	-	-	-	-	-	-	-
Thymus	1.07	1.40	5.80	8.98	1.50	6.21	9.61	1.50	6.19	9.70	0.06	0.24	0.95	1.00	1.00	1.00
Thyroid Gland	1.05	0.17	0.63	0.96	0.18	0.66	1.01	0.18	0.67	1.00	0.33	1.19	0.90	1.00	1.00	1.00
Ovaries (Mother)	1.03	1069.00	10.48	10.48		10.79	10.79									
Umbilical cord	1.04	15.51	26.50	29.68	16.13	27.56	30.87	-	-	-	-	-	-	-	-	-
Urinary Bladder	1.01	0.37	1.12	10.48	1.54	8.37	20.10	-	-	-	-	-	-	-	-	-
Uterus (Mother)	1.03	991.36	4807.00	5469.42	1021.10	4951.21	5745.08	430.00	683.30	950.00	81.47	151.49	143.24	0.75	0.52	0.55

## **2.7.2 FETAL POSITION IN UTERO**

The position or orientation of the fetus in the mother's uterus has not been clearly described in the literature on radiation dosage. The fetus is actively mobile throughout the pregnancy with a gradually increasing probability of being encountered in head-down presentation, as the pregnancy progresses to term. The described hybrid computational phantoms were adjusted to reflect the original fetal position inside the uterus in order to accurately estimate the radiation dose. In this work, all three models the 20-, 31-, as well as the 35-gestational week model were positioned head down.



(a) Segmented      (b) Contoured      (c) NURB      (d) NURBS vs. Original Mesh

**Figure 2.5** An example of the 31-week fetus model development, in this case, of the brain, eyes, and liver. (a) The original triangle mesh model extracted from 2D MR imaging. (b) The extracted contours from the original mesh model. (c) The completed 3D non-uniform rational basis spline (NURBS) surface, constructed from the original mesh polygons. (d) A comparison between the constructed 3D NURBS surface and the original mesh model.

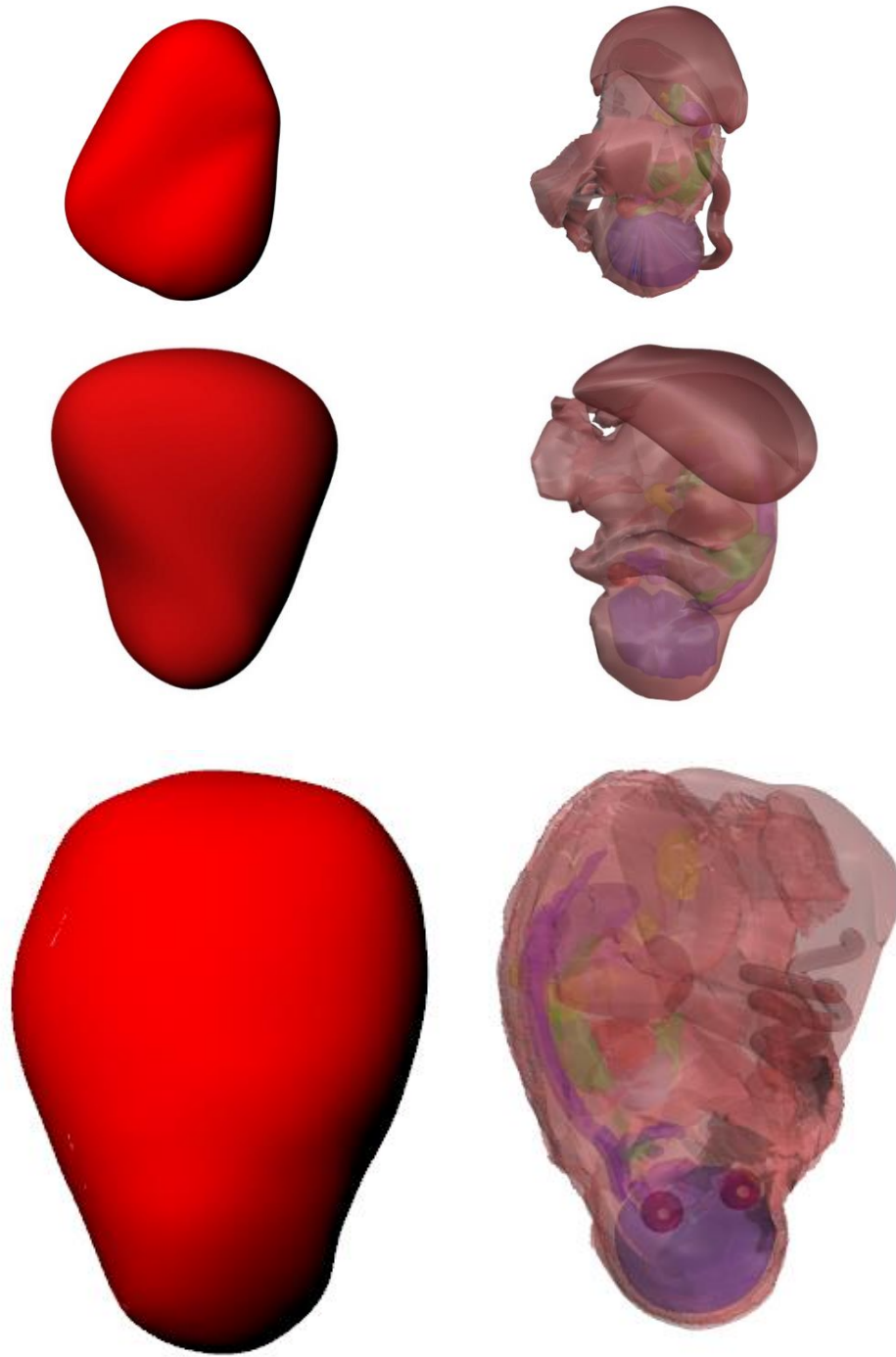


**Figure 2.6 A snapshot of the 20-, 31-, and 35-week uterus with the fetus inside it.**

## 2.8 DISCUSSION

In this study, three hybrid fetus phantom models were constructed, representing fetuses at 20, 31, and 35 weeks. Each fetus model contains 27 different organs and tissues, as presented in Figure 2.6 and Figure 2.7. These hybrid fetus models have many advantages, as they offer the flexibility of maintaining the original mesh shapes and the anatomical realism of the real medical image sets used for each model. The fetus phantoms which were built in this study include NURBS and polygon meshes, which can be used for the evaluations of fetal doses in radiological protection, medical imaging, and radiological therapy, where hybrid fetus phantoms are needed.

For each fetus phantom, the original, natural position of the fetus in the maternal uterus was carefully adopted. While both the 20- and 35-week fetus models were in right occiput posterior (ROP) configurations, the 31-week fetus model was in a left occiput anterior (LOA) presentation, surrounded by the maternal tissues, including the placenta and uterus. A complete list of fetal organ volumes and masses is presented in Table 2.1. Percentage differences between the finished hybrid fetus phantom models and ICRP reference data are listed in Table 2.2. Ultrasound (US) data taken nine days before the MR images were acquired indicated that the 20-week fetus was in the 60<sup>th</sup> percentile for overall fetal growth, with a total mass of 353 grams. US data of the 31-week fetus, recorded two days after MR images had been taken, also indicates that the fetal weight was larger than the typical fetus, with a total mass of 2,223 grams, placing the fetus in the 75<sup>th</sup> percentile for overall growth. While the 20- and 31-week fetuses were larger than the typical fetus, US data records of 35 weeks, taken nine days after MR images were acquired, indicate a total fetal mass of

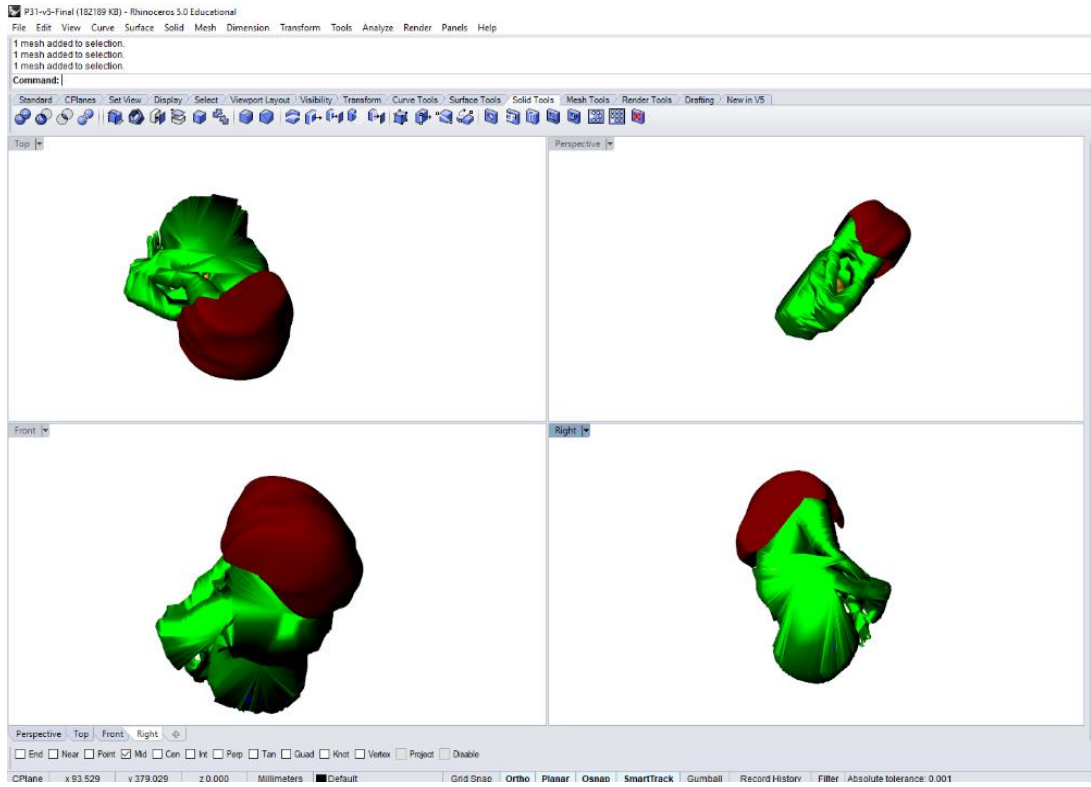
2,630 grams, which is in the 45<sup>th</sup> percentile of overall weight. This variation in data mass explains the change in data mass reported in Table 2.2. These hybrid fetus models have many advantages that make them suitable for various applications since they offer the flexibility to maintain the original mesh shapes and the anatomic accuracy by using real medical image sets for each model. Fetus position and orientation can be adjusted easily as shown in the front view head down orientations for all three models in Figure 2.6.

All three fetal phantom models are based on patient-specific MR images and illustrate a wide variety of organ sizes and exact positions, away from the standardized mean. The existing ICRP-89 reference phantoms represent the population average and are designed for systematic epidemiological studies with normalized data to provide recommendations for the general public. However, diagnostic imaging or radiation treatment planning requires patient-specific data for accurate dosimetry and risk assessment. Especially the heavy weight and obese cases will help to better understand limitations and uncertainties associated with these tasks when these fetal models are combined with standard, heavy weight or obese pregnant female phantom models available in the literature.

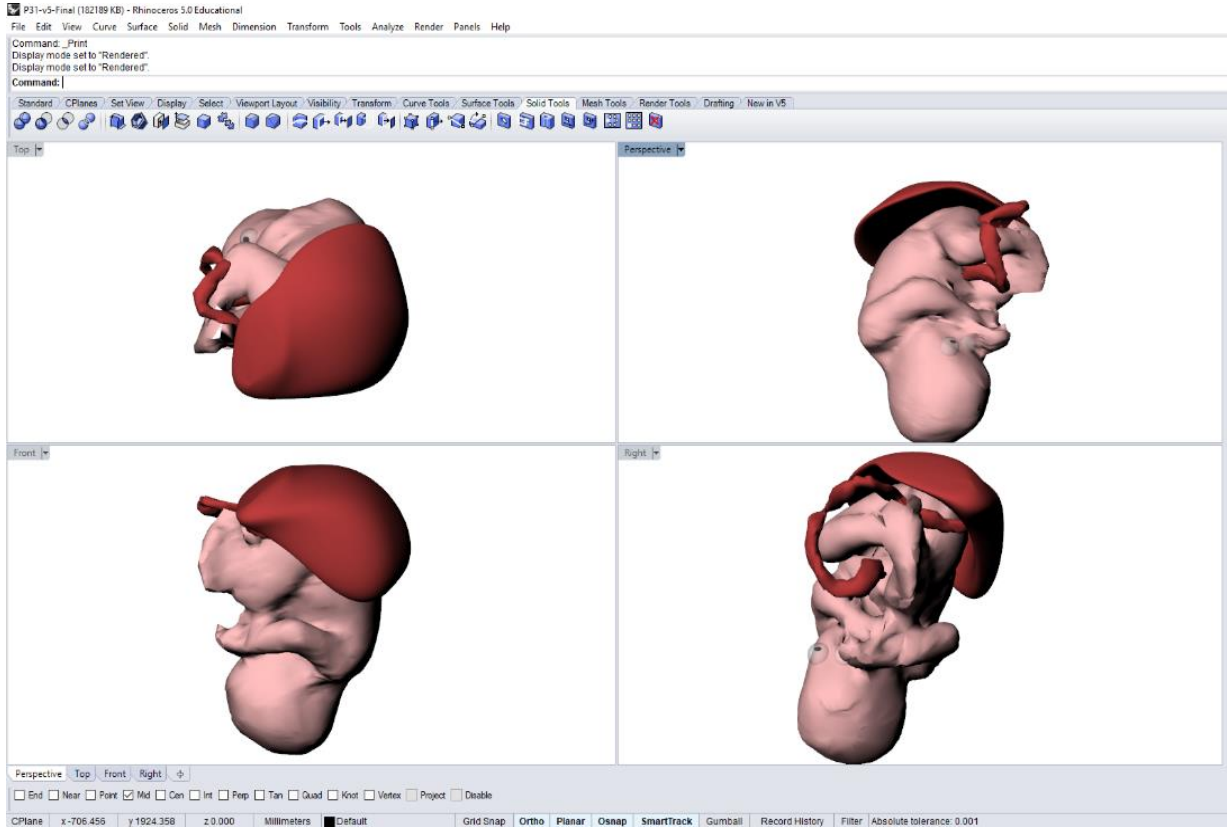
The fetus phantoms in this work including the NURBS and polygon meshes can be used for future evaluations of the radiation dose and radiation risk to the fetus and fetus organs in radiation protection, medical imaging, and radiation therapy in conjunction with Monte Carlo radiation transport simulations. Hybrid phantoms, including the hybrid fetus phantoms, are used to provide average and extreme geometries for radiation transport calculations. This will allow for better estimate mean doses including uncertainties, and more realistic risks.



(a) P20-Week



(b) P31-Week



(c) P35-Week

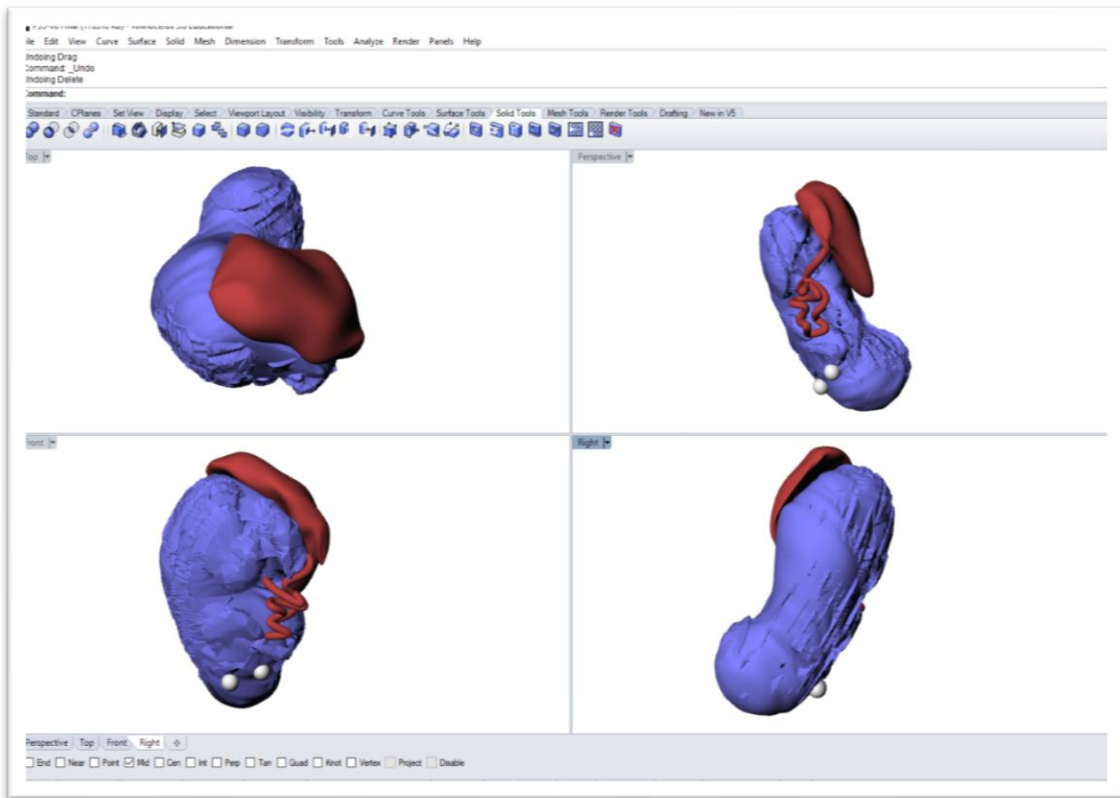


**Figure 2.7 A Snapshot of the 20- (a), 31- (b), and 35-week (c) fetus, showing the fetal body, the placenta, and the umbilical cord, with the help of Rhinoceros software.**

## **CHAPTER THREE: HYBRID COMPUTATIONAL PREGNANT FEMALE PHANTOM CONSTRUCTIONS**

The specific aim of this chapter is to construct a hybrid computational female phantom model for the fetus phantom set developed in the previous chapter, in order to create the hybrid computational pregnant phantom series. An adult female ICRP reference phantom was adopted for this study, to complete the pregnant phantom model set. The focus was on developing the female surface organ shapes and locations, and on preventing internal organ surfaces from overlapping with one another. After the female organs had been developed, the fetus phantom was inserted into the developed ICRP reference female, to complete the computational pregnant phantom model for each gestational period. This chapter details the efforts undertaken to meet research aim number 2, the construction of female organs: The construction of an ICRP reference female phantom, using an ICRP adult voxel reference female, to construct a hybrid computational female phantom to carry the fetus phantom constructed in the previous chapter. This chapter also describes the steps taken to meet research aim number 3: Adding the finished fetus phantom set to the ICRP reference female phantom, using 3D-modeling software to establish a complete standard pregnant phantom set at 20, 31, and 35 weeks of pregnancy. Finally, with the aid of radiological image sets, which had initially been used to construct the fetus models, each fetus' position and rotation inside the uterus is adopted for the corresponding fetus phantom, as outlined in research aim number 4.

### 3.1 ICRP FEMALE AND FILE FORMAT

In this study, an adult female ICRP reference phantom in voxel format [47] was used to construct the hybrid computational pregnant female phantom. The female polygon mesh model was constructed from the voxel model, utilizing a Visualization Toolkit VTK-based marching cubes algorithm, which is an open source software used for manipulating and displaying 3D rendering objects [48]. This algorithm generates a rendering surface describing a full geometry of the 3D model in triangle meshes [49]. Standard Triangle Length (STL) represents a 3D solid object constructed from triangle facets which are easy to manipulate [49]. Gaussian filters were applied to smoothen the overall organ shapes, which, however, generated some differences in organ volumes, especially in small organs.

The process started by generating a polygon mesh in STL file format for each organ, using the VTK, and importing the polygon meshes into 3D modeling software Rhinoceros. Triangle mesh organs of an adult ICRP reference female in STL file format were imported into a readable file format by Rhinoceros [50], with a mesh model resolution of 2 mm x 2 mm x 2 mm. Rhinoceros software offers several useful 3D tools for geometry checking, such as the MeshRepair, PatchSingleFace, FillMeshHoles, and RebuildMesh rendering options. The Boolean operator was a very useful tool to separate between two surfaces or polygon meshes, by creating a space between overlapping organs. Some female organ models were kept in polygon mesh, such as the brain, entire skeletal joints, and vertebrae, to maintain the realistic topology of each organ feature model as shown in Figure 3.1.

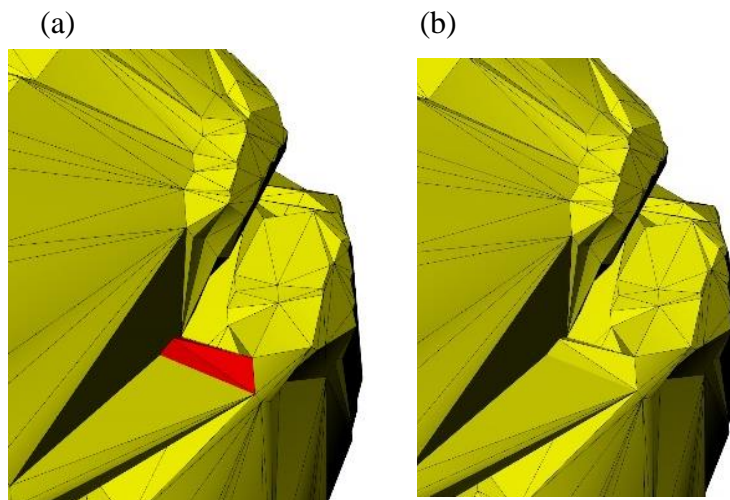


**Figure 3.1 Illustration of a polygon mesh object with triangle facets of a 35-week fetal brain organ. (a) The red gab between triangle faces. (b) The red hole was repaired using the FillMeshHoles command in Rhinoceros software [50].**

## **3.2 NURBS AND POLYGON MESH MODELING**

In order to effectively manipulate the polygon mesh anatomy of the computational phantom, STL files were generated and imported into Rhinoceros software in many different layers which can be turned off and on, without interrupting other organs' locations on other layers. To generate a non-uniform rational basis spline (NURBS) surface, the “contouring” and “lofting” tools were used in Rhinoceros. The contours were constructed from native polygon mesh organs,

by creating a space series of planar curves through the polygon mesh surface; the lofting tool was used to generate NURBS surfaces from those contours, by fitting surfaces through those series of curves to define and match the same native surface shape. NURBS surfaces were generated for the lungs, heart, thyroid glands, thymus, spleen, liver, stomach, kidneys, adrenal gland, gallbladder, pancreas, urinary bladder, and uterus. The essential step in this process is that the final NURBS surfaces have to be made to match precisely the polygon mesh surfaces so that the original realistic anatomy for each NURBS surface is preserved, without creating surface collisions between adjacent organs -- except in some cases, where manual adjustments were necessary to prevent overlapping collisions during the 3D modeling process. Eyeballs and lenses were later replaced with spherical and ellipsoidal shapes, in order to achieve smooth 3D modeling surfaces. Some organs were modeled by their walls and contents such as gallbladder, small and large intestines. The most effective way to extract the contents from their walls is to narrow down the generated NURBS surfaces and to create another NURBS surface that is smaller than the contents [20]. NURBS surfaces for the breasts were modeled based on the initial female polygon anatomy and were then replaced by matching NURBS surfaces.

The NURBS surfaces of the small and large intestines were designed differently than other organs, by using the pipe command in Rhinoceros. The uniform pipe NURBS surfaces were inserted manually from a single line to build cylinder pipes that match the polygon mesh volume and location of the original small and large intestines. While the small intestines, including the duodenum, jejunum, and ileum, start from the stomach and go to the beginning of the large intestines, the large intestines including the ascending colon, transverse colon, descending colon and sigmoid colon begin from the small intestine and go to the end of the rectum. In order to build

the contents and the walls of the intestines, two pipes were modeled, using the same single line. It took about one month to design the small and large intestines and to successfully fit them with the mother's internal organs for each gestational period.

### **3.3 STANDARD HYBRID FEMALE PHANTOM**

Matching the NURBS or polygon mesh surfaces of the adult ICRP reference female model with the corresponding original adult female ICRP reference phantom reported in the ICRP 110 report represented an essential step [47]. The ICRP reference data were recorded in organ and tissue masses; however, since the phantom's organs and tissue are based on volume, it was necessary to find their densities, listed in ICRU Report 46 [46], in order to calculate the organ mass reference values provided in ICRP 89 Publication [18]. Therefore, the female NURBS and polygons organs and tissues generated from the voxel model were individually matched with the reference values provided in ICRP 89 Publication [18]. The best way to match the ICRP reference values is to use the "3D scale" command in Rhinoceros<sup>TM</sup> software. Another way to approach the same ICRP reference values is to use "control points," controlled by NURBS in 3D modeling. In order to preserve realistic human organs and tissue, sometimes it was easier to manipulate the "control points," rather than to carry out a "3D scale." Great attention was devoted to constructing organ walls and their contents, such as the gallbladder, small intestines, and large intestines. To eliminate any gaps between the organs, the scaling method was accomplished at once for the entire



organs. The most crucial and challenging step was to prevent any collision between adjacent organs and tissues, in order to avoid any future complications during the voxelization step.

### **3.4 STANDARD FETUS POSITION IN UTERO**

As mentioned in Chapter two, section 2.7.2, the orientation of the fetus has not been taken into account in the literature on radiation dosage, and some research indicates that fetal position periodically changes during the first and second trimesters. During the second trimester, there is an equal likelihood of the fetus facing head up or head down. In the third trimester, the fetus' head is very likely to be down, in preparation for birth as suggested by Jing Chen reference [19]. In this study, two pregnant woman phantom models were used to study the whole-body exposure of the fetus to radiofrequency electromagnetic fields (8 and 32 weeks of pregnancy). The fetus' position in this study was chosen to be either head down head up [19].

In this dissertation study, the hybrid computational fetus phantom set was carefully developed to reflect the original location and orientation of the fetus in the maternal uterus, in order to build realistic fetus models for accurately estimating radiation doses. The original MR image sets were used to determine the initial fetal and uterus location among the other maternal organs and to adopt them for each model; first, the brain and spine orientations were taken into account, followed by the direction of the fetal extremities (hands and feet). The 20-week, the 31-week as well as the 35-week fetus model were all head down. While both the 20- and 35-week

fetus models were in right occiput posterior (ROP) configurations, the 31-week fetus model was in the left occiput anterior (LOA) position, surrounded by the maternal tissues, including the placenta and uterus. Organ volume adjustment was necessary to match within 1% the reference values reported in ICRP 89 Publication [18], in order to represent a standard fetus, set. The complete fetal anatomy was reviewed by a clinical obstetrician and facility specialist and suggested modifications were applied.

### **3.5 PREGNANT FEMALE PHANTOM CONSTRUCTIONS**

Both the standard computational female model and the fetus phantom sets developed in NURBS or polygon mesh were used to construct a pregnant model set at three different gestational periods. Major abdominal soft tissue organs below the diaphragm were removed from the non-pregnant females, using the Rhinoceros software: the small intestine, large intestine, liver, gall bladder, stomach, pancreas, uterus, and uterine bladder. With the help of Rhinoceros 3D modeling software, the finished fetus phantom was positioned in the appropriate location, matching the original radiological image sets [50]. The flexible nature of the NURBS or polygon mesh format of these phantoms has significant advantages, as their shape and volume can be changed to match the original MR image data.

### **3.5.1 PREGNANT FEMALE PHANTOM – 20 WEEKS**

In order to construct a hybrid computational pregnant phantom model at 20 weeks of gestation, the first step is to remove the internal maternal soft organs and tissues, using Rhinoceros software. The second step is to add the maternal uterus and the finished 20-week fetus to the finished female adult ICRP reference model. As a starting point, it was best to locate the maternal uterus and its contents roughly where the female's uterus had been, and then to use the radiological MR image set as a guide to adjust the location of the mother's uterus and of the fetus phantom. Once the 20-week fetus phantom model closely matched the corresponding location of the fetus in the radiological image set, the remaining maternal organs had to be gradually added to complete the pregnant phantom model. In this process, however, some adjustments were necessary, such as moving the small and large intestines slightly away from the uterus, thereby creating enough space for the 20-week fetal phantom to fit without any overlaps. Because at the 20-week stage the fetus was small, no major soft tissue modification was needed for this model. The only maternal organs which needed to be modified were the uterus, ovaries, urinary bladder, large intestines, and small intestines.

### **3.5.2 PREGNANT FEMALE PHANTOM – 31 WEEKS**

The pregnant female model was developed by changing the ICRP female phantom model and adding the 31-week fetus phantom that had been developed in Chapter 2. The abdomen of the female phantom was completely removed, and then the developed fetus phantom was added to the

female pelvis. The rest of the female anatomical tissues were reshaped and modified to match the shape of the abdomen at 31 weeks of pregnancy. This process required much work because at this stage of the pregnancy, the fetus is bigger and the position and shape of most of the mother's internal organs have changed to accommodate the growing size of the fetus. New small and large intestines were modeled, along with internal and external wall constructions for each intestine. Figure 3.2 shows the finished fetus model inside the mother's uterus. A control point technique was also used to modify the urinary bladder, the gall bladder, the stomach, the spleen, and the liver. The Boolean operator was a useful tool to separate overlapping organs and tissues. These organs and tissues were modified based on the original MR image set which had been used to construct the 31-week phantom, which reflects real anatomical organs. The deformed organs and tissues were replaced by the female phantom's other organs and tissues. The location of the 31-week fetus phantom is deeper inside the mother's pelvis than the 20-week fetus phantom. This is due to the extra fetal weight added to the uterus, which pushes the location of the urinary bladder in a horizontal direction. As a final step, the final fetal model was confirmed by an OBGYN specialist.

### **3.5.3 PREGNANT FEMALE PHANTOM – 35 WEEKS**

The realistic anatomy of the whole-body pregnant phantom was developed by combining the newly constructed fetus phantom at 35 weeks of pregnancy and the deformed ICRP female phantom model. After removing the abdominal organs of the ICRP female phantom, the 35-week

fetus phantom was added. The fetus size is big at this stage and located further inside the pelvis than at 31 weeks of pregnancy. In this model, many maternal anatomical organs were newly modeled, such as the small and large intestines, the urinary bladder, while some other maternal anatomical organs were modified, such as the liver, the stomach, the spleen, and the gall bladder. The fetal body, the placenta, and the umbilical cord inside the mother's uterus were positioned according to the original MR image set that had been used. Many factors had to be considered in order to build an accurate representation of a 35-weeks pregnant woman's shape, especially regarding the abdominal area, and to adjust the mother's posture and the fetal location inside the uterus.

### **3.6 RESULTS**

The voxelized ICRP adult reference female in polygon mesh view and the completed computational ICRP adult reference female phantom modeled in NURBS surfaces are shown in Figure 3.2. Frontal and back views of the ICRP adult reference female in NURBS surfaces of the standard reference female model are shown in Figure 3.3. Three-dimensional front representations of the hybrid fetus phantom models at 20, 31, and 35 weeks of gestation are represented in Figure 3.4. A snapshot of the completed hybrid pregnant computational phantom series showing the fetal body and its organs, the placenta, the umbilical cord, and the maternal organs were also taken from Rhinoceros software as shown in Figure 3.4 and Figure 3.5. Figure 3.5 represents the steps necessary to add the developing fetus phantoms inside the mother's uterus to create the pregnant

phantom model sets. All volume masses values of the pregnant female models were matched with the reference data provided in ICRP 89 Publication. Their mass and density values were listed in Table 3.2, Table 3.3, and Table 3.4. Flow chart describing the steps for developing hybrid computational pregnant phantom models is described in Table 3.5

### **3.6.1 THE ICRP ADULT FEMALE MODEL**

In this study, an adult ICRP voxel reference female [47] was used to construct a hybrid computational pregnant female phantom based on polygon mesh and NURBS surfaces. The female model created in this study includes 40 different anatomical structures that are necessary for organ dose calculations. Table 3.1 summarizes the female organ volumes, masses, densities, and the tissue or organs constructed method types (NURBS or polygon mesh). To make a standard hybrid computational phantom model set, all female NURBS and polygon mesh organs were carefully checked and matched with the reference data provided in ICRP 89 Publication. The polygon mesh model before 3D modeling is represented in Figure 3.2, and the NURBS surface developed model is also shown in Figure 3.3.

**Table 3.1 An Adult ICRP reference female mass, volume, and density.**

Female Phantom	Density (g/cm <sup>3</sup> )	ICRP Mass (g)	ICRP-89 Female Volume (cm <sup>3</sup> )	Female Phantom Volume (cm <sup>3</sup> )	NURBS or Mesh
Adrenals (2)	1.03	13.00	12.62	12.43	mesh
Brain	1.05	1300.00	1238.10	1190.67	nurbs
Breast Exterior (2)	0.98	172.54	176.65	176.65	nurbs
Breast glands (2)	0.98	500.00	511.90	512.53	mesh
Branchi	1.07	-	-	0.25	nurbs
Eyeballs (2)	1.05	15.00	14.30	14.22	nurbs
Eye Lenses (2)	1.00	0.40	0.40	0.40	nurbs
Gall Bladder wall	0.81	8.00	9.90	10.00	nurbs
Gall Bladder Content	1.08	48.00	44.44	53.98	nurbs
Gall Bladder Contents	1.08	48.00	44.40	53.98	nurbs
Heart	1.06	620.00	587.20	578.90	nurbs
Small Intestine Wall	1.03	600.00	582.52	575.18	nurbs
Small Intestine Content	1.03	280.00	271.84	278.01	nurbs
Large Intestine Wall	1.04	360.00	346.15	345.00	nurbs
Large Intestine Contents	1.04	320.00	307.69	306.00	nurbs
Kidneys (2)	1.05	275.00	261.90	260.33	nurbs
Larynx	1.07	19.00	17.76	17.66	nurbs
Liver	1.05	1400.00	1333.33	1345.84	nurbs
Lungs (2)	0.41	950.00	2300.80	2309.76	mesh
Nasal Septum	1.03	-	-	4.36	mesh
Oesophagus	1.03	35.00	33.98	33.81	nurbs
Ovaries (2)	1.04	11.00	10.60	10.48	nurbs
Pancreas	1.05	120.00	114.39	115.57	nurbs
Pituitary gland	1.00	0.60	0.60	0.61	nurbs
Pharynx	1.03	-	-	12.17	mix
Skeleton (total)	1.03	7800.00	7572.82	7262.19	-
Skin	1.10	2300.00	2090.91	2496.80	nurbs
Spleen	1.04	130.00	125.00	12.44	mesh
Spinal cord	1.02	-	-	17.43	mesh
Spin	1.03	-	-	1015.51	nurbs
Stomach wall	1.03	140.00	135.92	137.26	nurbs
Stomach contents	1.00	230.00	230.00	228.31	mesh
Tongue	1.05	60.00	57.14	56.84	mesh
Tooth Buds	2.74	40.00	14.60	14.70	mesh
Tonsils (2)	1.03	3.00	2.90	2.90	nurbs
Trachea	1.07	8.00	7.48	7.80	nurbs
Thymus	1.03	20.00	19.40	18.67	nurbs
Thyroid Gland	1.04	17.00	16.40	16.05	nurbs
Total Body	1.01	60000.00	59258.00	59258.00	nurbs
Urinary Bladder	1.04	40.00	38.50	38.94	nurbs
Uterus	1.03	80.00	77.67	78.36	nurbs

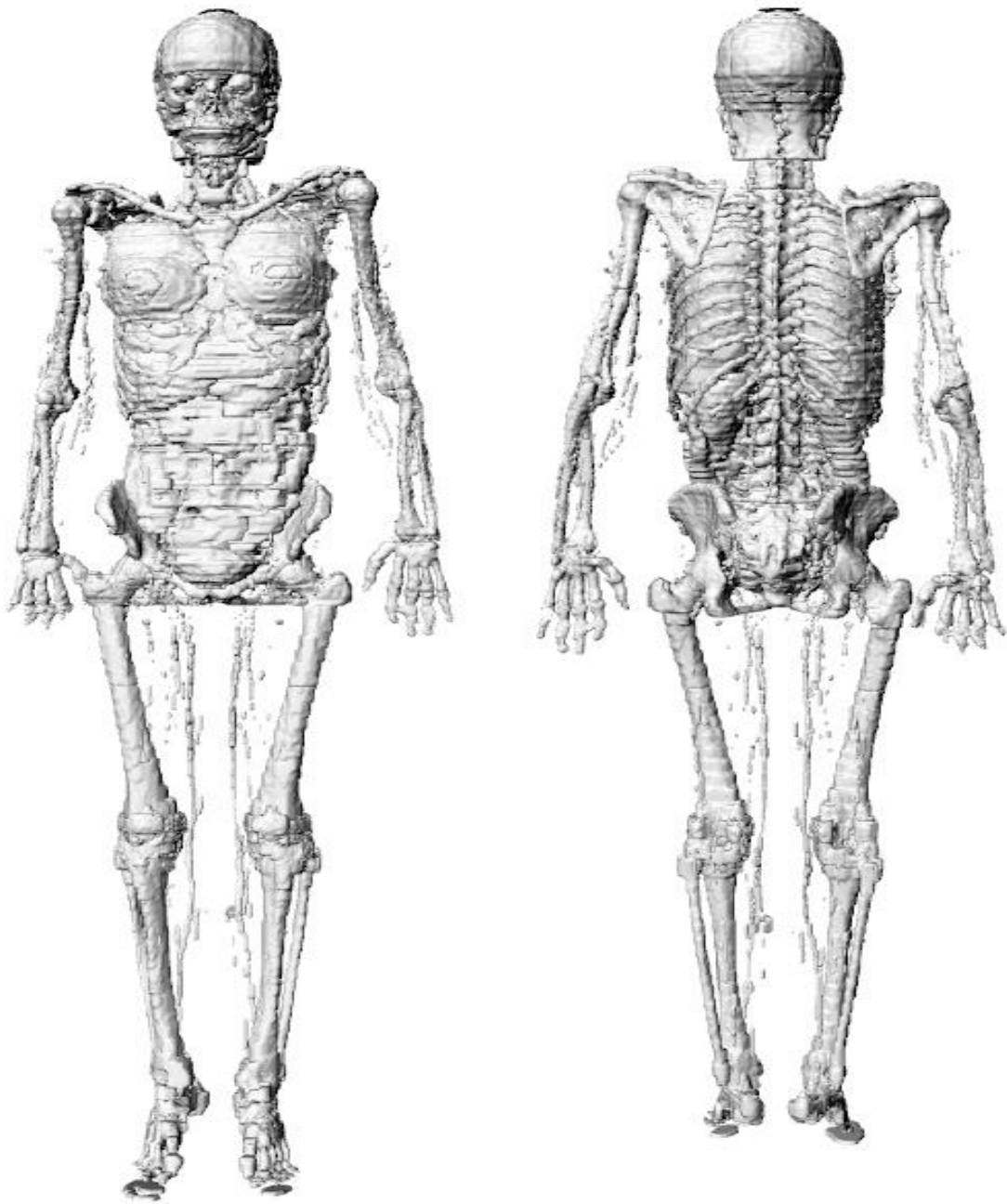


**Figure 3.2 Frontal and back views of the standard reference female model, after removing the skin of the initial voxels in a polygon mesh.**



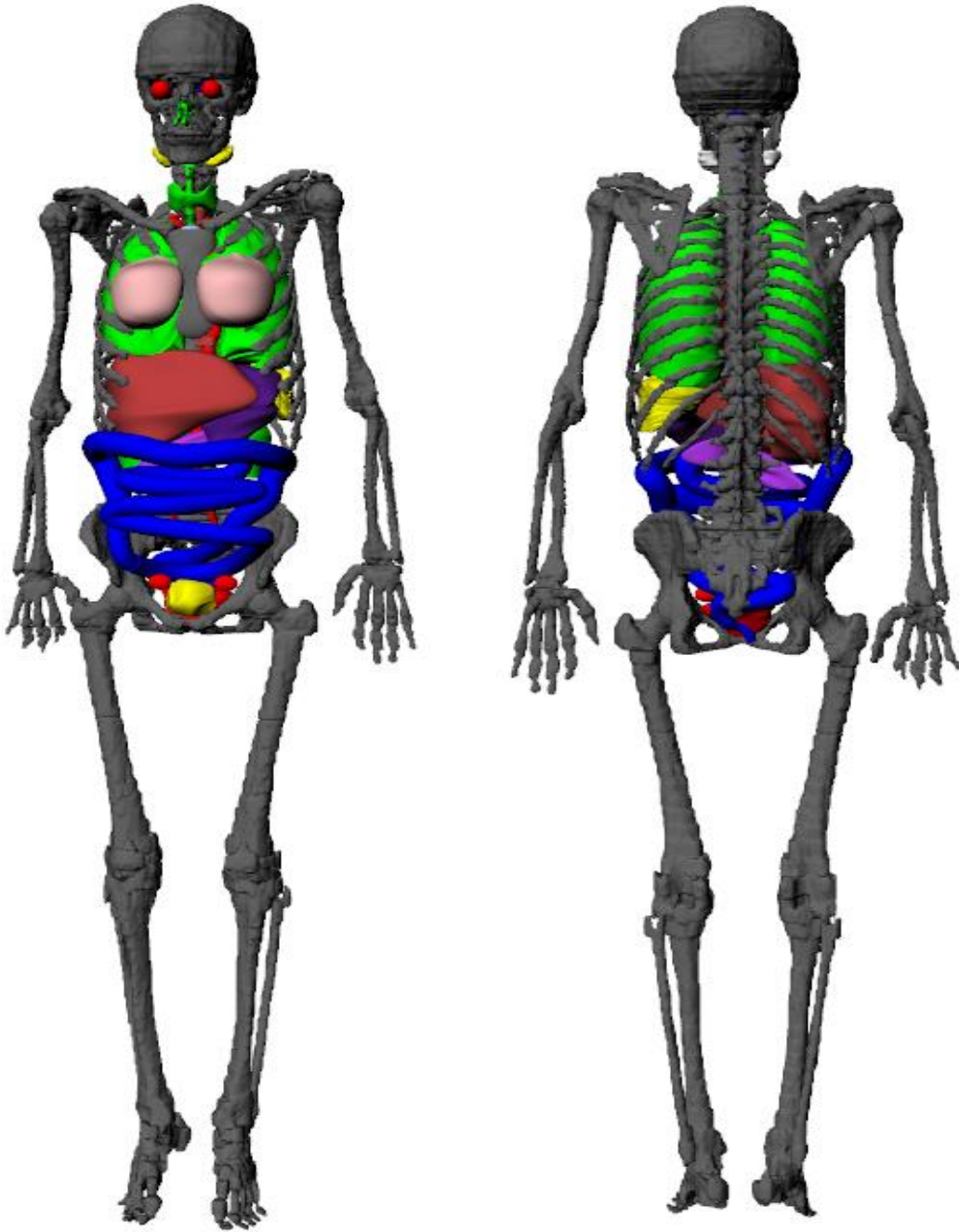


**Figure 3.3 Frontal and back views of the ICRP adult reference female in NURBS surfaces of the standard reference female model.**

### **3.6.2 THE FETUS PHANTOMS INSIDE THE UTERO**

The shape of the maternal organs changes to fit the growing size of the fetus as the pregnancy progresses. At 20 weeks of gestation, the fetal anatomical organs were relatively small. Thus, the anatomy of the female abdominal-pelvic region was adopted, with minor organ corrections. At 31 and 35 weeks of pregnancy, the fetus grows bigger, and much of the anatomical abdomen of the female pelvis were either remodeled or significantly changed to fit the correct fetus position that matches the MR image sets. The final maternal external envelope, as well as the fetus, the placenta, and the umbilical cord, are different for each model.

To preserve the realistic fetal positions inside the mother's uterus, we used all the information available from the MR image sets that had been used earlier to construct the realistic three hybrid computational phantoms. The maternal uterus was made transparent in order to make the internal fetal organs more visible. The final computational fetus phantoms include 27 different anatomical structures.

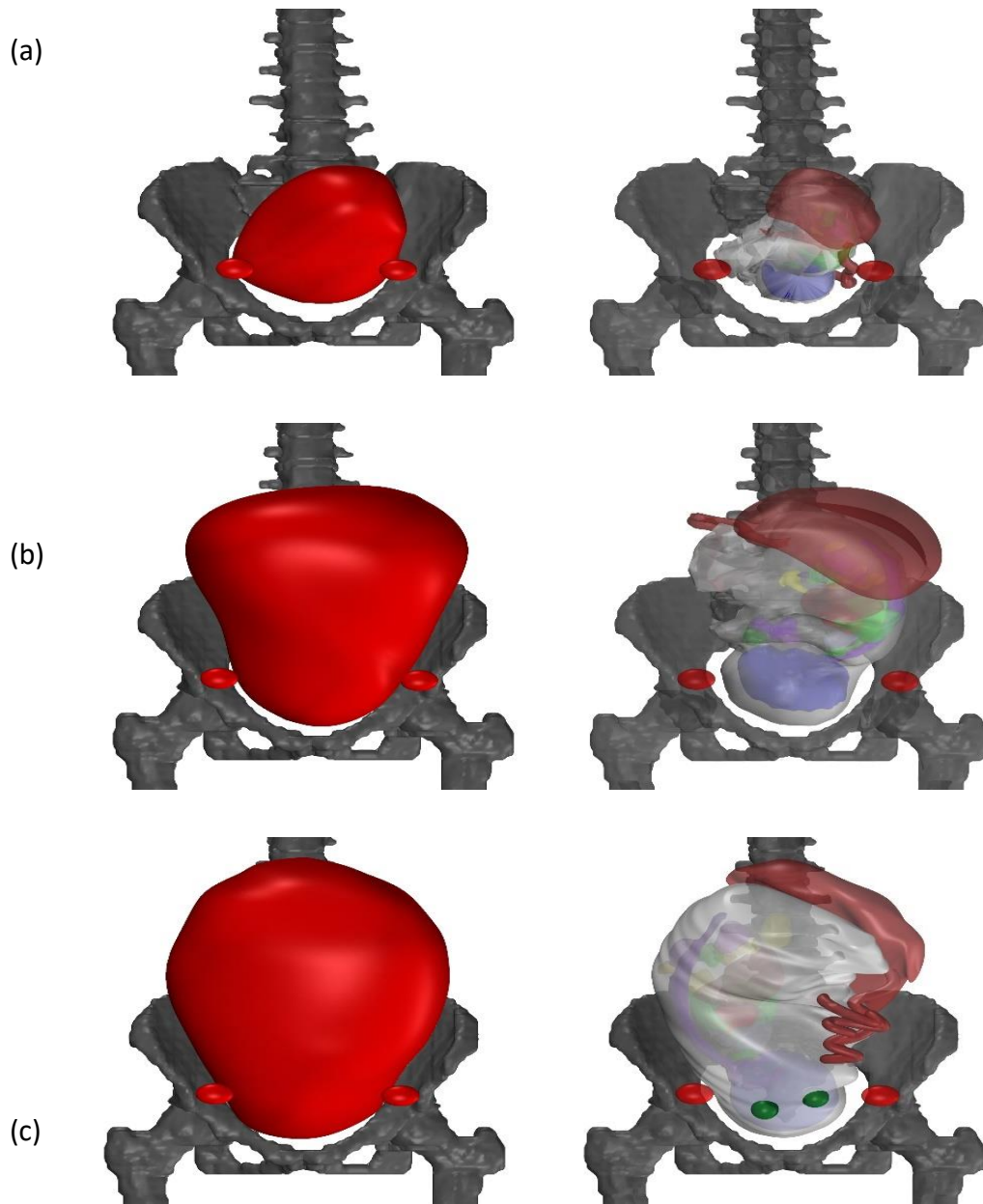


**Figure 3.4 Three-dimensional front representations of hybrid fetus phantom models at 20, 31, and 35 weeks of gestation. (a) 20-week of gestation, (b) 31-week of gestation, (c) 31 week of gestation.**

### 3.6.3 THE HYBRID PREGNANT COMPUTATIONAL PHANTOMS

The pregnant female model was developed from an ICRP adult reference, voxelized female. The hybrid computational pregnant models were developed based on anatomical data which was provided by MR image sets for all the individual models. The pregnant female anatomical structures changed during each gestational period of pregnancy. Significant variations in tissue anatomy and physiology during each gestational period in the pregnancy were taken into account. All volume masses values were matched with the reference data provided in ICRP 89 Publication [18]. These masses and densities are listed in Table 3.2, Table 3.3, and Table 3.4. The abdomen of a non-pregnant female model was either modified or made to match the abdominal shape of each pregnant model, based on radiological images used for constructing these models. To add the skin for the generated pregnant female models, the head's, leg's, and hand's skin of ICRP reference female were kept in the same mesh surface except for the abdominal skin area. The abdominal skin contours of the ICRP reference female were converted to NURBS surfaces in order to undergo the necessary adjustments after adding the fetus inside the mother's abdomen. Figure 3.6, Figure 3.7, and Figure 3.8 are the completed pregnant female phantom models after modifying the skin.

**Table 3.2 20-Weeks pregnant female phantom model mass, volume, and density.**

<b>20-Weeks Pregnant Female Phantom</b>	<b>Density (g/cm<sup>3</sup>)</b>	<b>ICRP Mass (g)</b>	<b>ICRP-89 Female Volume (cm<sup>3</sup>)</b>	<b>Pregnant Female Volume (cm<sup>3</sup>)</b>	<b>Modified Organs Yes/No</b>
Adrenals (2)	1.03	13.00	12.60	12.43	-
Brain	1.05	1300.00	1238.10	1190.67	-
Breast Exterior ( 2)	0.98	500.00	511.90	551.62	Yes
Breast glands ( 2)	0.98	0.17	176.65	190.12	Yes
Breast-Total	0.98	360.00	367.35	370.87	Yes
Branchi	1.07	-	-	0.25	-
Eyeballs (2)	1.05	15.00	14.30	14.22	-
Eye Lenses (2)	1.00	0.40	0.40	0.40	-
Gall Bladder Wall	1.08	48.00	54.30	53.99	Yes
Gall Bladder Content	0.81	8.00	9.90	9.99	Yes
Heart	1.06	620.00	587.20	578.90	-
Small Intestine Wall	1.03	600.00	582.50	394.40	Yes
Small Intestine Content	1.03	280.00	280.00	281.00	Yes
Large Intestine Wall	1.04	360.00	414.84	414.84	Yes
Large Intestine Contents	1.04	320.00	239.92	239.92	Yes
Kidneys (2)	1.05	275.00	261.90	260.33	-
Larynx	1.07	19.00	17.75	17.66	-
Liver	1.05	1400.00	1333.30	1345.84	-
Lungs (2)	0.41	950.00	2300.80	2309.76	-
Nasal Septum	1.03	-	-	4.36	-
Oesophagus	1.03	35.00	34.00	33.81	-
Ovaries (2)	1.04	11.00	10.60	10.48	-
Pancreas	1.05	120.00	116.50	115.57	-
Pituitary gland	1.00	0.60	0.60	0.61	-
Pharynx	1.03	-	12.17	12.17	-
Skeleton (total)	1.03	7800.00	7572.80	7262.19	-
Skin	1.10	2300.00	2496.80	-	-
Spleen	1.04	130.00	125.00	124.39	-
Spinal cord	1.02	-	-	17.43	-
Spin	1.03	-	-	1015.51	-
Stomach Wall	1.03	140.00	135.92	136.59	Yes
Stomach Contents	1.00	230.00	230.00	227.50	Yes
Tongue	1.05	60.00	57.10	56.84	-
Tooth Buds	2.74	40.00	14.60	14.70	-
Tonsils (2)	1.03	3.00	2.90	2.90	-
Trachea	1.07	8.00	7.74	7.80	-
Thymus	1.03	20.00	18.70	18.67	-
Thyroid Gland	1.04	17.00	16.10	16.05	-
Total Body	1.01	-	-	66607.58	Yes
Urinary Bladder	1.04	40.00	38.50	38.53	Yes
Uterus	1.03	80.00	77.67	988.43	Yes

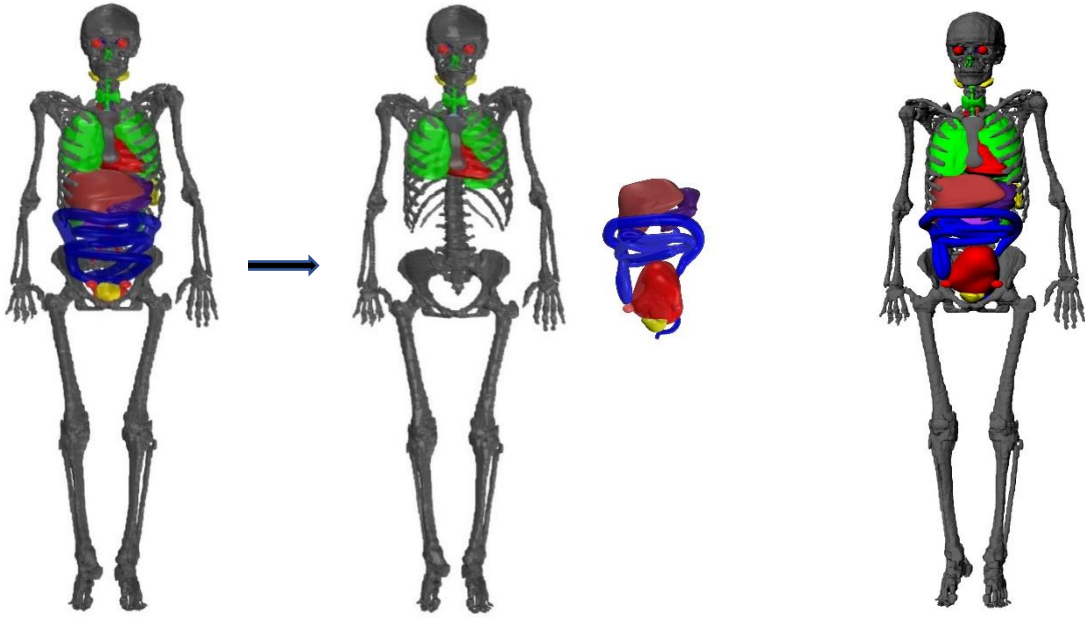
**Table 3.3 31-Weeks pregnant female phantom model mass, volume, and density.**

<b>31-Weeks Pregnant Female Phantom</b>	<b>Density (g/cm<sup>3</sup>)</b>	<b>ICRP Mass (g)</b>	<b>ICRP-89 Female Volume (cm<sup>3</sup>)</b>	<b>Pregnant Female Volume (cm<sup>3</sup>)</b>	<b>Modified Organs Yes/No</b>
Adrenals (2)	1.03	13.00	12.60	12.43	-
Brain	1.05	1300.00	1238.10	1190.67	-
Breast Exterior ( 2)	0.98	500.00	511.90	559.41	Yes
Breast glands ( 2)	0.98	0.17	176.65	192.80	Yes
Breast-Total	0.98	740.00	755.10	752.21	Yes
Branchi	1.07	-	-	0.25	-
Eyeballs (2)	1.05	15.00	14.30	14.22	-
Eye Lenses (2)	1.00	0.40	0.40	0.40	-
Gall Bladder Wall	1.08	48.00	54.30	52.32	Yes
Gall Bladder Content	0.81	8.00	9.90	9.97	Yes
Heart	1.06	620.00	587.20	578.90	-
Small Intestine Wall	1.03	600.00	582.50	581.50	Yes
Small Intestine Content	1.03	280.00	280.00	280.10	Yes
Large Intestine Wall	1.04	360.00	414.84	415.00	Yes
Large Intestine Contents	1.04	320.00	239.92	238.00	Yes
Kidneys (2)	1.05	275.00	261.90	260.33	-
Larynx	1.07	19.00	17.75	17.66	-
Liver	1.05	1400.00	1333.30	1305.44	Yes
Lungs (2)	0.41	950.00	2300.80	2309.76	-
Nasal Septum	1.03	-	-	4.36	-
Oesophagus	1.03	35.00	34.00	33.81	-
Ovaries (2)	1.04	11.00	10.60	10.48	-
Pancreas	1.05	120.00	116.50	108.04	Yes
Pituitary gland	1.00	0.60	0.60	0.61	-
Pharynx	1.03	-	12.17	12.17	-
Skeleton (total)	1.03	7800.00	7572.80	7262.19	-
Skin	1.10	2300.00	2496.80	-	-
Spleen	1.04	130.00	125.00	124.39	-
Spinal cord	1.02	-	-	17.43	-
Spin	1.03	-	-	1015.51	-
Stomach Wall	1.03	140.00	135.92	137.23	Yes
Stomach Contents	1.00	230.00	230.00	225.50	Yes
Tongue	1.05	60.00	57.10	56.84	-
Tooth Buds	2.74	40.00	14.60	14.70	-
Tonsils (2)	1.03	3.00	2.90	2.90	-
Trachea	1.07	8.00	7.74	7.80	-
Thymus	1.03	20.00	18.70	18.67	-
Thyroid Gland	1.04	17.00	16.10	16.05	-
Total Body	1.01	-	-	78907.98	Yes
Urinary Bladder	1.04	40.00	38.50	38.08	Yes
Uterus	1.03	80.00	77.70	4539.85	Yes

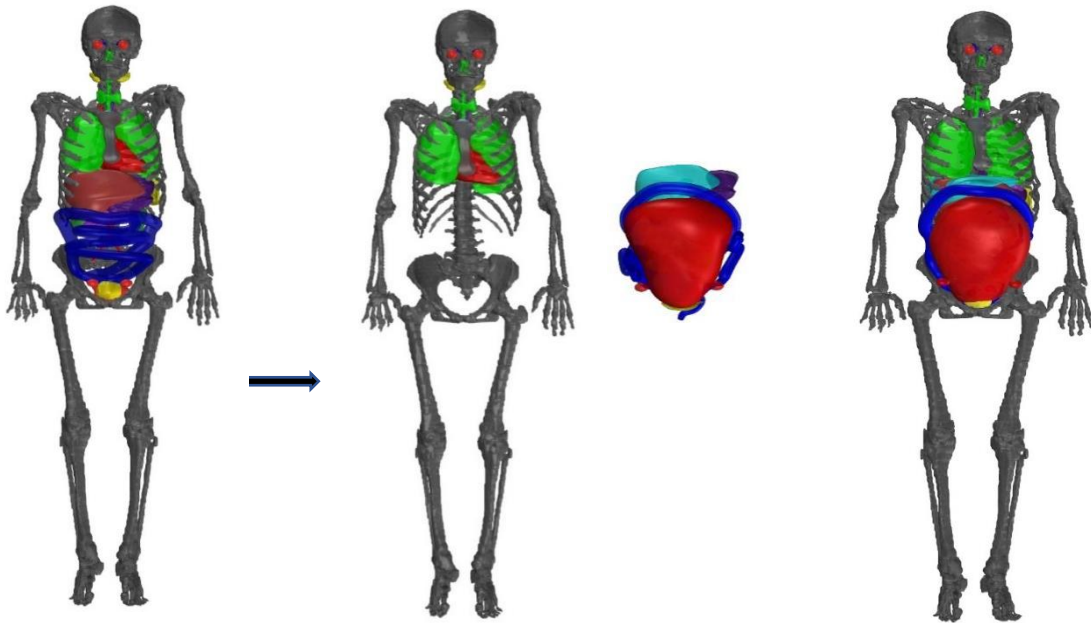
**Table 3.4 35-Weeks pregnant female phantom model mass, volume, and density.**

<b>35-Weeks Pregnant Female Phantom</b>	<b>Density (g/cm<sup>3</sup>)</b>	<b>ICRP Mass (g)</b>	<b>ICRP-89 Female Volume (cm<sup>3</sup>)</b>	<b>Pregnant Female Volume (cm<sup>3</sup>)</b>	<b>Modified Organs Yes/No</b>
Adrenals (2)	1.03	13.00	12.60	12.43	-
Brain	1.05	1300.00	1238.10	1190.67	-
Breast Exterior ( 2)	0.98	500.00	511.90	576.53	Yes
Breast glands ( 2)	0.98	176.00	176.65	198.70	Yes
Breast-Total	0.98	760.00	775.51	775.23	Yes
Branchi	1.07	-	-	0.25	-
Eyeballs (2)	1.05	15.00	14.30	14.22	-
Eye Lenses (2)	1.00	0.40	0.40	0.40	-
Gall Bladder Wall	1.08	48.00	54.30	53.98	Yes
Gall Bladder Content	0.81	8.00	9.90	10.00	Yes
Heart	1.06	620.00	587.20	578.90	-
Small Intestine Wall	1.03	600.00	582.50	580.00	Yes
Small Intestine Content	1.03	280.00	271.84	272.20	Yes
Large Intestine Wall	1.04	360.00	346.15	346.15	Yes
Large Intestine Contents	1.04	320.00	307.69	306.50	Yes
Kidneys (2)	1.05	275.00	261.90	260.33	-
Larynx	1.07	19.00	17.75	17.66	-
Liver	1.05	1400.00	1333.30	1330.00	Yes
Lungs (2)	0.41	950.00	2317.07	2309.76	-
Nasel Septum	1.03	-	-	4.36	-
Oesophagus	1.03	35.00	34.00	33.81	-
Ovaries (2)	1.04	11.00	10.60	10.48	-
Pancreas	1.05	120.00	116.50	117.24	Yes
Pituitary gland	1.00	0.60	0.60	0.61	-
Pharynx	1.03	-	12.17	12.17	-
Skeleton (total)	1.03	7800.00	7572.80	7262.19	-
Skin	1.10	2300.00	2496.80	-	-
Spleen	1.04	130.00	125.00	124.39	-
Spinal cord	1.02	-	-	17.43	-
Spin	1.03	-	-	1015.51	-
Stomach Wall	1.03	140.00	135.92	205.16	Yes
Stomach Contents	1.00	230.00	230.00	128.29	Yes
Tongue	1.05	60.00	57.10	56.84	-
Tooth Buds	2.74	40.00	14.60	14.70	-
Tonsils (2)	1.03	3.00	2.90	2.90	-
Trachea	1.07	8.00	7.74	7.80	-
Thymus	1.03	20.00	18.70	18.67	-
Thyroid Gland	1.04	17.00	16.10	16.05	-
Total Body	1.01	60000.00	59258.00	79936.61	Yes
Urinary Bladder	1.04	40.00	38.50	17.56	Yes
Uterus	1.03	80.00	77.70	5181.57	Yes

(a)



(b)





(c)

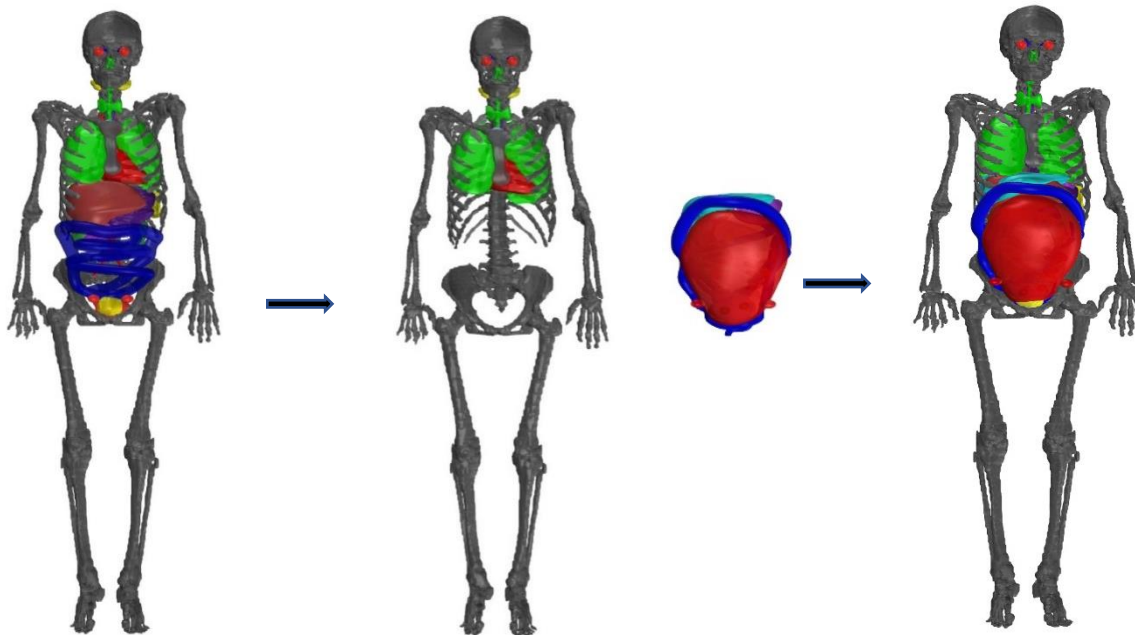


**Figure 3.5** The steps necessary to create ICRP pregnant computational phantom sets by adding the fetus phantom developed inside ICRP reference female after removing selected organs from the non-pregnant model at (a) 20, (b) 31, and (c) 35 weeks of gestation.

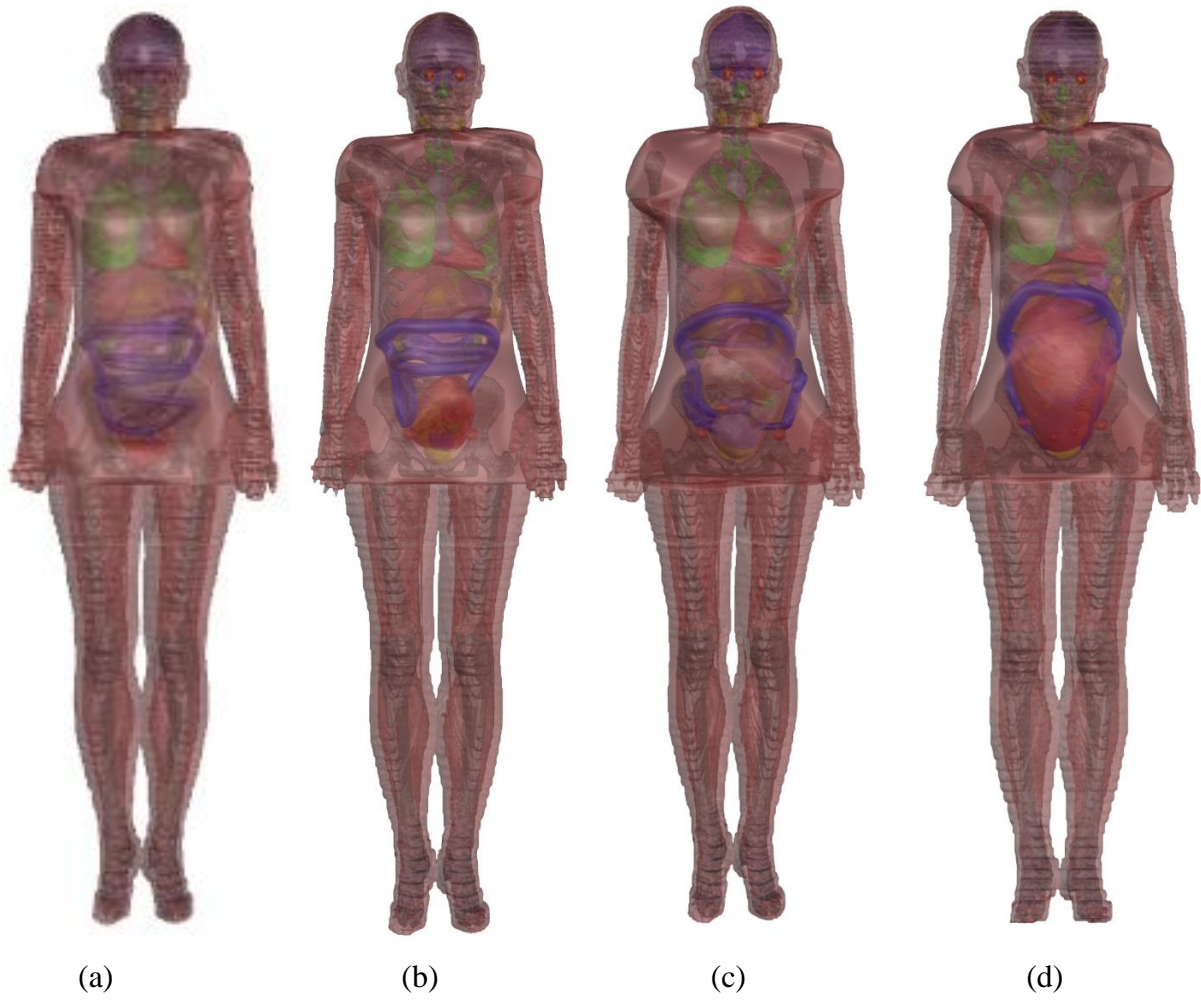


**Figure 3.6 Frontal views of pregnant female phantom series. (a) ICRP female phantom, (b) 20-week pregnant phantom, (c) 31-week pregnant phantom, (d) 35-week pregnant phantom.**

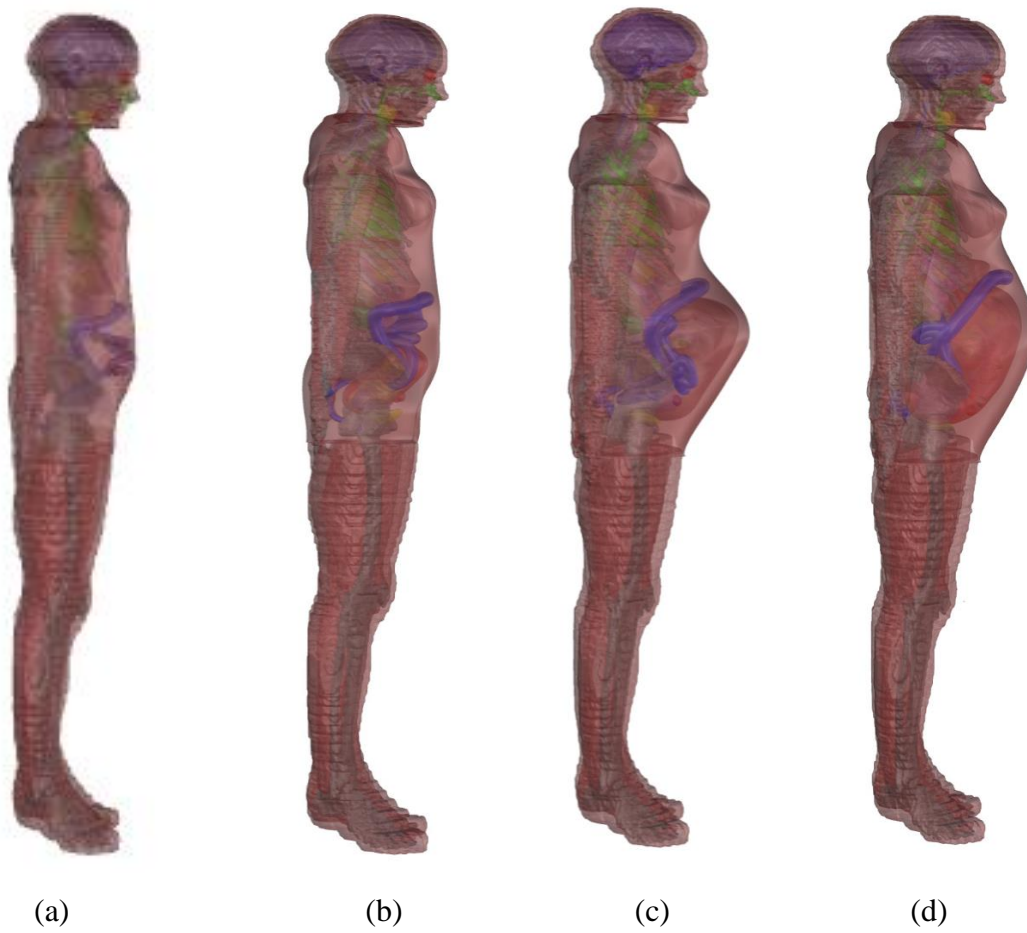


**Figure 3.7 Side views of pregnant female phantom series. (a) ICRP female phantom, (b) 20-week pregnant phantom, (c) 31-week pregnant phantom, (d) 35-week pregnant phantom.**

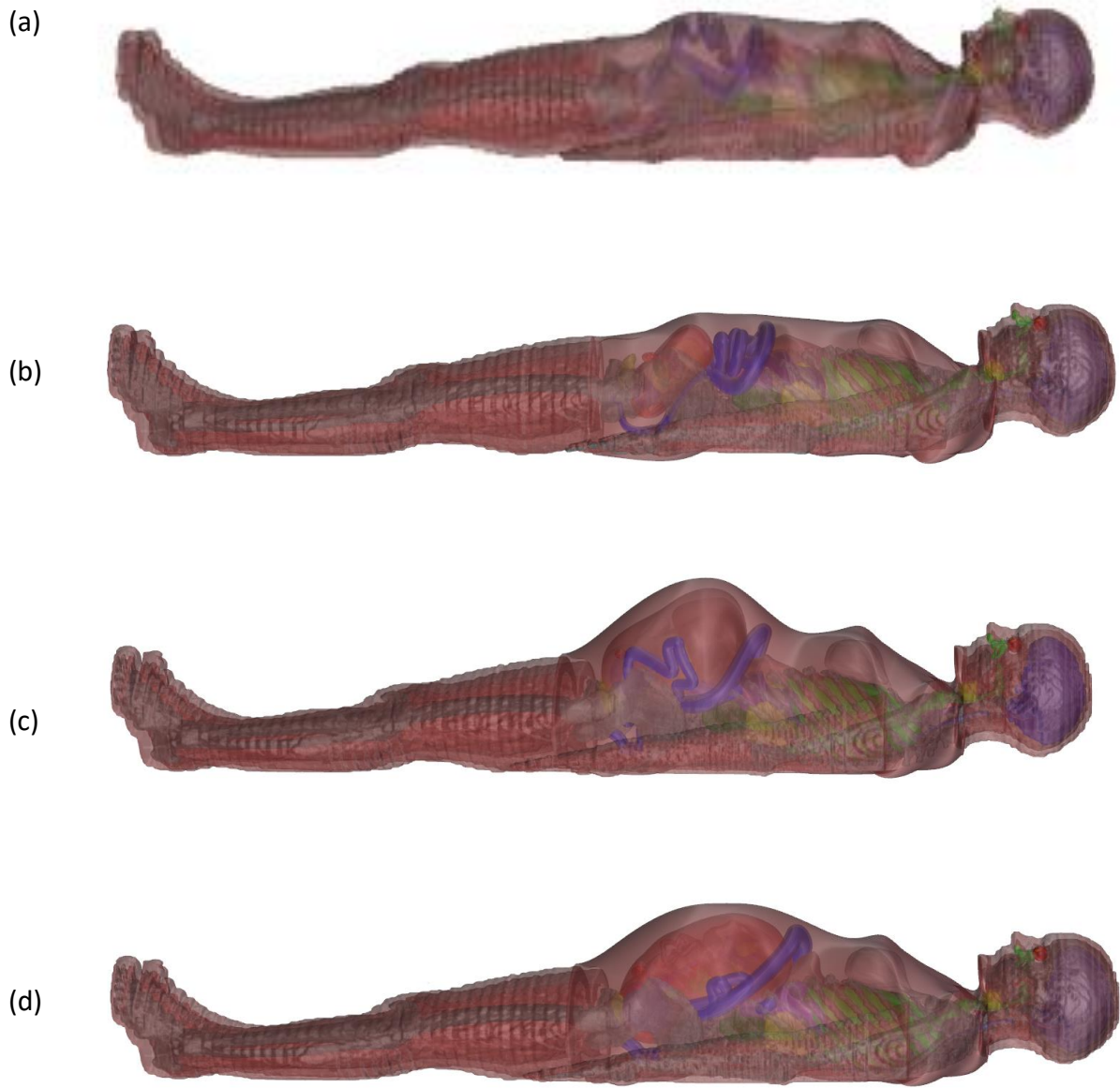
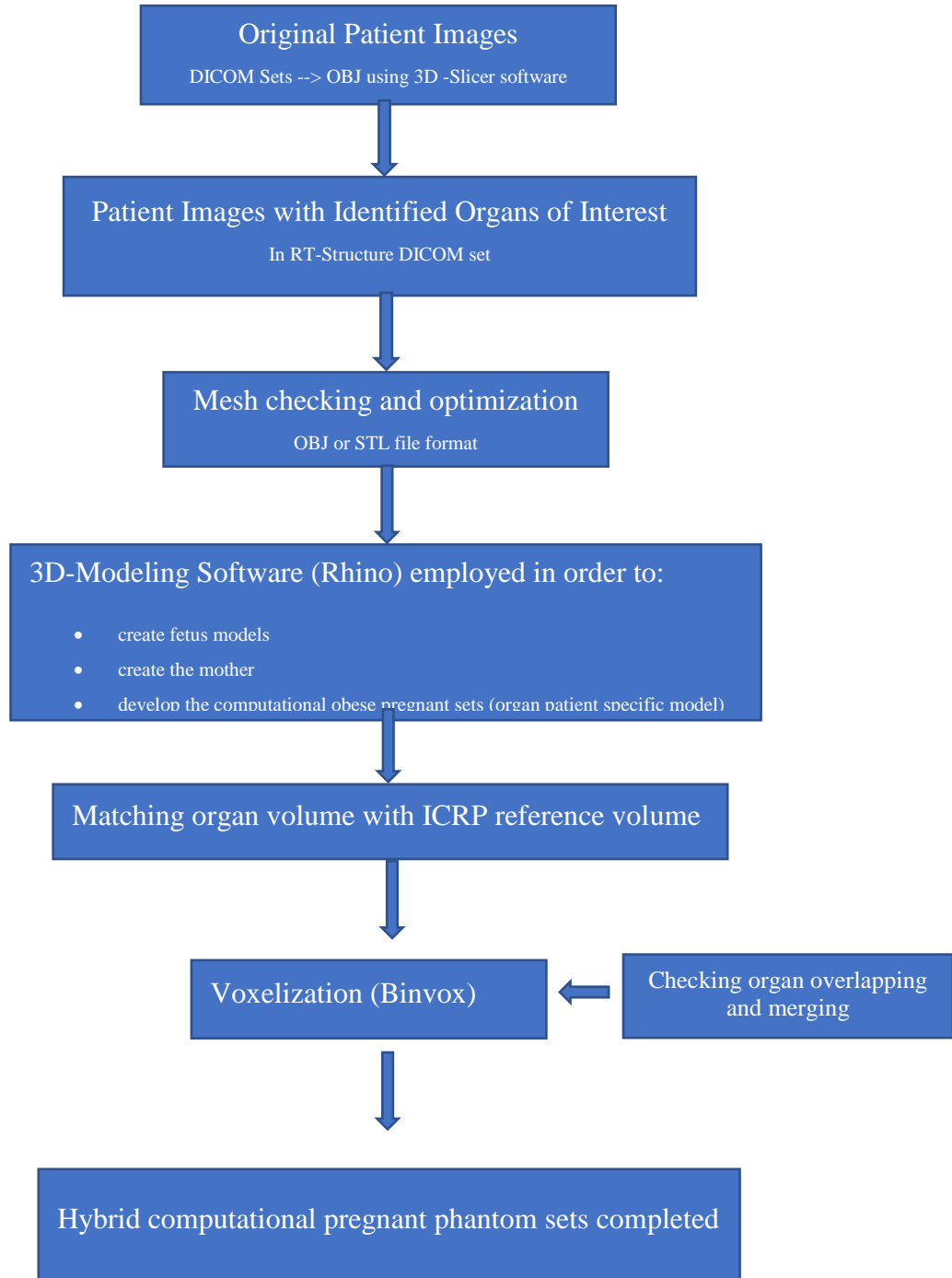


**Figure 3.8 Side and the original views of pregnant female phantom series. (a) ICRP female phantom, (b) 20-week pregnant phantom, (c) 31-week pregnant phantom, (d) 35- week pregnant phantom.**

**Table 3.5 Flow chart describing the steps for developing hybrid computational pregnant phantom models.**



### 3.7 DISCUSSION

The three state-of-the-art hybrid computational pregnant phantom models were developed based on advanced polygon mesh and NURBS surface methods. The pregnant models were developed in this study by applying these methods to the adult ICRP reference voxelized female phantom and three segmented computational fetus phantoms. As shown in Figure 3.2, distinguishing most of the female internal soft organs represented a difficulty because the outlines of the organs were lines with gaps which were not always smooth and visible. The original ICRP female voxel size model is 2 mm x 2 mm x 2 mm.

In reverse view, the lines representing the bones and skeleton of the ICRP female were continuing and smooth, therefore, they were left in polygon mesh representation. The voxelized reference female in the polygon mesh model was constructed with the help of the Visualization Toolkit VTK-based marching cubes algorithm [46]. This algorithm generates a rendering surface which describes the full geometry of the 3D model in triangle mesh, as represented in Figure 3.2 [47]. Gaussian filters were applied to smooth the organ shapes; however, these filters caused differences, especially in the size of the organs. Those organs were later corrected and matched with the ICRP adult female reference data [39]. Most organs and tissues were converted in NURBS surface modeling, except for a few organs which were kept in polygon mesh, such as the brain, all the joints of the skeleton, and the vertebrae, in order to maintain the realistic topology of each organ feature model.

NURBS surfaces in the computational female and the fetal phantoms enhanced the continuity and the overall smoothness of the internal anatomy of the soft organs, as shown in

Figure 3.3. The surfaces of the NURBS-based phantom are defined by a set of control points. The shape and volume of a NURBS surface vary according to the coordinates of these control points. The polygonal mesh has three remarkable advantages when it comes to developing whole-body phantoms. Bones and skeletons were left in mesh surfaces, showing the human anatomy, in order to obtain real patient anatomical images or commercial human anatomy mesh models. For the purposes of radiation transport simulation studies, computational phantoms in NURBS surfaces were directly implemented to the code for radiation simulation studies[20]. The adult ICRP reference female model, as well as the woman, finished female models, has a height of 168 cm, a weight of 60 kg, with over 140 organ and tissues.

The fetus can be in different locations, at different angles inside the mother's uterus. In general, occiput position means that the baby's head is aimed down towards the pelvis, and the baby is facing the mother's abdomen. A posterior presentation aims the top of the head into the pelvis. Anterior position means that the baby's head enters the pelvis with the crown of the head first. In this research, the 20-, 31-, and 35-gestational-week fetus models were all head down. While both the 20- and 35-week fetus models were in a right occiput posterior (ROP) configuration, the 31-week fetus model was in left occiput anterior (LOA) position, surrounded by maternal tissue, including the placenta and the uterus. The fetal organ and female organ volume adjustments were necessary to match the average reference values reported in ICRP 89 Publication within 1% [38]. The complete fetal anatomy was reviewed by a clinical obstetrician and facility specialist and suggested modification was applied.

## **CHAPTER FOUR: HYBRID OBESE COMPUTATIONAL PREGNANT PHANTOM CONSTRUCTIONS**

The goal of this chapter is to develop hybrid computational overweight and obese pregnant female phantoms. Obesity is defined as having a body mass index of  $30 \text{ kg/m}^2$  and more. This chapter details the efforts undertaken to meet research aim number 5, the construction of overweight phantoms to include: one overweight female model, and three overweight pregnant female models at different gestation ages: 20, 31, and 35 weeks. These models are derived from an ICRP reference female and the whole pregnant female models created in chapter three. This chapter also describes the ultimate aim of this dissertation to meet research aim number 6: four obese models are created: one obese female model and three obese pregnant models at three gestation periods: 20, 31 and 35 weeks. Both the overweight models and the obese models are created by adding different amounts of fat layers underneath the skin. The developed overweight and obese models were voxelized for future dosimetry studies.

### **4.1 PREGNANT FEMALE MODELS COMPLETED**

The pregnant female models as described in chapter 3 are used as a starting point. These pregnant phantoms are based on the ICRP standard female, from which major abdominal soft tissue organs below the diaphragm were removed, the fetus added, and the missing organs carefully restored in the proper location to create pregnant phantom sets. After the fetus was added, the pregnant female phantom was voxelized for future dose calculation.



## 4.2 VOXELIZATION

In order to be able to use the developed pregnant phantom models for future dosimetry calculations, it was important to convert NURBS and polygon mesh surfaces into voxels. The goal of this step was to convert the 3D pregnant female phantom models into discrete voxels and assemble them into a whole-body voxel model, with the help of the Binvox software package [51]. Binvox performs the conversion from a polygonal mesh surface to an object which consists of less than  $1024 \times 1024 \times 1024$  voxels. It is capable of reading 3D model files and of writing the information into voxel files [52]. To cover the entire body, the body was divided into many organs and tissues, as listed in Appendix B. This appendix includes each organ type and its given identity (ID) that was added prior to exporting it from Rhinoceros. Thus, these voxelized organs were already assembled into a whole-body voxel, using Binvox software.

To start the voxelization process, each organ from the female pregnant phantom model was given an ID to create a library of organs and all organs of the female pregnant model were exported from Rhinoceros and saved in a single 3D mesh object wavefront (\*.WRL) file format, a standard file format [50]. This file format represents an object which can convert NURBS surfaces into polygon meshes directly using Rhinoceros software. Binvox software recognizes this wavefront (\*.WRL) file format as an input file and can start the voxelization process. The WRL file format contains all the organ identity and coordinate position information originally assigned to the organs, before exporting the files into WRL file format. The identities (ID) were assigned as reference names to each organ, and a bounding box was built to create a linear box object that encloses the pregnant female phantom model [50]. The process of how to add an ID to each organ is illustrated in Figure 4.1. Due to memory issues, the pregnant female phantom model was

voxelized with 200 voxels per matrix size, which was chosen for most of the pregnant phantom models.

To maintain the smoothness of all surfaces and polygon meshes, the voxelization step was accomplished in several stages. Binvox applies the parity count method and the ray stabbing method for voxelization [52]. The voxel grid size used for each pregnant phantom model is listed in Appendix B. The voxel resolution must be good enough to represent the pregnant phantom anatomy with sufficient accuracy, in order to maintain the shape of the voxelized organs. The pregnant female phantoms developed in this project represented a challenge in the voxelization process. Each fetus and pregnant phantom model are represented with a fairly good resolution. Binvox can change the mesh surface to voxels organ by organ. In order to voxel each organ smoothly and effectively, the organ should have no duplicate surfaces, no naked edges, no gaps, no degenerate faces, and no overall object artifacts. The organs should be on good surfaces or mesh objects before exporting them from Rhinoceros software. The voxelization process can convert the object data format of the 3D mesh geometry into a binary voxelized data file format. The object data file format stores the 3D geometry as vertex position and normal. The faces that make each polygon are defined as a list of vertices. To process this project and, in particular, the voxelization step smoothly and with a relatively short computation time, we used a laptop with CoreI7-7700HQ CPU at 2.80 GHz, a 64-bit operating system, 8 GB of memory, and an FX880M graphics card.

To convert a three-dimensional object from its continuous geometric representation into a set of voxels that shape the original three-dimensional object, each phantom pregnant model was individually voxelized by scanning along the three axes of the coordinate system. Binvox uses two different methods to carry out the voxelization process: the parity count method and the ray

stabbing method [51-52]. The parity count method is used for an open surface, while the ray stabbing method is used for a closed surface.

The parity count method is useful for polygon mesh phantom models and can differentiate between an element volume being inside the element volume or outside of it: an odd number of intersections means that the voxel is inside the model, while an even number of intersections means it is outside surface. The parity count method was also upgraded to work well for polygonal models with various degeneracies, such as cracks or holes in the surface. Because most of the organs developed in this project were carefully checked for any cracks or holes before the voxelization step, in our case, this method was mainly used for open organs, such as the small and large intestines.

Binvox also uses the ray stabbing method for closed surfaces, such as the heart and the brain. The ray stabbing method is used for polygonal models that might cause a problem with the parity count method, such as double-walled building models or ones that have intersecting surfaces or several interpenetrating sub-parts. The ray stabbing method consists in cutting or stabbing the surface in two opposite directions: all voxels that are deep between two different rays are considered to be inside the model, where the parity count method would create an empty interior for such a model [52]. This method works well with voxelizing the skin in the models, which will be discussed later. It differs from the parity count method, however, in the way it interprets the depth samples of rays because the ray stabbing method only retains the first and last depth sample along each ray. More details on the voxelization algorithms can be found in this reference [52].

An example of the voxelization input of lungs is shown in Figure 4.1. It illustrates how to extract the bounding box information for a given right and left lung organ's ID. Binvox also has a nice feature to visually see and check the voxelized phantom generated with Binvox extension

only (\*. binvox). Because it was important to check the pregnant model in detail, the Binvox file extension was important in reviewing the model. If the voxelization process was successfully accomplished using Binvox file format, a \*.RAW file was generated as a final output file, following the input shown in Figure 4.2. This proved to be the most effective way to check the final voxelization output file. It is worth noting that using the maximum voxel resolution of 1024 was not very effective and could be processed due to memory issues. To solve this issue, the voxel resolution was changed to a 200 x 200 x 200 voxel so that it would be possible to voxelize smoothly and to review the final pregnant female phantom models effectively as shown in Figure 4.3. Figure 4.4, and Figure 4.5 illustrate the back, front and side views of the voxelized ICRP reference female, 20, 31, and 35-week pregnant female models.

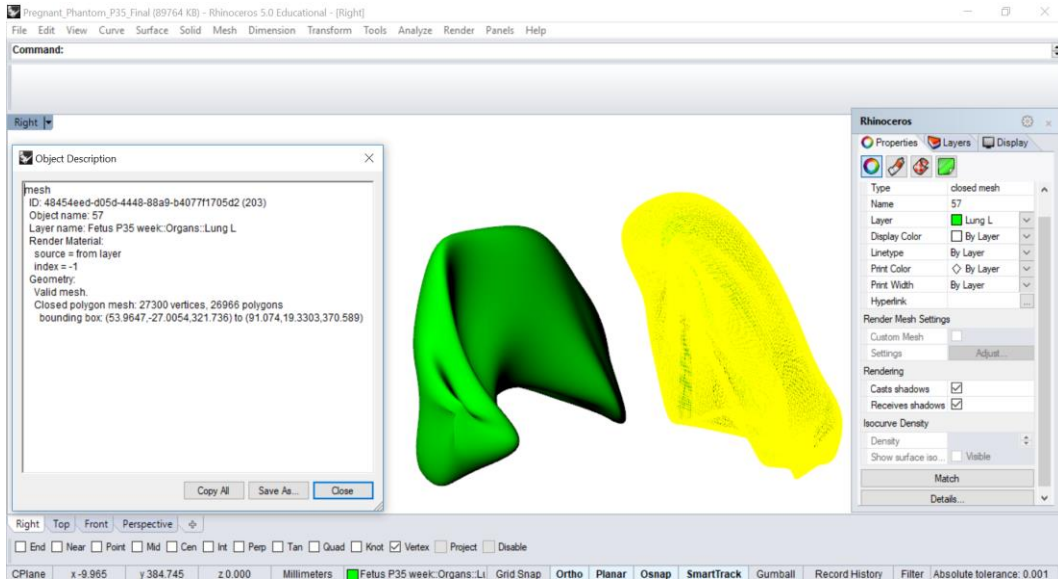
## **4.2 OVERWEIGHT AND OBESE PREGNANT FEMALE PHANTOM**

An individual is classified as overweight if they have a body index (BMI) range between 25 and 29.9 kg/m<sup>2</sup>, while a BMI range between 30 and 39.9 kg/m<sup>2</sup> is considered obese [2].

There are two types of fat: subcutaneous (SAT), which is external fat underneath the skin, and visceral (VAT), which is fat surrounding the internal abdominal organs. The overweight and obese pregnant female phantom, which is the main and ultimate goal of this dissertation project, were created by modifying the finished female pregnant model. As mentioned earlier, the pregnant female masses and height were matched to the average ICRP female reference values defined by the ICRP 89 Publication [18].

A total of eight new overweight and obese phantoms were developed with different BMI values. These phantoms were produced using Rhinoceros software by adding fat underneath the original skin, and by binding them together as one thick fat layer surrounding the skin, using several tools this software offers. The SAT fat was mainly added under the abdominal skin and thigh skin areas. Figure 4.6 and Figure 4.7 show the side and top views of the ICRP reference female, the overweight female, and the obese female phantom models. Table 4.1 shows the weight classifications of the newly generated phantom models, including the ICRP reference female, the overweight female, and the obese female phantom weight. The height of these new models was kept the same as the ICRP reference female value (168 cm). This table also included the BMI of the 20-, 31-, and 35-weeks pregnant female model, the overweight and the obese pregnant female weights. The female organs were kept the same and no change was made toward their organ mass, except in the external boundary, which is the skin. Figure 4.8, Figure 4.9 and Figure 4.10 show the front, side, and top views of the ICRP reference female, the overweight female, and the obese female of the 20-weeks pregnant phantom models. Figure 4.11, Figure 4.12 and Figure 4.13 show the front, side, and top views of the ICRP reference female, the overweight female, and the obese female of the 31-weeks pregnant phantom models. Figure 4.14, Figure 4.15 and Figure 4.16 show the front, side, and top views of the ICRP reference female, the overweight female, and the obese female of the 35-weeks pregnant phantom models.

(a)



(b)

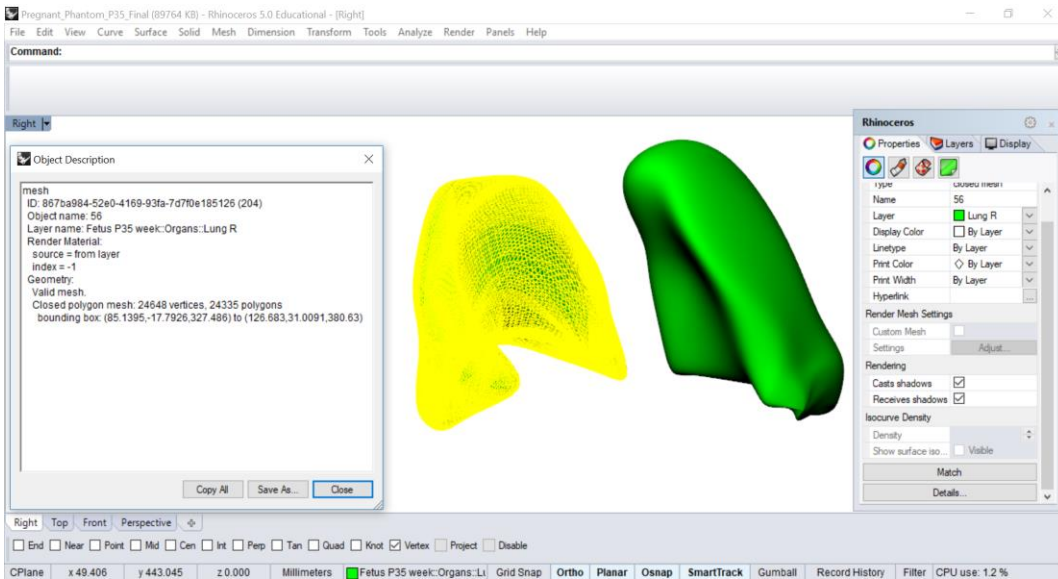


**Figure 4.1** An example of the left lung at 35 weeks of gestation, in a closed polygon mesh after it has been given (a) an identity of 57 and a it's bounding box, and (b) an identity of 56 and it's bounding box.

(a)

```
Command Prompt
-cb: center model inside unit cube
-rotx: rotate object 90 degrees ccw around x-axis before voxelizing
-rotz: rotate object 90 degrees cw around z-axis before voxelizing
  both -rotx and -rotz can be used multiple times
-aw: _also_ render the model in wireframe (helps with thin parts)
-fit: only write the voxels in the voxel bounding box
-bi <id>: when converting to schematic, use block ID <id>
-down: downsample voxels by a factor of 2 in each dimension (can be used multiple times)
-dmin <nr>: when downsampling, destination voxel is on if >= <nr> source voxels are (default 4)
Supported 3D model file formats:
  VRML V2.0: almost fully supported
  UG, OBJ, OFF, DXF, XGL, POV, BREP, PLY, JOT: only polygons supported
Example:
binvox -c -d 200 -t mira plane.wrl

C:\Users\makki\Desktop\Binvox\vox_package> binvox -d 212.576 -c -v 57195.42.WRL

--- [binvox] mesh voxelizer, version 1.17, build #586 on 2012/11/11 18:48:05
--- written by Patrick Min, 2004-2012

  using carving method only
  using parity voting method only
you specified both carving and voting method (which is the default)
loading model file...
MeshFileIdentifier::~create_mesh_file(57195.42.WRL)
error: unrecognized first line in VRML file [pju]
  Is the model file in the same directory as binvox?

C:\Users\makki\Desktop\Binvox\vox_package> binvox -d 195.42 -c -v 57.WRL
```

(b)

```
Command Prompt
-c: z-buffer based carving method only
-dc: dilated carving, stop carving 1 voxel before intersection
-v: z-buffer based parity voting method only (default is both -c and -v)
-e: exact voxelization (any voxel with part of a triangle gets set)(does not use graphics card)
Additional parameters:
  -bb <minx> <miny> <minz> <maxx> <maxy> <maxz>: force a different input model bounding box
  -ri: remove internal voxels
  -cb: center model inside unit cube
  -rotx: rotate object 90 degrees ccw around x-axis before voxelizing
  -rotz: rotate object 90 degrees cw around z-axis before voxelizing
    both -rotx and -rotz can be used multiple times
  -aw: _also_ render the model in wireframe (helps with thin parts)
  -fit: only write the voxels in the voxel bounding box
  -bi <id>: when converting to schematic, use block ID <id>
  -down: downsample voxels by a factor of 2 in each dimension (can be used multiple times)
  -dmin <nr>: when downsampling, destination voxel is on if >= <nr> source voxels are (default 4)
Supported 3D model file formats:
  VRML V2.0: almost fully supported
  UG, OBJ, OFF, DXF, XGL, POV, BREP, PLY, JOT: only polygons supported
Example:
binvox -c -d 200 -t mira plane.wrl

C:\Users\makki\Desktop\Binvox\vox_package>viewvox 56.binvox
```

(c)

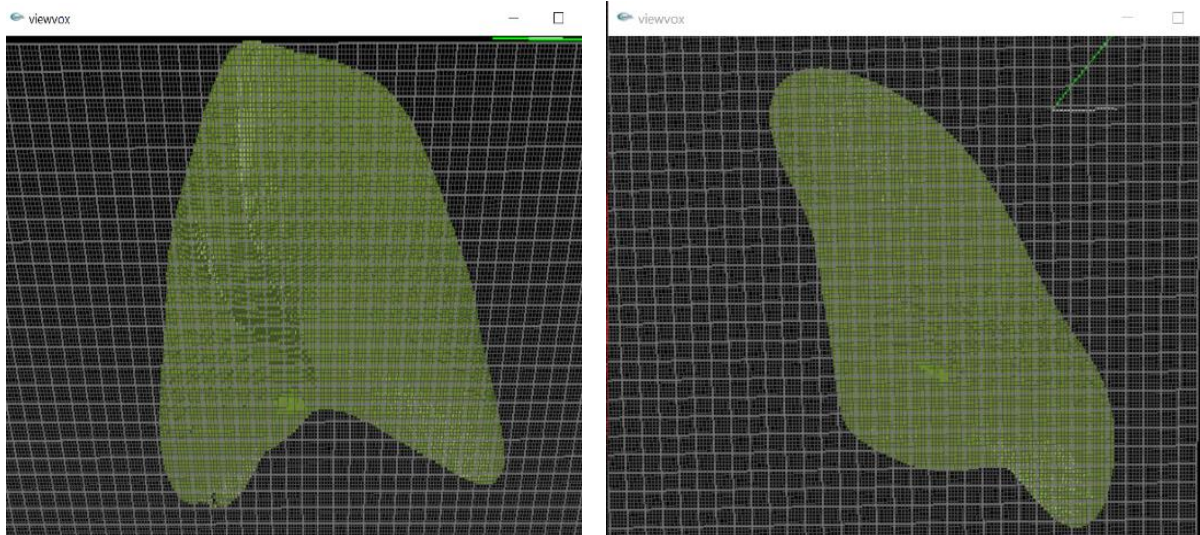


**Figure 4.2** The same example of the left lung at 35 weeks of gestation, in a closed polygon mesh, after it has been given (a) a Binvox command prompt of the left lung, as an example of the left lung voxelization process, using the same ID and maximum voxel resolution calculated from its bounding box, and (b) a Viewvox command prompt, in order to visualize and check the initial voxelization step in (a). (c) The output result from step (b), showing the resulting voxelized left and right lungs, repeating the steps outlined above.



**Table 4.1 The weight classifications of ICRP reference model and female pregnant phantoms, excluding fetus weight.**

<b>Female Weight Classification (no fetus weight included)</b>	<b>Weight (Kg)</b>	<b>BMI (Kg/m<sup>2</sup>)</b>
ICRP Female Model	60.00	22.58
Overweight Female Model	76.70	28.87
Obese Female Model	90.01	33.88
Overweight 20 week Female Pregnant Model	75.80	28.53
Obese 20 week Female Pregnant Model	90.01	33.88
Overweight 31 week Female Pregnant Model	76.14	28.66
Obese 31 week Female Pregnant Model	88.57	33.34
Overweight 35 week Female Pregnant Model	76.12	28.65
Obese 35 week Female Pregnant Model	90.97	34.24

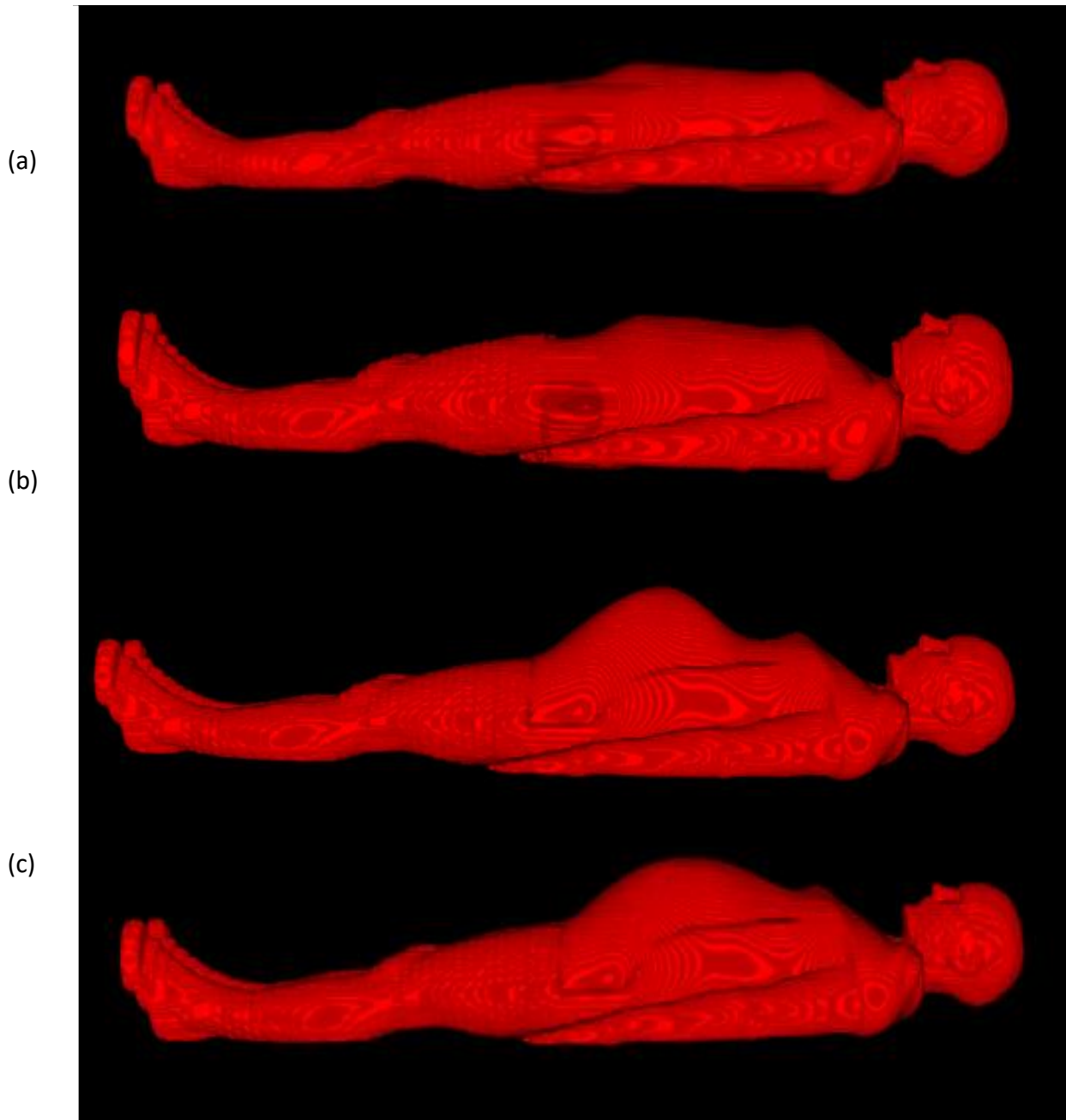
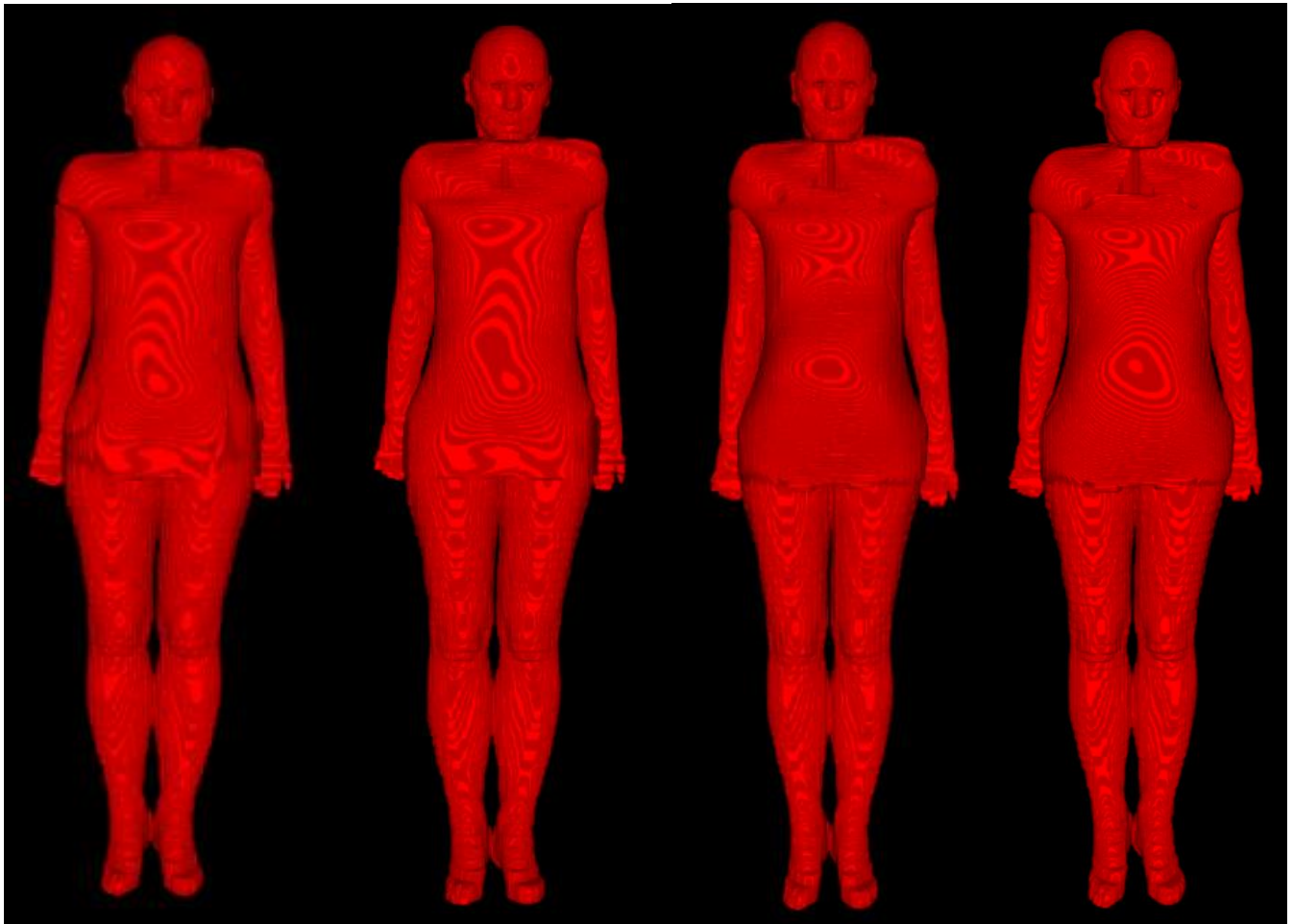


**Figure 4.3** The side and original orientation of the voxelized pregnant female phantom series, using ImageJ 3D viewer. (a) ICRP female phantom, (b) 20-weeks pregnant phantom, (c) 31-weeks pregnant phantom, (d) 35-weeks pregnant phantom.



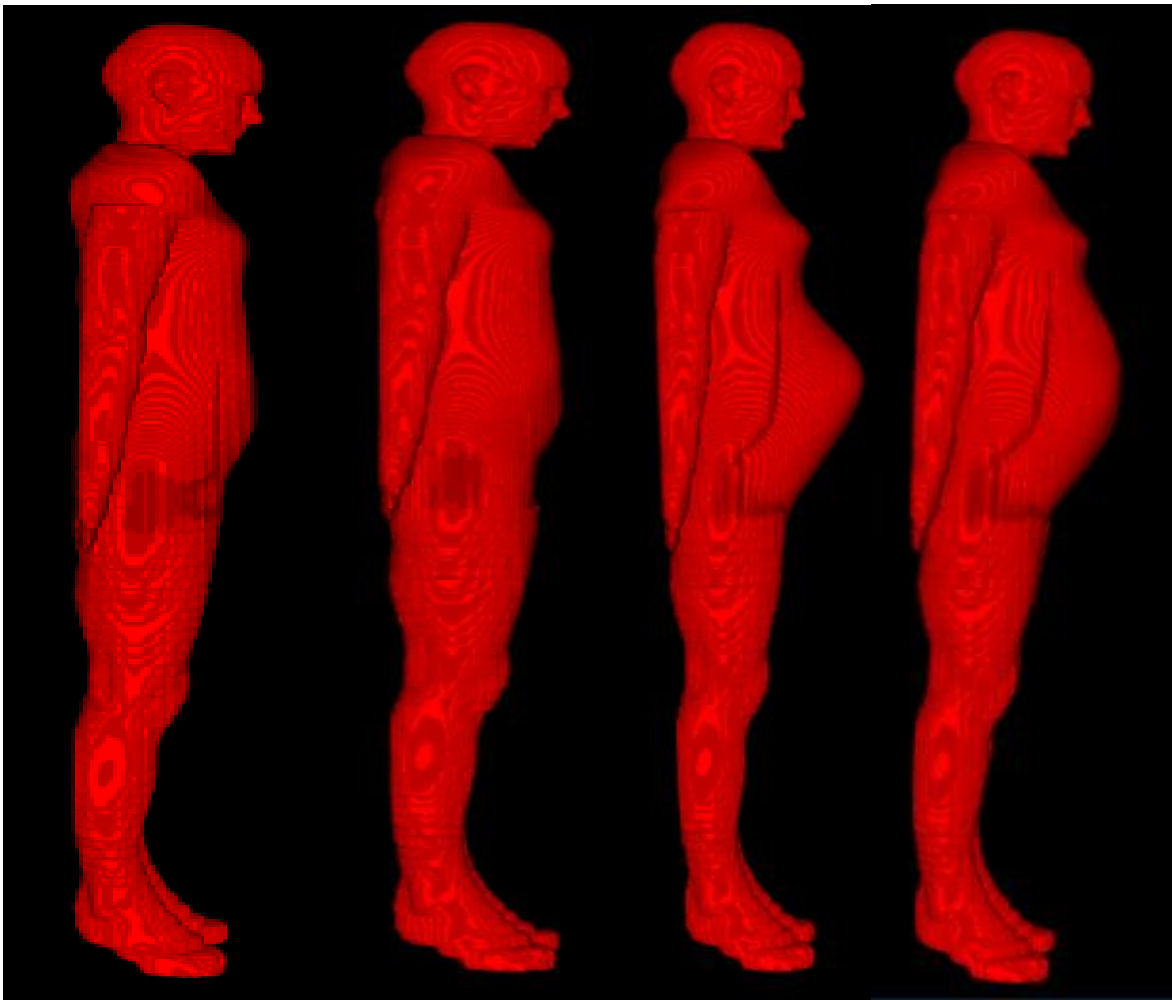
(a)

(b)

(c)

(d)

**Figure 4.4 Frontal views of voxelized pregnant female phantom series, using ImageJ 3D viewer. (a) ICRP female phantom, (b) 20-weeks pregnant phantom, (c) 31-weeks pregnant phantom, (d) 35-weeks pregnant phantom.**



(a)

(b)

(c)

(d)

**Figure 4.5 Side views of the voxelized pregnant female phantom series, using ImageJ 3D viewer. (a) ICRP female phantom, (b) 20-weeks pregnant phantom, (c) 31-weeks pregnant phantom, (d) 35-weeks pregnant phantom.**

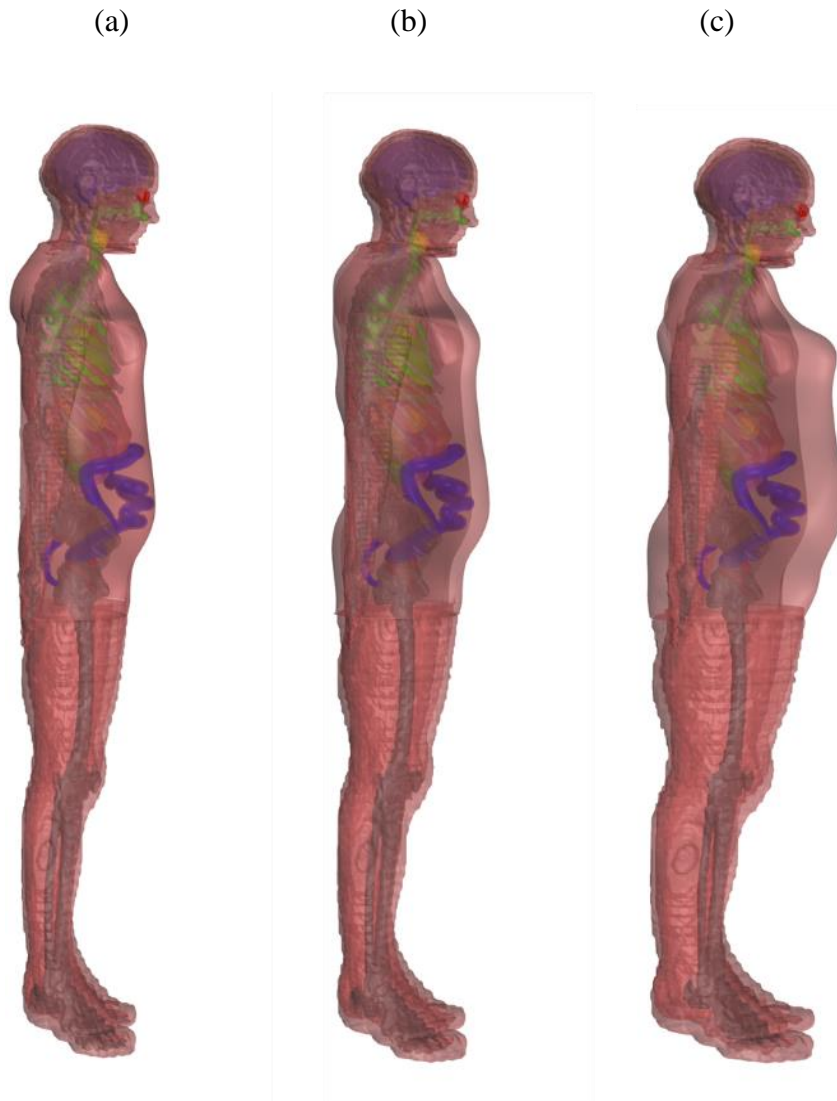
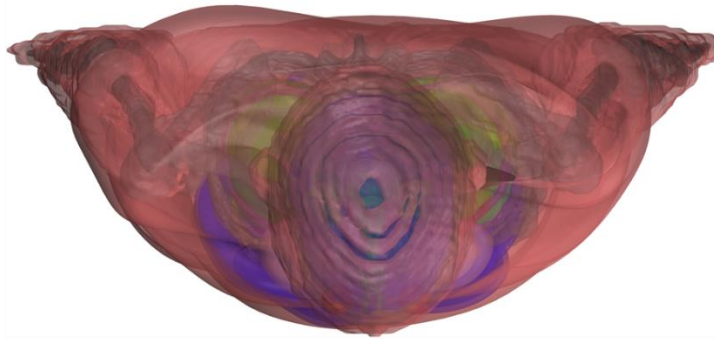
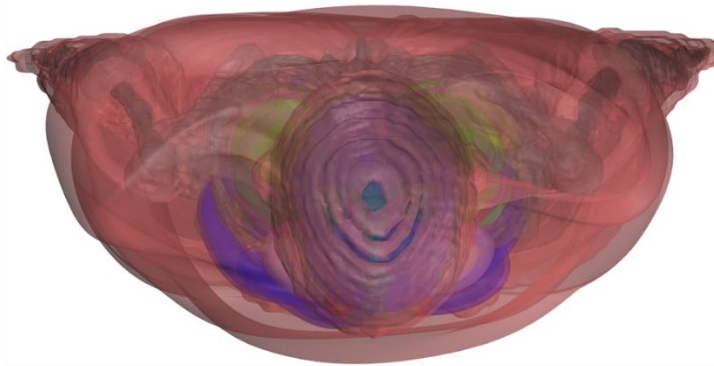


**Figure 4.6 Side view ICRP reference female phantom series. (a) ICRP female phantom, (b) Overweight female phantom (c) Obese pregnant phantom.**

(a)



(b)



(c)

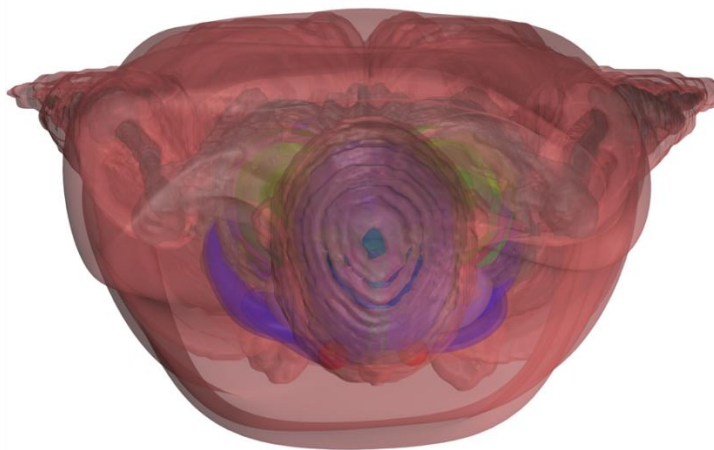


**Figure 4.7** Top views of the ICRP reference female phantom series. (a) ICRP female phantom, (b) Overweight female phantom (c) Obese pregnant phantom.

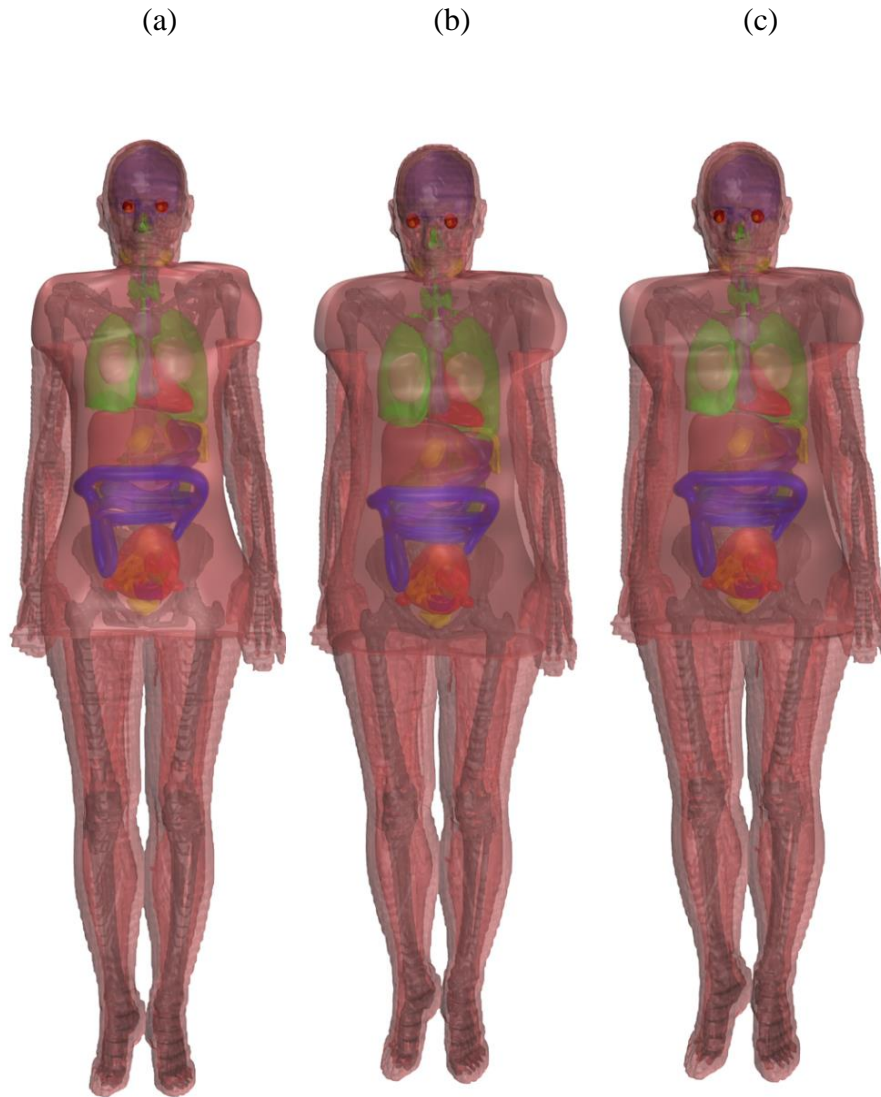


**Figure 4.8 Frontal views of 20-weeks voxelized pregnant female phantom series. (a) ICRP pregnant phantom, (b) Overweight pregnant phantom, (c) Obese pregnant phantom.**

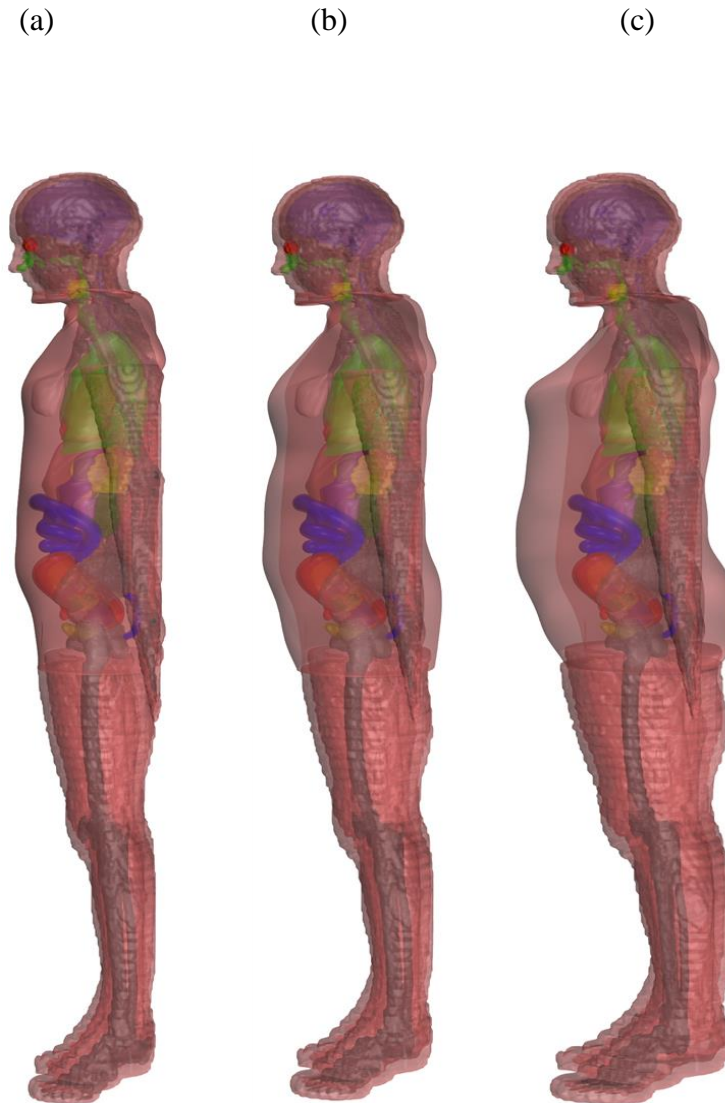


**Figure 4.9** Side views of 20-weeks voxelized pregnant female phantom series. (a) ICRP pregnant phantom, (b) Overweight pregnant phantom, (c) Obese pregnant phantom.



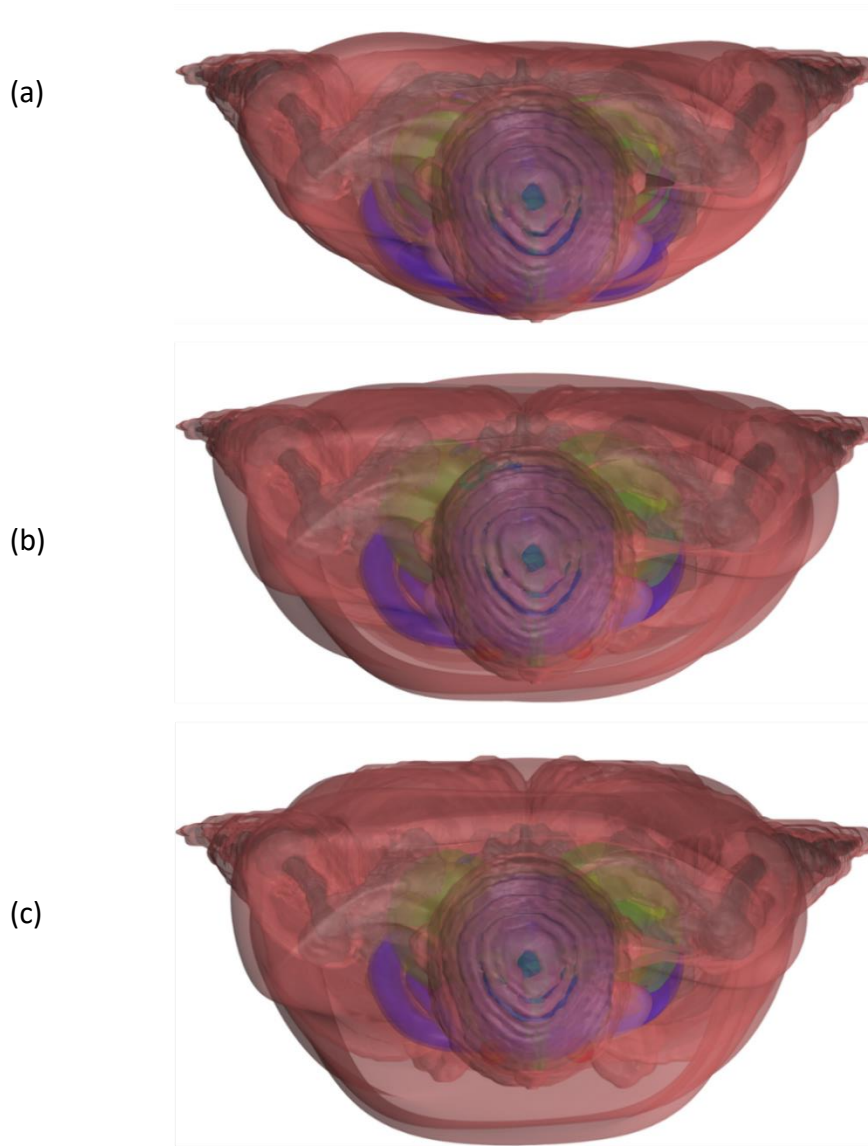


**Figure 4.10 Top views of voxelized 20-week pregnant female phantom series. (a) ICRP pregnant phantom, (b) Overweight pregnant phantom, (c) Obese pregnant phantom.**

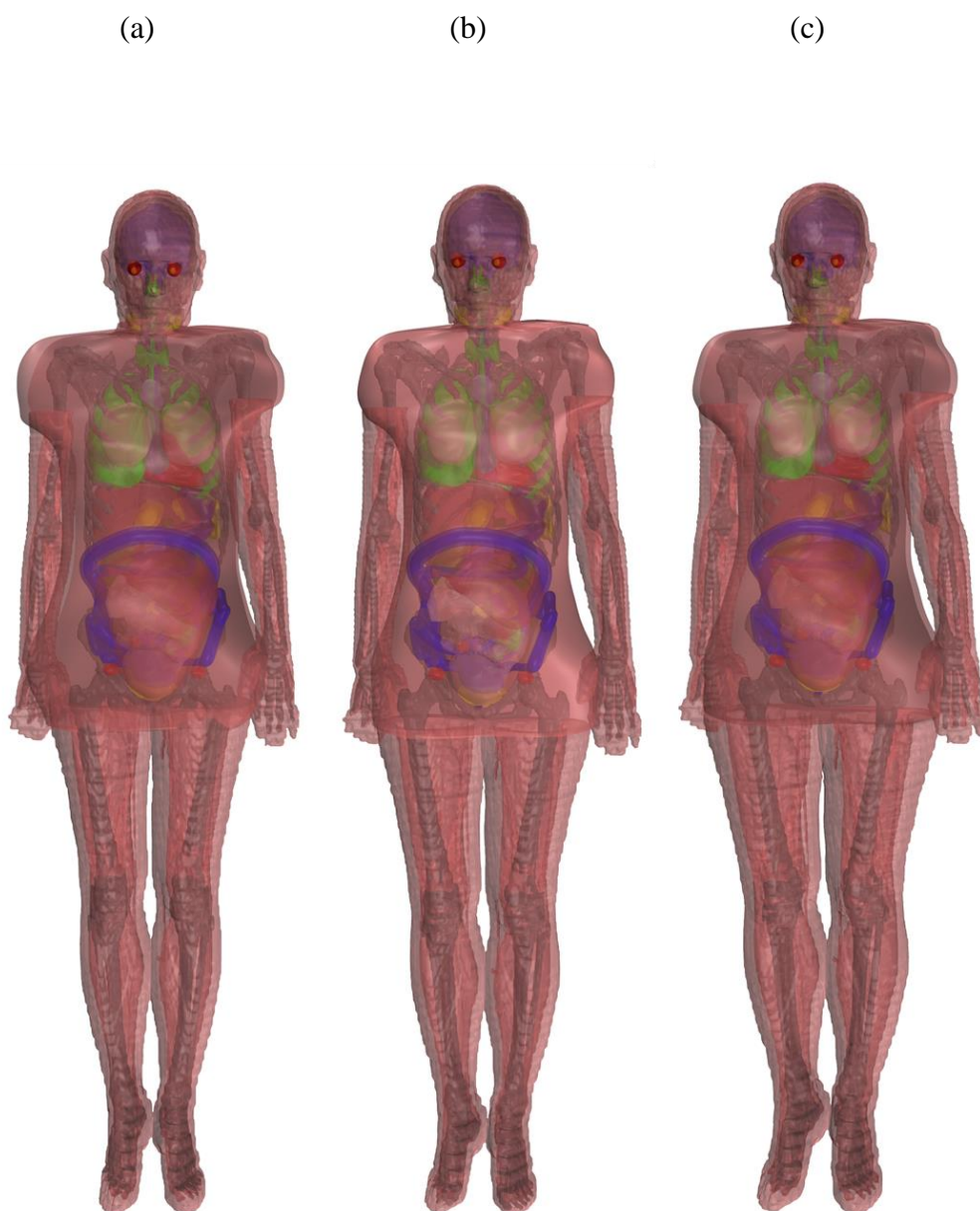


**Figure 4.11 Front views of 31-weeks voxelized pregnant female phantom series. (a) ICRP pregnant phantom, (b) Overweight pregnant phantom, (c) Obese pregnant phantom.**

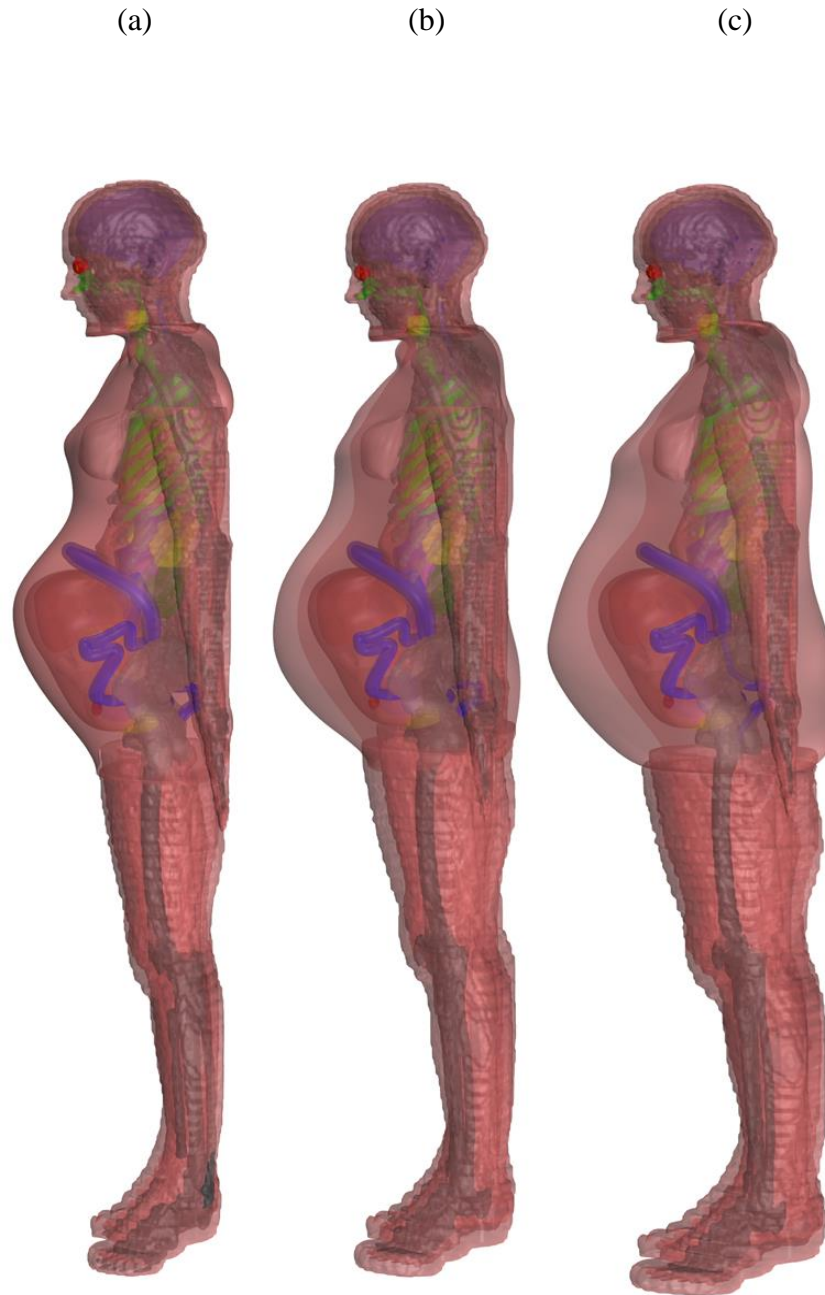


**Figure 4.12 Side views of 31-weeks pregnant female phantom series. (a) ICRP female phantom, (b) 20-weeks pregnant phantom, (c) 20-weeks overweight pregnant phantom.**

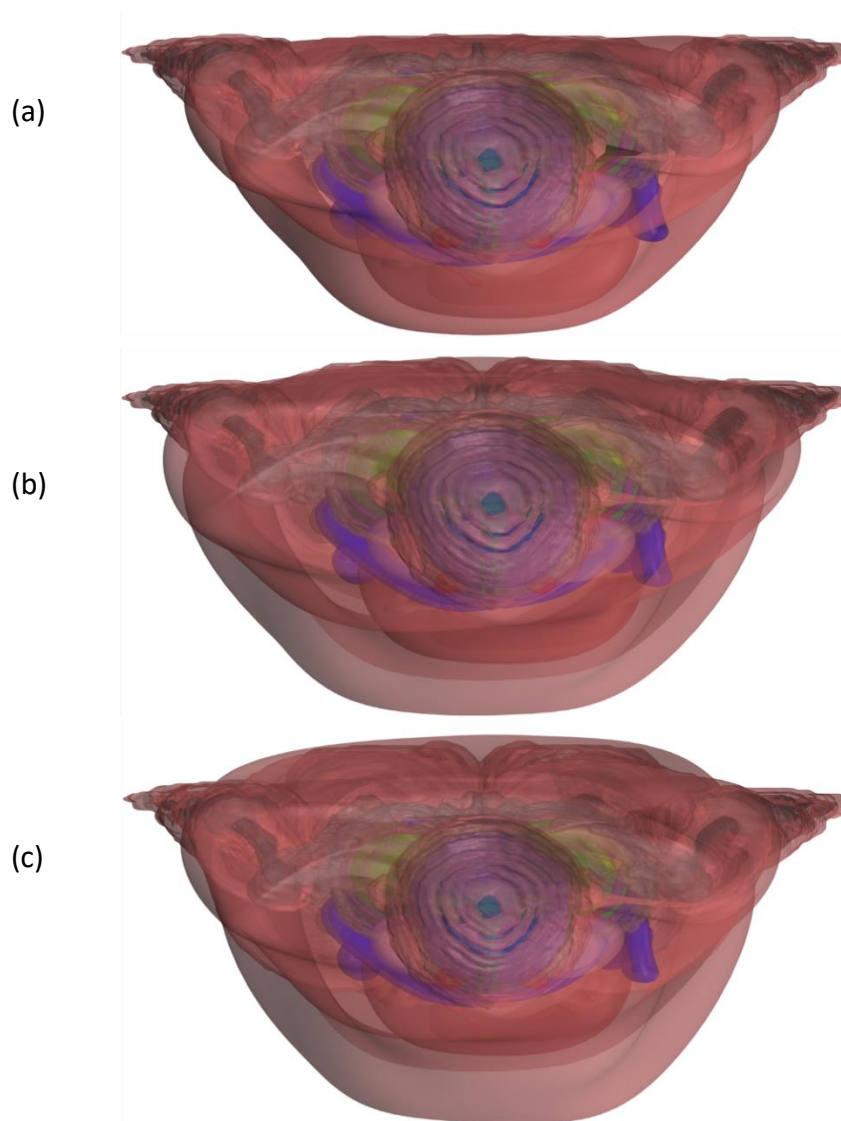


**Figure 4.13** Top views of 31-weeks voxelized pregnant female phantom series. (a) ICRP pregnant phantom, (b) Overweight pregnant phantom, (c) Obese pregnant phantom.

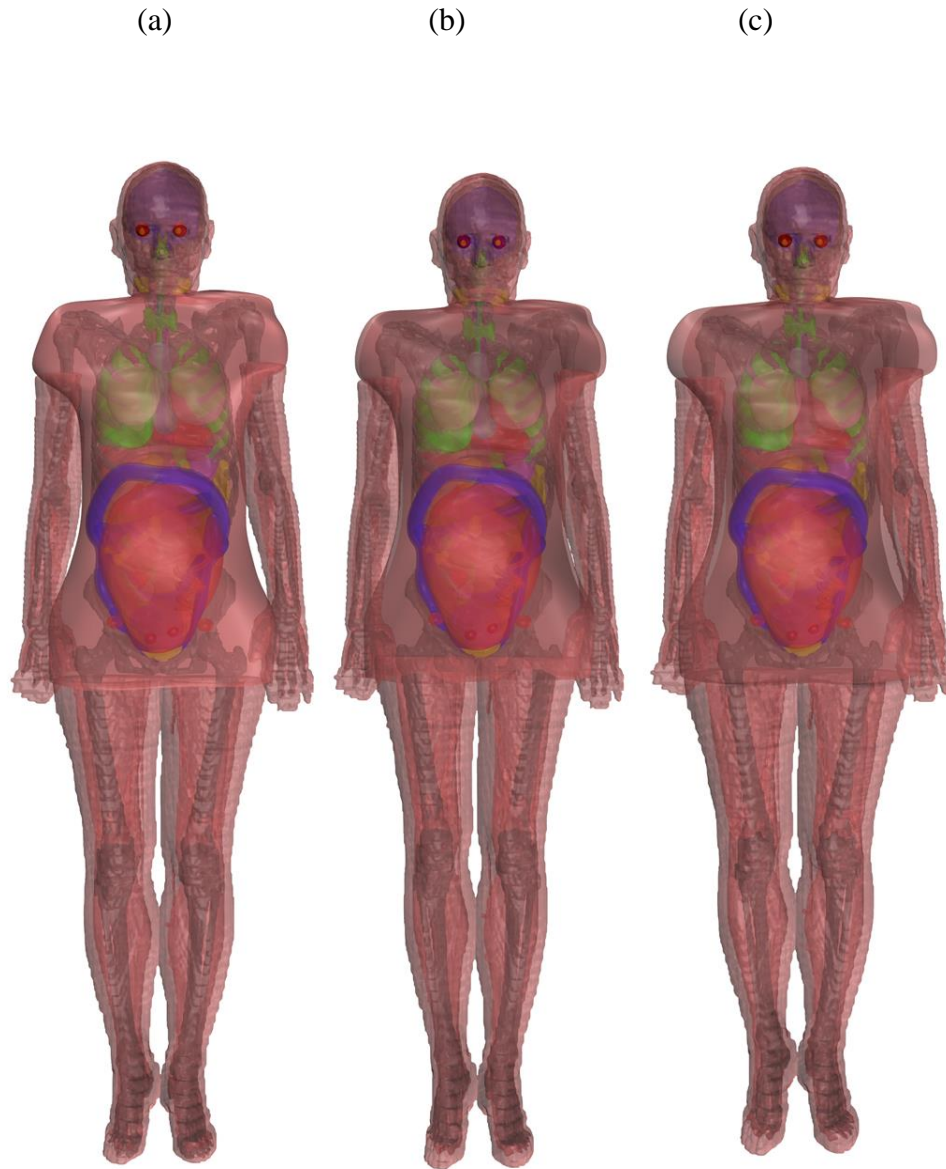


**Figure 4.14 Front views of 35-weeks voxelized pregnant female phantom series. (a) ICRP pregnant phantom, (b) Overweight pregnant phantom, (c) Obese pregnant phantom.**

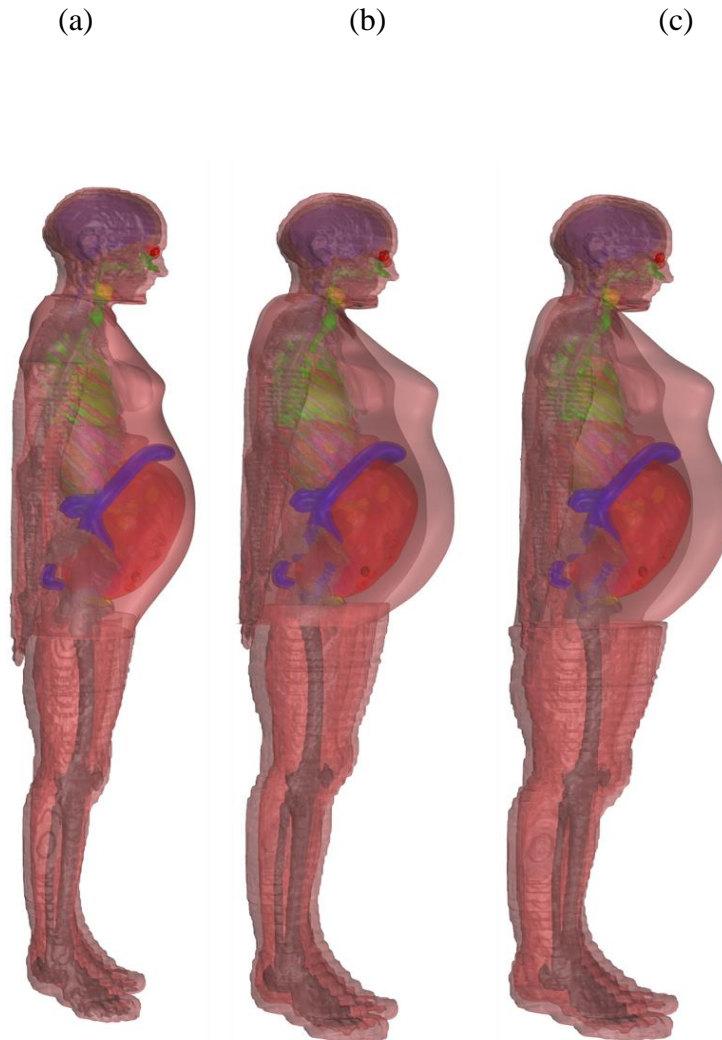


**Figure 4.15 Front views of 35-weeks voxelized pregnant female phantom series. (a) ICRP pregnant phantom, (b) Overweight pregnant phantom, (c) Obese pregnant phantom.**

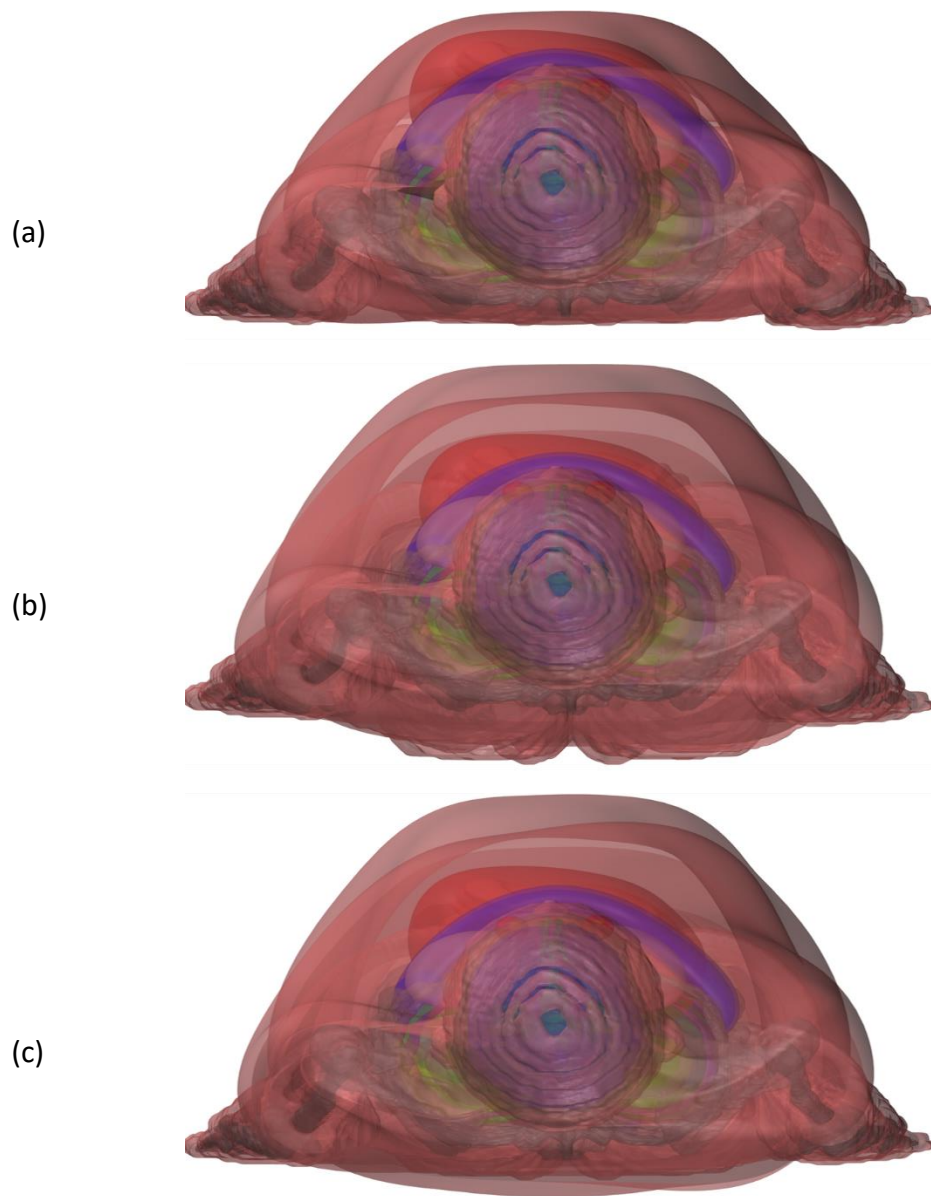


**Figure 4.16 Top views of voxelized 35-week pregnant female phantom series. (a) ICRP pregnant phantom, (b) Overweight pregnant phantom, (c) Obese pregnant phantom.**

## **CHAPTER FIVE: CONCLUSION AND FUTURE WORK**

### **5.1 CONCLUSION**

This dissertation research presents the development of realistic hybrid obese pregnant female phantoms at three different gestational stages. In order to achieve this aim, three realistic computational fetus phantom models, derived from human pregnant patients, were developed at 20, 31 and 35 weeks of gestation. Each phantom developed in this study represents the reference data from the ICRP 89 Publication. An adult ICRP reference female computational model was also constructed in order to build computational overweight and obese pregnant model sets by taking into consideration all the factors that can contribute to the fetal dose. Such factors include the weight a patient has gained, patient body changes, fetal development, fetal position, and the detailed anatomy of the fetus inside the patient's body, which can be accomplished using radiological images of pregnant patients. US data has also been used to reflect the detailed patient body, which can lead to designing realistic model sets that are specific to the standard pregnant computational phantom series and to the obese pregnant computational phantom series. Thus, the field of medical physics can rely on them in the future when estimations regarding the fetal dose are made in order to avoid any future cancer in the patient or the fetus. Below is a short project description of each chapter included in this dissertation.

Chapter One is an introduction that illustrates the specific goals of this research. It describes the previous pregnant phantoms, their classifications, and their limitations. It highlights the principal effects of ionization radiation on the fetus during pregnancy and explains why it is



essential to develop these hybrid computational phantoms. It also shows the common diagnostic imaging modalities during pregnancy.

Chapter Two describes the detailed procedure for developing hybrid fetal computational models. The process starts with segmenting the fetal organs and creating NURBS surface models for most fetal organs and tissues. A total of 29 fetal organs and tissues were identified from real imaging sets of pregnant patients. The NURBS and polygon mesh surface geometries are carefully described in this chapter. The fetal organ and tissue masses were modified to match the reference organ masses. Therefore, each fetal hybrid phantom represents the realistic human fetal anatomy and fetal position inside the uterus. The masses of fetal soft tissue and organs were matched with the ICRP reference values provided in ICRP 89 Publication. The hybrid fetal computational models accurately reflect the existing ICRP reference data and can be useful in evaluating radiation doses to the fetus and in estimating the risk for the pregnant patient who is seeking radiotherapy or diagnostic imaging procedures where realistic fetal computational human-based phantoms are required. These newly developed fetus models can also be used for radiation protection purposes, to expand the current definition of the fetal references of a given fetal population concerning the change in body weight.

Chapter Three describes how an adult ICRP reference female was used to construct the pregnant female phantom. The female reference model comes in voxels, which were converted into NURBS or mesh surface models for further surface modifications and manipulations. A total of 35 different organs and tissues were identified from the reference voxel female model. The three hybrid computational fetus phantoms were individually added to the adult ICRP reference female NURBS surface or polygon mesh model to create three realistic hybrid computational pregnant phantom models. Some maternal organs were either modified or remodeled with the help of

radiological images sets. The masses of maternal organs and tissues were re-matched with ICRP reference values (their original voxel model). The three standard pregnant phantoms were finally converted into voxels for future radiation transport study. It is important to mention that the new pregnant female phantom models created in this study represent improvements in the anatomical representation of the developing fetus, particularly with respect to individual fetal soft tissue and organs for each fetus model, because they are constructed from real radiological image sets from pregnant patients for each gestational period. In addition, no scaling method on the fetus phantom set was used for this study, which makes the final fetus models more realistic and reliable. Since radiological image guides were used in this project, these new pregnant female phantoms also account for natural changes in maternal organ masses and positions.

Chapter Four summarizes the steps necessary to voxelize the pregnant phantom models. It also includes the steps necessary to build a skin for each model and to voxelize it accordingly. Overweight and obese pregnant phantom models are also addressed in this chapter, by adding layers of fat to the skin, except in the eye regions. This process required considerable software and programming in order to successfully build the obese pregnant phantom models.

The complete steps for developing computational obese phantom models are described in Table 3.4. A comparison table of the total organ segmentation of this work as well as of the previous pregnant phantom is presented in Appendix A. The voxelized phantom models' information is listed in Appendix B. Selected published abstracts and awards are listed in Appendix C. The completed fetus phantom set, the female phantom, and the pregnant phantom sets are depicted in Figure 2.6, 3.3, and 4.1. Figure 3.4 represents the steps necessary to add the developing fetus phantoms inside the mother's uterus to create the pregnant phantom model sets. The total body masses of the fetus models, matched with ICRP reference data with a percentage error of less

than 2%, are listed in Tables 2.1 and 2.2. ICRP reference mass volumes and densities of the computational female phantom are listed in Table 3.1. Fetal body compositions of the developed computational fetus phantom set are listed in Table 3.2. The total body mass of fetus models are matched with ICRP reference data with a percentage error of less than 2%, as listed in Tables 3.3, 3.4, and 3.5.

This project was carried out in approximately three years, given that the medical images used for this dissertation project were and still are very difficult to obtain and were approved under IRB protocol in order to complete this project. The three realistic fetus phantom ages were solely based on what was available in the archive. It took approximately three to four months to finish the segmentation task in each fetus model, and about one year to finish creating the surface modeling, which also required focused work and time.

## **5.2 FUTURE WORK**

These new hybrid computational pregnant phantoms can be used in dose evaluations to the fetus and pregnant patient for internal or external radiation dosimetry studies. They can also be used in radiation protection, diagnostic imaging, and radiation therapy applications. The phantoms are based on real medical images; therefore, they represent the realistic anatomy of the human pregnant patient body. The three hybrid fetus phantoms include spine skeletons only because CT medical images for pregnant patients were limited and normally, the fetuses were shielded during diagnostic imaging and radiation therapy procedures.

The first future clinical application of this project is to compare the finished fetus models with an existing CT model for fetal dose reconstruction and risk assessment study. Another future examination would be to apply different fetal positions and orientations in utero, and study how these changes would affect fetal dose estimates. Automatic segmentation and machine learning applications can be studied since the treatment plan system (TPS) lacks identifying the anatomy organs of the fetus. This application would save a lot of time and labor work for dosimetrist and physicist and could decrease the variation raised from the manual segmentation.

The obese pregnant female models can be used to study the effect of image quality and radiation dosage in various diagnostic image modalities, such as external radiation (CT scan) or internal radiation (PRT CT or DPRCT), which can be accomplished with Monte Carlo simulation. They can also be used to check the existing protocol used for the obese patient in order to potentially decrease the doses to healthy organs.

## REFERENCES

- [1] T. Kulie, A. Slattengren, J. Redmer, H. Counts, A. Eglash, S. Schragger, “Obesity and Women’s Health: An Evidence-Based Review.,” *J. Am. Board Fam. Med.*, vol. 24, no. 1, pp. 75–85, Jan. 2011.
- [2] A. Ding, M. M. Mille, T. Liu, P. F. Caracappa, and X. G. Xu, “Extension of RPI-adult male and female computational phantoms to obese patients and a Monte Carlo study of the effect on CT imaging dose.,” *Phys. Med. Biol.*, vol. 57, no. 9, pp. 2441–59, May 2012.
- [3] S. James, P. Matsangas, D. Connelly, “Knowledge of Obesity Risks and Women’s Health: What do we know?.,” *Invest Gynecol Res Women’s Heal.*, vol. 1, no. 1, pp. 1–6, 2017.
- [4] B. Rimawi, V. Green, and M. Lindsay, “Fetal Implications of Diagnostic Radiation Exposure During Pregnancy : Recommendations.,” *Clin. Obstet.*, vol. 59, no. 2, pp. 412–418, 2016.
- [5] M. Stovall, C. Blackwell, J. Cundiff, D. Novack, J. Palta, L. Wagner, E. Webster, and R. Shalek, “Fetal dose from radiotherapy with photon beams: report of AAPM Radiation Therapy Committee Task Group No. 36.,” *Med. Phys.*, vol. 22, no. 1, pp. 63–82, Jan. 1995.
- [6] C. Geng, M. Moteabbed, J. Seco, Y. Gao, X. Xu, J. Ramoss-Mendez, B. Faddegon, H. Paganetti, “Dose assessment for the fetus considering scattered and secondary radiation from photon and proton therapy when treating a brain tumor of the mother.,” *Phys. Med. Biol.*, vol. 61, no. 2, pp. 683–695, 2016.
- [7] S. F. Kry, D. Followill, R. A. White, M. Stovall, D. A. Kuban, and M. Salehpour, “Uncertainty of calculated risk estimates for secondary malignancies after radiotherapy.,” *Int. J. Radiat. Oncol. Biol. Phys.*, vol. 68, no. 4, pp. 1265–71, Jul. 2007.
- [8] B. Bednarz and X. G. Xu, “A feasibility study to calculate unshielded fetal doses to pregnant patients in 6-MV photon treatments using Monte Carlo methods and anatomically realistic phantoms,” *Med. Phys.*, vol. 35, no. 7, pp. 3054–3061, 2008.
- [9] A. Owrangi, D. Roberts, E. Covington, J. Hayman, K. Masi, C. Lee, J. Moran, and J. Prisciandaroa, “Revisiting fetal dose during radiation therapy: Evaluating treatment techniques and a custom shield,” *J. Appl. Clin. Med. Phys.*, vol. 17, no. 5, pp. 34–46, 2016.
- [10] E. Pantelis, C. Antypas, M. Frassanito, L. Sideri, K. Salvara, L. Lekas, O. Athanasiou, M. Piperis, N. Salvaras, and P. Romanelli, “Radiation dose to the fetus during CyberKnife radiosurgery for a brain tumor in pregnancy,” *Phys. Medica*, vol. 32, no. 1, pp. 237–241, 2016.
- [11] S. F. Kry, G. Starkschall, J. A. Antolak, and M. Salehpour, “Evaluation of the accuracy of fetal dose estimates using TG-36 data.,” *Med. Phys.*, vol. 34, no. 4, pp. 1193–1197, 2007.
- [12] R. M. Howell, S. B. Scarboro, S. F. Kry, and D. Z. Yaldo, “Accuracy of out-of-field dose calculations by a commercial treatment planning system.,” *Phys. Med. Biol.*, vol. 55, no.

- 23, pp. 6999–7008, 2010.
- [13] M. Mazonakis, A. Tzedakis, and J. Damilakis, “Monte Carlo Simulation of Radiotherapy for Breast Cancer in Pregnant Patients: How to Reduce the Radiation Dose and Risks to Fetus?,” *Radiat. Prot. Dosimetry.*, vol. 175, pp. 10–16, Sep. 2016.
- [14] C. Lee and J. Lee, “Computational anthropomorphic phantoms for radiation protection dosimetry: evolution and prospects,” *Nucl. Eng. Technol.*, vol. 38, pp. 239–250, 2006.
- [15] X. G. Xu, V. Taranenkov, J. Zhang, and C. Shi, “A boundary-representation method for designing whole-body radiation dosimetry models: pregnant females at the ends of three gestational periods--RPI-P3, -P6 and -P9.,” *Phys. Med. Biol.*, vol. 52, no. 23, pp. 7023–44, Dec. 2007.
- [16] H. Zaidi and B. M. W. Tsui, “Review of Computational Anthropomorphic Anatomical and Physiological Models,” *Proc. IEEE*, vol. 97, no. 12, pp. 1938–1953, Dec. 2009.
- [17] M. G. Stabin, E.E. Watson, M. Cristy, J.C. Ryman, K.F. Eckerman, J.L. Davis, D. Marshall, and M.K. Gehlen, “Mathematical models and specific absorbed fractions of photon energy in the nonpregnant adult female and at the end of each trimester of pregnancy,” Oak Ridge National Laboratory, May. 1995.
- [18] ICRP, “Basic anatomical and physiological data for use in radiological protection: reference values ICRP Publication 89,” *Annals ICRP*, Oxford: Pergamon, vol. 32, 2002.
- [19] J. Chen, “Mathematical models of the embryo and fetus for use in radiological protection,” *Health Phys.*, vol. 86, no. 3, pp. 285–295, 2004.
- [20] X. Xu and K. Eckerman, *Handbook of anatomical models for radiation dosimetry.*, vol. 143, pp. 1-721, 2010.
- [21] J. Becker, M. Zankl, U. Fill, and C. Hoeschen, “Katja — the 24th week of virtual pregnancy for dosimetric calculations,” *Polish J. Med. Phys. Eng.*, vol. 14, no. 1, pp. 13–19, 2009.
- [22] C. Shi, X. Xu, “Development of a 30-week-pregnant female tomographic model from computed tomography (CT) images for Monte Carlo organ dose calculations,” *Med. Phys.*, vol. 31, no. 9, pp. 2491–7, Sep. 2004.
- [23] R. Cech, N. Leitgeb, and M. Pediaditis, “Fetal exposure to low frequency electric and magnetic fields,” *Phys. Med. Biol.*, vol. 52, no. 4, pp. 879–888, 2007.
- [24] S. Nagaoka, T., Togashi, T., Saito, K., Takahashi, M., Ito, K., Ueda, T., Osada, H., Ito, H., Watanabe, “An anatomically realistic voxel model of the pregnant woman and numerical dosimetry for a whole-body exposure to RF electromagnetic fields,” *Annu. Int. Conf. IEEE Eng. Med. Biol. - Proc.*, pp. 5463–5467, 2006.
- [25] K. Akimoto, S., Nagaoka, T., Saito, K., Watanabe, S., Takahashi, M., Ito, “Comparison of SAR in realistic fetus models of two fetal positions exposed to electromagnetic wave from business portable radio close to maternal abdomen,” in *2010 Annual International Conference of the IEEE Engineering in Medicine and Biology*, pp. 734–737, 2010.
- [26] M. Angel, E., Wellnitz, C., Goodsitt, M., Yaghamai, N., DeMarco, J., Cagnon, C., Sayre, J., Cody, D., Stevens, D., Primak, A., McCollough, C., McNitt-Gray, “Radiation Dose to

- the Fetus for Pregnant Patients Undergoing Multidetector CT Imaging: Monte Carlo Simulations Estimating Fetal Dose for a Range of Gestational Age and Patient Size,” *Radiology*, vol. 249, no. 1, pp. 220–227, Oct. 2008.
- [27] T. Xie, P.Z. Fregonara and H. Zaidi, “Construction of a computational model of pregnant patients with twins for radiation dosimetry,” *Proc. 6th Int. Work. Comput. Hum. Phantoms, Annapolis*, vol. 27, pp. 120–121, 2017.
- [28] L. Bibin, J. Anquez, E. Angelini, and I. Bloch, “Hybrid 3D pregnant woman and fetus modeling from medical imaging for dosimetry studies,” *Int. J. Comput. Assist. Radiol. Surg.*, vol. 5, no. 1, pp. 49–56, 2010.
- [29] M. Maynard, N. Long, N. Moawad, R. Shifrin, A. Geyer, G. Fong, W. Bolch, “The UF Family of hybrid phantoms of the pregnant female for computational radiation dosimetry,” *Phys. Med. Biol.*, vol. 59, no. 15, pp. 4325–4343, 2014.
- [30] E. Azghadi, L. Motavalli, H. Hakimabad, “Development of a 9-months pregnant hybrid phantom and its internal dosimetry for thyroid agents,” *J. Radiat. Res.*, vol. 55, no. 4, pp. 730–747, 2014.
- [31] L. Motavalli, H. Hakimabad, E. Azghadi, “Fetal and maternal dose assessment for diagnostic scans during pregnancy,” *Phys. Med. Biol.*, vol. 61, no. 9, pp. 3596–3608, 2016.
- [32] T. Xie and H. Zaidi, “Development of computational pregnant female and fetus models and assessment of radiation dose from positron-emitting tracers,” *Eur. J. Nucl. Med. Mol. Imaging*, vol. 43, no. 13, pp. 2290–2300, Dec. 2016.
- [33] T. Xie and H. Zaidi, “Fetal and Maternal Absorbed Dose Estimates for Positron-Emitting Molecular Imaging Probes,” *J. Nucl. Med.*, vol. 55, no. 9, pp. 1459–1466, Sep. 2014.
- [34] T. Xie, P. Zanotti-Fregonara, A. Edet-Sanson, and H. Zaidi, “Patient-Specific Computational Model and Dosimetry Calculations for PET/CT of a Patient Pregnant with Twins,” *J. Nucl. Med.*, vol. 59, no. 9, pp. 1451–1458, Sep. 2018.
- [35] M. R. Maynard, “Hybrid Computational Phantoms of the Developing Fetus and Pregnant Female : Construction and Application To Select Internal Radiation Dosimetry Studies,” PhD dissertation, The University of Florida, 2013.
- [36] D. D. Martin, “Review of radiation therapy in the pregnant cancer patient.,” *Clin. Obstet. Gynecol.*, vol. 54, no. 4, pp. 591–601, Dec. 2011.
- [37] A. Surbone, F. Peccatori, and N. Pavlidis, "*Cancer and Pregnancy*. Springer, vol. 178, 2008.
- [38] M. P. Hande and D. P. U. Uevi, “Effect of In Utero Exposure to Diagnostic Ultrasound on the Postnatal Survival and Growth of Mouse,” *Teratology*, vol. 48, no. 1993, pp. 405–411, 1993.
- [39] N. M. Rofsky, D. J. Pizzarello, J. C. Weinreb, M. M. Ambrosino, and C. Rosenberg, “Effect on fetal mouse development of exposure to MR imaging and gadopentetate dimeglumine.,” *J. Magn. Reson. Imaging*, vol. 4, no. 6, pp. 805–7, 1994.
- [40] J. Gu, B. Bednarz, P. F. Caracappa, and X. G. Xu, “The development, validation and

- application of a multi-detector CT (MDCT) scanner model for assessing organ doses to the pregnant patient and the fetus using Monte Carlo simulations.," *Phys. Med. Biol.*, vol. 54, no. 9, pp. 2699–2717, 2009.
- [41] B. Bednarz and X. G. Xu, "Monte Carlo modeling of a 6 and 18 MV Varian Clinac medical accelerator for in-field and out-of-field dose calculations: development and validation.," *Phys. Med. Biol.*, vol. 54, no. 4, pp. N43-57, 2009.
- [42] ICRP 60," 1990 Recommendations of the International Commission on Radiological Protection ICRP Publication 60."Annal ICRP, Oxford: Pregamon.", vol.31, 1991.
- [43] G. Isaacson, M. C. Mintz, and E. S. Crelin, *Atlas of Fetal Sectional Anatomy With Ultrasound and Magnetic Resonance Imaging*. Springer New York, 1986.
- [44] L. H. Nelson, W. J. Bo, and G. C. Lynch, *Fetal Sectional Anatomy and Ultrasonography*. Williams & Wilkins, 1988.
- [45] M. Maynard, J. Geyer, J. Aris, R. Shifrin, W. Bolch, "The UF family of hybrid phantoms of the developing human fetus for computational radiation dosimetry.," *Phys. Med. Biol.*, vol. 56, no. 15, pp. 4839–79, Aug. 2011.
- [46] ICRU, "Photon, electron, proton and neutron interaction data for body tissues ICRU Report 46," Bethesda, MD: ICRU, 1992.
- [47] ICRP, "Adult Reference Computational Phantoms, ICRP Publication 110," Elsevier, 2009.
- [48] VTK, <http://www.vtk.org>.
- [49] M. Hafizah, T. Kok, and E. Spriyanto, "3D ultrasound image reconstruction based on VTK," pp. 102–106, 2010.
- [50] Rhinoceros software, version 5.0, <https://www.rhino3d.com>.
- [51] Binvox software, <http://www.cs.princeton.edu/~min/binvox>.
- [52] F. S. Nooruddin and G. Turk, "Simplification and repair of polygonal models using volumetric techniques," *IEEE Trans. Vis. Comput. Graph.*, vol. 9, no. 2, pp. 191–205, 2003.



## APPENDIX A: SEGMENTED ORGANS OF PREVIOUS PREGNANT PHANTOMS IN COMPARISON WITH THE CURRENT DEVELOPED MODEL.

Organs	Stabin 1995 ORNL, US	ICRP-89	Chen 2004 Canada	Xu 2007 NY(CT)	Dimbylow 2006 UK (CT+MR)	Wu 2006 US (MRI)	Cech 2007 Austria (MRI+CT)	Nagaoka 2007 Japan (MRI)	Bibin 2010 France(MR+US)	Maynard 2011 FL (MR+CT)	Hus.2013 IRAN (MRI+CT)	This work
Uterus of the mother	v		v	v	v	v	v	v	v	v	v	v
Placenta	v		v	v	v	v	v	v		v	v	v
Amniotic cord									v	v	v	v
Amniotic Fluid					v	v		v	v	v	v	v
Brain		v	v	v	v			v	v	v	v	v
Pitulary Gland										v		v
Branchia										v		v
Liver		v								v	v	v
Heart		v							v	v	v	v
Lungs		v							v	v	v	v
Stomach										v	v	v
SI										v	v	v
LI										v	v	v
Urinary Bladder			v					v	v	v	v	v
Kidneys		v								v	v	v
Gall Bladder						v				v	v	v
Eyes								v	v	v	v	v
Spin										v		v
Spinal Cord										v	v	v
Adrenals		v								v	v	v
Spleen		v								v	v	v
Pancreas		v								v	v	v
Thymus										v	v	v
Thyroid		v								v	v	v
Trachea										v		v
Skeleton	v		v	v	v	v	v			v	v	v
Soft Tissue	v		v	v			v			v	v	v
Colon										v		v
Esophagus wall										v		
Skin/whol body			v	v	v	v		v		v	v	v
<b>Total Organs</b>	<b>4</b>	<b>9</b>	<b>7</b>	<b>6</b>	<b>6</b>	<b>6</b>	<b>4</b>	<b>7</b>	<b>8</b>	<b>30</b>	<b>24</b>	<b>29</b>

## **APPENDIX B: VOXELIZED PREGNANT PHANTOM MODELS INFORMATION**

This appendix presents the following tables of fetal and pregnant female phantom developed as follows:

1. Voxelization bounding box, organ ID, and voxel resolution for 20-week Pregnant Female Phantom.
2. Voxelization bounding box, organ ID, and voxel resolution for 31-week Pregnant Female Phantom.
3. Voxelization bounding box, Organ ID and voxel resolution for 35-week Pregnant Female Phantom.

## B-1 Voxelization bounding box, organ ID, and voxel resolution for 20-week Pregnant Female Phantom.

Female Organs- 20 Weeks	ID	Bounding Box: From			Bounding Box: To			Dimentions			Max
		u	v	i	u	v	i	$\Delta u$	$\Delta v$	$\Delta i$	
EyeR	1	157.23	-50.63	889.42	180.99	-26.88	913.48	23.75	23.75	24.07	24.07
EyeL	2	100.07	-50.63	890.06	123.82	-26.88	914.12	23.75	23.75	24.07	24.07
LensR	3	162.13	-46.02	893.62	171.86	-42.04	903.35	9.74	3.99	9.74	9.74
LensL	4	106.42	-46.02	892.62	116.15	-42.04	902.35	9.74	3.99	9.74	9.74
Brain	5	72.72	-52.64	874.00	196.38	118.74	1015.25	123.66	171.38	141.25	171.38
Pituary Gland	6	129.66	19.50	891.25	140.34	30.18	901.40	10.68	10.68	10.16	10.68
Tonsiles (1)	7	133.57	3.78	814.91	152.83	21.68	827.20	19.26	17.90	12.29	19.26
Spin	8	121.10	62.23	466.73	139.22	132.49	859.85	18.12	70.26	393.13	393.13
Lymph Nodes (1)	9	87.11	15.82	811.20	114.29	48.51	840.40	27.18	32.70	29.19	32.70
Teeth	10	103.72	-32.47	843.74	163.33	15.00	862.74	59.61	47.47	19.00	59.61
Tongue	11	112.64	-22.42	823.77	158.33	41.04	856.21	45.69	63.46	32.43	63.46
Skin	12	-125.67	-657.35	-178.75	390.84	1025.61	74.26	516.51	1682.96	253.00	1682.96
Oesophagus	13	107.34	24.20	781.21	157.30	53.33	812.34	49.96	29.13	31.14	49.96
Thyroid Gland	14	102.47	33.19	753.55	160.23	64.98	791.13	57.77	31.79	37.58	57.77
Pharynx	15	119.58	-11.36	833.87	147.34	48.14	886.99	27.75	59.50	53.13	59.50
Trachea	16	120.65	52.82	690.47	135.08	86.62	756.65	14.43	33.80	66.18	66.18
Larynx	17	117.85	26.90	748.21	143.01	63.09	845.21	25.15	36.19	97.00	97.00
Branchi	18	100.47	78.31	657.28	171.12	96.68	691.34	70.64	18.37	34.05	70.64
Nasle Cartilage	19	126.87	-57.51	853.10	136.01	-23.04	887.64	9.14	34.48	34.54	34.54
LungR	20	140.64	8.78	529.35	248.56	147.12	753.38	107.91	138.33	224.03	224.03
LungL	21	18.95	9.31	556.80	138.15	140.98	748.11	119.19	131.66	191.32	191.32
Stomach wall	22	146.67	0.80	429.69	238.02	93.73	545.75	91.35	92.93	116.06	116.06
Stomach Content	23	157.66	5.81	437.84	234.98	84.47	535.86	77.32	78.66	98.01	98.01
Gall Bladder wall	24	98.29	19.58	483.16	152.12	66.26	537.06	53.84	46.68	53.90	53.90
Gall Bladder Content	25	110.97	29.91	493.26	141.49	56.43	524.75	30.52	26.51	31.48	31.48
Pancreas	26	57.02	13.62	390.07	201.49	68.40	459.30	144.47	54.78	69.23	144.47
Thymus	27	109.53	44.94	684.00	150.22	70.31	736.81	40.70	25.37	52.81	52.81
Liver	28	24.21	-23.90	424.20	217.91	129.35	567.01	193.70	153.24	142.81	193.70
Heart	29	97.55	7.31	555.56	224.03	104.59	681.04	126.48	97.28	125.49	126.48
Spleen	30	163.67	51.76	470.18	250.30	125.68	549.84	86.63	73.92	79.66	86.63
SI Wall	31	32.92	-35.51	263.92	240.51	51.08	443.51	207.59	86.59	179.60	207.59
SI content	32	33.85	-34.62	264.02	239.67	50.92	442.47	205.82	85.55	178.45	205.82
LI Wall	33	3.75	-46.15	184.36	251.31	139.53	463.64	247.56	185.68	279.28	279.28
LI Content	34	6.84	-43.01	184.65	248.12	135.88	460.47	241.28	178.89	275.82	275.82
OvaryR	35	79.75	37.91	235.90	107.90	54.14	257.81	28.15	16.22	21.91	28.15
OvaryL	36	179.88	6.67	241.00	208.03	22.90	262.91	28.15	16.22	21.91	28.15
KidneyR	37	37.71	45.68	388.29	104.28	105.22	471.28	66.57	59.54	82.99	82.99
KidneyL	38	153.20	59.73	390.42	219.89	115.17	493.40	66.69	55.45	102.98	102.98
AdrenalR	39	75.29	75.49	471.12	101.42	111.32	490.37	26.12	35.84	19.25	35.84
AdrenalL	40	146.36	60.16	489.63	168.01	100.96	506.26	21.65	40.80	16.63	40.80
Urinary Bladder	41	99.69	6.51	196.99	163.31	68.33	228.50	63.61	61.82	31.51	63.61
Uterus	42	71.35	-38.41	216.94	200.63	110.49	360.54	129.28	148.90	143.60	148.90
BreastR	43	51.81	-42.01	602.64	123.39	20.34	685.10	71.57	62.35	82.47	82.47
BreastL	44	51.81	-42.01	602.64	123.39	20.34	685.10	71.57	62.35	82.47	82.47
BrestFatR	45	56.44	-33.04	605.11	106.62	8.56	664.14	50.18	41.60	59.03	59.03
BrestFatL	46	56.44	-33.04	605.11	106.62	8.56	664.14	50.18	41.60	59.03	59.03
Skeletons	85-102	38.59	-17.19	-654.05	113.84	159.91	-539.68	75.24	177.10	114.38	177.10

Fetus Organs-20 Weeks	ID	Bounding Box: From			Bounding Box: To			Dimentions			Max
		u	v	i	u	v	i	$\Delta u$	$\Delta v$	$\Delta i$	
Fetus Nasel Septum	48	113.24	54.28	268.53	122.09	58.76	273.96	8.85	4.48	5.43	8.85
Placenta	49	112.96	-34.17	274.10	198.11	45.31	359.17	85.14	79.47	85.07	85.14
Umbilical cord	50	106.75	4.50	233.58	182.54	107.31	297.19	75.79	102.81	63.61	102.81
Fetus Brain	51	109.86	46.34	220.71	163.79	94.99	270.13	53.93	48.65	49.42	53.93
Fetus Pituitary gland	52	123.31	67.83	251.03	127.79	72.30	255.50	4.47	4.47	4.47	4.47
Fetus Bronchi	53	146.20	37.88	257.19	152.59	49.80	267.93	6.39	11.91	10.74	11.91
Fetus Liver	54	132.92	4.36	267.82	170.64	49.24	311.15	37.72	44.87	43.34	44.87
Fetus Heart	55	139.18	33.65	267.77	159.41	49.26	291.91	20.22	15.61	24.14	24.14
Fetus Lung R	56	138.50	37.31	265.63	174.72	65.36	286.49	36.22	28.05	20.86	36.22
Fetus Lung L	57	137.71	19.02	252.63	175.60	43.52	277.51	37.89	24.49	24.88	37.89
Fetus Stomach	58	152.89	37.91	293.55	165.85	50.04	308.26	12.96	12.14	14.71	14.71
Fetus Urinary Bladder	61	148.66	11.32	308.68	155.86	23.06	320.76	7.19	11.75	12.07	12.07
Fetus Kidney R	62	159.66	7.25	281.41	176.57	25.37	298.80	16.91	18.12	17.39	18.12
Fetus Kidney L	63	159.66	7.25	281.41	176.57	25.37	298.80	16.91	18.12	17.39	18.12
Fetus Gall Bladder	64	145.62	10.32	287.75	156.12	18.28	298.23	10.50	7.95	10.48	10.50
Fetus Eyeball R	65	122.50	63.33	268.24	134.58	75.41	280.48	12.08	12.08	12.24	12.24
Fetus Eyeball L	66	122.50	63.33	268.24	134.58	75.41	280.48	12.08	12.08	12.24	12.24
Fetus Eye Lens R	67	121.72	46.35	258.29	126.25	48.29	262.84	4.52	1.94	4.55	4.55
Fetus Eye Lens L	68	121.72	46.35	258.29	126.25	48.29	262.84	4.52	1.94	4.55	4.55
Fetus Adrenal R	69	166.45	35.07	289.80	176.94	47.49	304.55	10.50	12.42	14.75	14.75
Fetus Adrenal L	70	167.65	18.60	275.87	178.07	33.51	287.69	10.42	14.91	11.82	14.91
Fetus Spleen	71	153.10	47.16	292.46	169.17	54.92	307.11	16.08	7.76	14.65	16.08
Fetus Pancreas	72	153.60	8.89	297.35	165.55	41.25	316.85	11.95	32.36	19.50	32.36
Fetus Thymus	73	127.98	30.08	262.25	142.04	45.20	284.26	14.06	15.12	22.01	22.01
Fetus Thyroid Gland	74	129.68	47.56	253.76	139.85	57.89	263.34	10.16	10.34	9.59	10.34
Fetus Tongue	75	128.10	50.13	265.31	136.61	57.93	274.10	8.52	7.81	8.80	8.80
Fetus Trachea	77	127.37	45.02	256.97	146.88	55.11	263.32	19.51	10.09	6.35	19.51
Fetus body	80	74.21	-15.48	217.91	184.20	100.97	346.42	109.99	116.45	128.51	128.51
Fetus Tooth Buds	81	125.92	44.11	264.80	137.95	56.20	281.52	12.04	12.09	16.72	16.72
Fetus Spinal Cord	83	153.10	7.03	250.32	179.39	54.93	312.80	26.29	47.90	62.48	62.48
Fetus Spin	84	153.10	7.03	250.32	179.39	54.93	312.80	26.29	47.90	62.48	62.48

## B-2 Voxelization bounding box, organ ID, and voxel resolution for 31-week Pregnant Female Phantom.

Female Organs- 31 Weeks	ID	Bounding Box: From			Bounding Box: To			Dimentions			Max
		u	v	i	u	v	i	$\Delta u$	$\Delta v$	$\Delta i$	
EyeR	1	-	-	-	-	-	-	-	-	-	-
EyeL	2	-	-	-	-	-	-	-	-	-	-
LensR	3	-	-	-	-	-	-	-	-	-	-
LensL	4	-	-	-	-	-	-	-	-	-	-
Brain	5	-	-	-	-	-	-	-	-	-	-
Pituary Gland	6	-	-	-	-	-	-	-	-	-	-
Tonsiles (1)	7	-	-	-	-	-	-	-	-	-	-
Spin	8	-	-	-	-	-	-	-	-	-	-
Lymph Nodes (1)	9	-	-	-	-	-	-	-	-	-	-
Teeth	10	-	-	-	-	-	-	-	-	-	-
Tongue	11	-	-	-	-	-	-	-	-	-	-
Skin	12	-133.78	-655.15	-171.03	399.00	1025.61	148.46	532.78	1680.76	319.49	1680.76
Oesophagus	13	-	-	-	-	-	-	-	-	-	-
Thyroid Gland	14	-	-	-	-	-	-	-	-	-	-
Pharynx	15	-	-	-	-	-	-	-	-	-	-
Trachea	16	-	-	-	-	-	-	-	-	-	-
Larynx	17	-	-	-	-	-	-	-	-	-	-
Branchi	18	-	-	-	-	-	-	-	-	-	-
Nasle Cartilage	19	-	-	-	-	-	-	-	-	-	-
LungR	20	-	-	-	-	-	-	-	-	-	-
LungL	21	-	-	-	-	-	-	-	-	-	-
Stomach wall	22	161.58	7.02	452.59	239.67	85.68	547.32	78.09	78.66	94.72	94.72
Stomach Content	23	150.42	2.01	448.09	242.71	94.94	557.21	92.29	92.93	109.12	109.12
Gall Bladder wall	24	98.29	19.58	483.16	152.12	66.26	537.06	53.83	46.68	53.90	53.90
Gall Bladder Content	25	98.29	19.58	483.16	152.12	66.26	537.06	53.83	46.68	53.90	53.90
Pancreas	26	71.06	17.57	396.47	201.68	72.38	488.03	130.62	54.81	91.56	130.62
Thymus	27	-	-	-	-	-	-	-	-	-	-
Liver	28	24.18	-25.45	423.44	217.25	128.01	567.48	193.07	153.46	144.04	193.07
Heart	29	-	-	-	-	-	-	-	-	-	-
Spleen	30	-	-	-	-	-	-	-	-	-	-
SI Wall	31	18.57	-49.60	242.46	266.73	93.82	458.93	248.16	143.41	216.47	248.16
SI content	32	18.57	-49.60	242.46	266.73	93.82	458.93	248.16	143.41	216.47	248.16
LI Wall	33	5.67	-75.60	185.39	249.73	140.00	497.45	244.06	215.60	312.05	312.05
LI Content	34	5.67	-75.60	185.39	249.73	140.00	497.45	244.06	215.60	312.05	312.05
OvaryR	35	198.15	-31.14	244.82	226.30	-14.92	266.73	28.15	16.22	21.91	28.15
OvaryL	36	198.15	-31.14	244.82	226.30	-14.92	266.73	28.15	16.22	21.91	28.15
KidneyR	37	-	-	-	-	-	-	-	-	-	-
KidneyL	38	-	-	-	-	-	-	-	-	-	-
AdrenalR	39	-	-	-	-	-	-	-	-	-	-
AdrenalL	40	-	-	-	-	-	-	-	-	-	-
Urinary Bladder	41	90.82	10.76	202.46	176.33	71.12	231.23	85.50	60.36	28.77	85.50
Uterus	42	36.84	-130.84	207.92	245.88	60.06	458.36	209.04	190.90	250.43	250.43
BreastR	43	42.58	-51.44	592.17	134.09	28.28	697.61	91.51	79.72	105.44	105.44
BreastL	44	148.81	-46.43	593.34	240.73	24.98	699.67	91.92	71.40	106.33	106.33
BrestFatR	45	48.49	-39.97	595.33	112.66	13.22	670.81	64.16	53.19	75.48	75.48
BrestFatL	46	160.63	-38.68	600.85	225.08	9.26	676.57	64.45	47.93	75.73	75.73
Skeletons	85-102	-	-	-	-	-	-	-	-	-	-

Fetus Organs-31 Weeks	ID	Bounding Box: From			Bounding Box: To			Dimentions			Max
		u	v	i	u	v	i	$\Delta u$	$\Delta v$	$\Delta i$	
Fetus Nasel Septum	48	101.49	6.83	302.11	125.41	13.94	321.92	23.92	7.11	19.80	23.92
Fetus Placenta	49	89.11	-116.68	340.02	243.42	32.07	457.77	154.31	148.75	117.76	154.31
Umbilical cord	50	55.17	-97.17	347.66	132.02	13.61	431.01	76.85	110.78	83.35	110.78
Fetus Brain	51	92.29	-31.56	223.99	175.01	41.32	294.18	82.71	72.88	70.19	82.71
Fetus Pituitary gland	52	128.22	-0.65	263.25	133.44	4.55	268.27	5.22	5.20	5.02	5.22
Fetus Bronchi	53	184.14	-10.34	299.39	198.32	10.55	310.96	14.19	20.89	11.58	20.89
Fetus Liver	54	138.47	-64.62	318.72	200.89	12.30	358.87	62.42	76.91	40.15	76.91
Fetus Heart	55	152.66	-17.02	305.37	185.89	10.75	337.20	33.23	27.77	31.83	33.23
Fetus Lung R	56	170.80	-12.11	300.63	209.15	24.09	344.57	38.35	36.20	43.94	43.94
Fetus Lung L	57	162.69	-40.16	295.44	213.31	-3.19	331.97	50.62	36.97	36.53	50.62
Fetus Stomach	58	135.88	-13.92	356.76	164.30	2.24	369.60	28.42	16.15	12.84	28.42
Fetus Urinary Bladder	61	154.69	-49.55	389.63	171.47	-34.64	401.69	16.78	14.91	12.05	16.78
Fetus Kidney R	62	152.01	-38.59	365.74	175.70	-14.03	395.38	23.69	24.56	29.63	29.63
Fetus Kidney L	63	160.20	-62.84	355.25	187.47	-36.07	383.58	27.26	26.78	28.34	28.34
Fetus Gall Bladder	64	157.78	-37.63	351.32	172.58	-22.68	361.21	14.80	14.96	9.89	14.96
Fetus Eyeball R	65	93.74	-14.45	293.53	111.93	3.76	311.90	18.19	18.21	18.38	18.38
Fetus Eyeball L	66	93.74	-14.45	293.53	111.93	3.76	311.90	18.19	18.21	18.38	18.38
Fetus Eye Lens R	67	97.77	-8.74	305.92	103.63	-3.78	310.14	5.86	4.96	4.22	5.86
Fetus Eye Lens L	68	97.77	-8.74	305.92	103.63	-3.78	310.14	5.86	4.96	4.22	5.86
Fetus Adrenal R	69	165.38	-25.96	357.20	187.91	-11.18	377.84	22.53	14.77	20.64	22.53
Fetus Adrenal L	70	177.97	-43.94	350.72	201.86	-28.57	368.25	23.89	15.37	17.53	23.89
Fetus Spleen	71	122.69	-20.38	346.60	145.75	13.52	372.42	23.06	33.90	25.82	33.90
Fetus Pancreas	72	144.64	-50.45	355.59	168.16	-13.71	379.10	23.52	36.73	23.51	36.73
Fetus Thymus	73	155.32	-15.49	287.77	183.12	19.02	308.41	27.80	34.51	20.64	34.51
Fetus Thyroid Gland	74	156.97	-2.11	281.37	172.55	16.69	293.37	15.58	18.80	12.01	18.80
Fetus Tongue	75	121.28	-16.32	294.26	138.51	0.79	311.65	17.23	17.11	17.38	17.38
Fetus Trachea	77	156.29	0.76	283.00	186.20	11.01	302.11	29.91	10.25	19.10	29.91
Fetus Fetus body	80	55.84	-89.85	209.63	218.09	53.79	432.96	162.26	143.64	223.34	223.34
Fetus Tooth Buds	81	115.28	-26.71	299.13	136.44	6.29	322.86	21.15	33.01	23.73	33.01
Fetus Spinal Cord	83	155.87	-38.37	273.12	216.27	14.62	404.70	60.40	52.99	131.58	131.58
Fetus Spin	84	155.87	-38.37	273.12	216.27	14.62	404.70	60.40	52.99	131.58	131.58

### B-3 Voxelization bounding box, Organ ID and voxel resolution for 35-week Pregnant Female Phantom.

Female Organs- 35 Weeks	ID	Bounding Box: From			Bounding Box: To			Dimentions			Max
		u	v	i	u	v	i	$\Delta u$	$\Delta v$	$\Delta i$	
EyeR	1	-	-	-	-	-	-	-	-	-	-
EyeL	2	-	-	-	-	-	-	-	-	-	-
LensR	3	-	-	-	-	-	-	-	-	-	-
LensL	4	-	-	-	-	-	-	-	-	-	-
Brain	5	-	-	-	-	-	-	-	-	-	-
Pituary Gland	6	-	-	-	-	-	-	-	-	-	-
Tonsiles (1)	7	-	-	-	-	-	-	-	-	-	-
Spin	8	-	-	-	-	-	-	-	-	-	-
Lymph Nodes (1)	9	-	-	-	-	-	-	-	-	-	-
Teeth	10	-	-	-	-	-	-	-	-	-	-
Tongue	11	-	-	-	-	-	-	-	-	-	-
Skin	12	-133.78	-655.15	-171.03	399.00	1025.61	123.55	532.78	1680.76	294.58	1680.76
Oesophagus	13	-	-	-	-	-	-	-	-	-	-
Thyroid Gland	14	-	-	-	-	-	-	-	-	-	-
Pharynx	15	-	-	-	-	-	-	-	-	-	-
Trachea	16	-	-	-	-	-	-	-	-	-	-
Larynx	17	-	-	-	-	-	-	-	-	-	-
Branchi	18	-	-	-	-	-	-	-	-	-	-
Nasle Cartilage	19	-	-	-	-	-	-	-	-	-	-
LungR	20	-	-	-	-	-	-	-	-	-	-
LungL	21	-	-	-	-	-	-	-	-	-	-
Stomach wall	22	127.87	4.77	479.70	233.32	98.73	566.29	105.45	93.96	86.59	105.45
Stomach Content	23	136.91	9.62	482.23	230.39	89.43	557.06	93.48	79.81	74.83	93.48
Gall Bladder wall	24	83.08	20.26	495.46	136.62	66.78	550.69	53.54	46.52	55.24	55.24
Gall Bladder Content	25	95.76	29.62	507.33	126.28	56.14	538.82	30.52	26.51	31.48	31.48
Pancreas	26	63.31	26.54	434.45	192.04	78.44	508.81	128.73	51.90	74.36	128.73
Thymus	27	-	-	-	-	-	-	-	-	-	-
Liver	28	17.83	-44.58	431.07	217.11	138.58	577.09	199.27	183.16	146.02	199.27
Heart	29	-	-	-	-	-	-	-	-	-	-
Spleen	30	-	-	-	-	-	-	-	-	-	-
SI Wall	31	14.72	-10.58	202.09	247.90	113.94	484.57	233.18	124.52	282.48	282.48
SI content	32	15.70	-9.58	203.08	246.90	112.95	484.17	231.20	122.52	281.09	281.09
LI Wall	33	5.17	-88.40	185.22	250.19	143.48	530.22	245.02	231.88	345.00	345.00
LI Content	34	8.31	-84.25	185.85	247.54	135.84	526.41	239.23	220.08	340.56	340.56
OvaryR	35	43.00	-33.00	257.18	71.16	-16.77	279.09	28.15	16.22	21.91	28.15
OvaryL	36	194.24	-28.39	252.25	222.39	-12.17	274.16	28.15	16.22	21.91	28.15
KidneyR	37	-	-	-	-	-	-	-	-	-	-
KidneyL	38	-	-	-	-	-	-	-	-	-	-
AdrenalR	39	-	-	-	-	-	-	-	-	-	-
AdrenalL	40	-	-	-	-	-	-	-	-	-	-
Urinary Bladder	41	97.37	20.62	198.89	169.66	73.35	225.41	72.29	52.73	26.53	72.29
Uterus	42	28.90	-105.93	209.88	238.66	107.91	502.19	209.77	213.84	292.31	292.31
BreastR	43	42.58	-51.44	592.17	134.09	28.28	697.61	91.51	79.72	105.44	105.44
BreastL	44	148.81	-46.43	593.34	240.73	24.98	699.67	91.92	71.40	106.33	106.33
BrestFatR	45	48.49	-39.97	595.33	112.66	13.22	670.81	64.16	53.19	75.48	75.48
BrestFatL	46	160.63	-38.68	600.85	225.08	9.26	676.57	64.45	47.93	75.73	75.73
Skeletons	85-102	-	-	-	-	-	-	-	-	-	-

Fetus Organs-35 Weeks	ID	Bounding Box: From			Bounding Box: To			Dimentions			Max
		u	v	i	u	v	i	$\Delta u$	$\Delta v$	$\Delta i$	
Nasel Septum	48	122.21	-11.01	255.59	129.61	3.04	263.85	7.40	14.05	8.26	14.05
Placenta	49	87.97	-76.05	336.91	235.10	41.51	500.53	147.13	117.56	163.62	163.62
Umbilical cord	50	154.74	-74.00	288.08	217.09	-25.00	386.28	62.35	49.01	98.20	98.20
Brain	51	90.74	5.02	217.63	171.48	90.86	302.02	80.74	85.84	84.39	85.84
Pituitary gland	52	127.40	26.91	257.09	132.79	32.31	262.49	5.40	5.40	5.40	5.40
Bronchi	53	77.12	10.37	319.65	109.72	20.66	335.86	32.60	10.29	16.21	32.60
Liver	54	63.50	-54.27	347.08	131.69	25.59	412.09	68.18	79.86	65.00	79.86
Heart	55	80.45	-30.55	325.31	113.68	12.88	352.75	33.23	43.43	27.43	43.43
Lung R	56	85.14	-17.79	327.49	126.68	31.01	380.63	41.54	48.80	53.14	53.14
Lung L	57	53.96	-27.01	321.74	91.07	19.33	370.59	37.11	46.34	48.86	48.86
Stomach	58	52.59	-70.60	366.93	106.94	-22.46	403.69	54.34	48.14	36.76	54.34
Urinary Bladder	61	113.33	-59.61	407.67	136.52	-35.43	444.40	23.20	24.18	36.73	36.73
Kidney R	62	78.72	-6.90	402.26	106.20	20.65	436.35	27.48	27.55	34.09	34.09
Kidney L	63	45.92	-34.23	386.96	69.77	-4.78	418.24	23.84	29.46	31.28	31.28
Gall Bladder	64	93.62	-25.81	400.59	113.98	-4.55	418.03	20.36	21.26	17.44	21.26
Eyeball R	65	143.45	-21.88	242.45	158.81	-1.03	263.52	15.36	20.85	21.07	21.07
Eyeball L	66	106.43	-21.54	230.20	127.30	-0.69	251.26	20.87	20.85	21.07	21.07
Eye Lens R	67	152.61	-10.88	249.59	158.81	-8.01	255.65	6.20	2.86	6.06	6.20
Eye Lens L	68	152.61	-10.88	249.59	158.81	-8.01	255.65	6.20	2.86	6.06	6.20
Adrenal R	69	77.80	1.87	389.44	96.21	27.29	409.72	18.41	25.41	20.28	25.41
Adrenal L	70	37.34	-16.34	379.93	61.33	7.69	395.36	23.99	24.03	15.43	24.03
Spleen	71	51.53	-12.32	359.34	79.19	9.04	386.27	27.66	21.37	26.93	27.66
Pancreas	72	60.39	-27.23	387.69	86.94	10.83	413.22	26.55	38.05	25.53	38.05
Thymus	73	87.41	-24.48	301.94	122.49	-1.73	334.51	35.08	22.75	32.57	35.08
Thyroid Gland	74	89.86	17.53	286.65	113.63	31.85	306.45	23.77	14.32	19.80	23.77
Tongue	75	107.63	-7.98	276.42	117.06	1.00	285.33	9.44	8.97	8.91	9.44
Trachea*	77	89.22	17.87	289.34	108.07	29.49	321.91	18.85	11.62	32.57	32.57
Fetus body	80	33.62	-103.44	213.22	209.42	101.65	475.85	175.80	205.09	262.63	262.63
Tooth Buds	81	91.44	-9.06	276.33	127.88	9.66	301.91	36.43	18.73	25.58	36.43
Spinal Cord*	83	50.07	-44.33	267.83	96.97	24.01	417.73	46.90	68.34	149.90	149.90
Spin	84	45.69	-47.49	264.16	100.45	27.80	444.99	54.76	75.29	180.83	180.83




## **APPENDIX C: SELECTED PAPERS, PRESENTATIONS, ABSTRACTS AND AWARDS**

- Rasha Makkia, Keith Nelson, Habib Zaidi, Michael Dingfelder, “Contraction of realistic hybrid computational fetal phantoms from radiological images in three gestational ages for radiation dosimetry applications”, *Physics in Medicine and Biology*, under review April 10, 2019.
- Rasha Makkia, Keith Nelson, Habib Zaidi, Michael Dingfelder, “Construction of Realistic Hybrid Computational Pregnant Phantoms for Radiation Risk Assessment”, *Imaging General ePoster Viewing (PO-GePV-I-10)* presented at 61<sup>st</sup> Annual Meeting of the American Association of Physicists in Medicine (AAPM), July 14, 2019, San Antonio, TX.
- Rasha Makkia, Keith Nelson, Habib Zaidi, Michael Dingfelder, “Construction of Realistic Hybrid Computational Pregnant Phantoms for Radiation Risk Assessment”, Graduate Oral Presentation in the Natural Sciences Category at Annual Research and Creative Achievement Week (RCAW) at ECU, April, 11 2019, Greenville, NC
- Rasha Makkia, Keith Nelson, Michael Dingfelder, “Fetus Phantom Constructions for Organ Dose Assessment of Pregnant Patients Who Underwent Radiotherapy”, Best Poster Competition (PO-BPC-Foyer-01) presented at Annual Meeting of the American Association of Physicists in Medicine (AAPM) Spring Clinical Meeting, April 27, 2018, Las Vegas, NV.
- R. Makkia, K. Nelson, H. Zaidi, and M. Dingfelder, “Development of Obese Hybrid Computational Pregnant Phantom Models for Radiotherapy Applications”, Poster (SU-I-GPD-T-213) presented at the 60<sup>th</sup> Annual Meeting of the American Association of Physicists in Medicine (AAPM), July 29, 2018, Nashville, TN.

- R. Makkia, K. Nelson, M. Dingfelder, H. Zaidi, “Construction of Realistic Hybrid Computational Fetus Models for Radiotherapy Applications”, Poster (SU-I-GPD-T-301) presented at the 60<sup>th</sup> Annual Meeting of the American Association of Physicists in Medicine (AAPM), July 29, 2018, Nashville, TN.
- Rasha Makkia, Keith Nelson, Habib Zaidi, Michael Dingfelder, “Construction of Realistic Hybrid Computational Fetus Models for Radiotherapy Applications”, Graduate Oral Presentation in the Natural Sciences Category at Annual Research and Creative Achievement Week (RCAW) at ECU, March, 11 2018, Greenville, NC.
- Rasha Makkia, “Organ Dose Reconstruction for Wilms Tumor Patients Treated with Radiation Therapy”, First Winner of Student Research Competition, Oral presentation at Health Physics Society North Carolina Chapter, NCHPS, March 4, 2017, Carolina Beach, NC
- R Makkia, M Gopalakrishnan C Lee M Mille C Pelletier J Kalapurakal C Lee J Jung, “A Pilot Study of Organ Dose Reconstruction for Wilms Tumor Patients Treated with Radiation Therapy”, Therapy general poster discussion (SU-F-T-117), presented at 58<sup>st</sup> Annual Meeting of the American Association of Physicists in Medicine (AAPM), June 7, 2016, Washington, DC.
- Rasha Makkia, “Fetus Phantom Constructions for Organ Dose Assessment of Pregnant Patients Who Underwent Radiotherapy”, First Winner of Student Research Competition, Oral presentation at Health Physics Society North Carolina Chapter, NCHPS, March 3, 2016, Carolina Beach, NC

# APPENDIX D: THE UNIVERSITY & MEDICAL CENTER INSTITUTIONAL REVIEW BOARD (UMCIRB)



**EAST CAROLINA UNIVERSITY**  
**University & Medical Center Institutional Review Board**  
4N-64 Brody Medical Sciences Building · Mail Stop 682  
600 Moye Boulevard · Greenville, NC 27834  
Office 252-744-2914 · Fax 252-744-2284  
[www.ecu.edu/ORIC/irb](http://www.ecu.edu/ORIC/irb)

**Notification of Initial Approval: Expedited**

**From:** Biomedical IRB  
**To:** [Keith Nelson](#)  
**CC:** [Keith Nelson](#)  
[Keith Nelson](#)  
**Date:** 10/20/2017  
**Re:** [UMCIRB 17-001935](#)  
Fetus Phantom Construction

I am pleased to inform you that your Expedited Application was approved. Approval of the study and any consent form(s) is for the period of 10/20/2017 to 10/19/2018. The research study is eligible for review under expedited category #5. The Chairperson (or designee) deemed this study no more than minimal risk.

Changes to this approved research may not be initiated without UMCIRB review except when necessary to eliminate an apparent immediate hazard to the participant. All unanticipated problems involving risks to participants and others must be promptly reported to the UMCIRB. The investigator must submit a continuing review/closure application to the UMCIRB prior to the date of study expiration. The Investigator must adhere to all reporting requirements for this study.

Approved consent documents with the IRB approval date stamped on the document should be used to consent participants (consent documents with the IRB approval date stamp are found under the Documents tab in the study workspace).

The approval includes the following items:

Name	Description
Makkia Research Protocol Rev 1.docx	Study Protocol or Grant Application

The Chairperson (or designee) does not have a potential for conflict of interest on this study.

---

IRB0000705 East Carolina U IRB #1 (Biomedical) IORG0000418  
IRB00003781 East Carolina U IRB #2 (Behavioral/SS) IORG0000418

IRB00000705 East Carolina U IRB #1 (Biomedical) IORG0000418

IRB000003781 East Carolina U IRB #2 (Behavioral/SS) IORG0000418

